Cation Exchange (Ag^{+}, Zn^{2+}, Cu^{2+}) Behavior of Natural Zeolites

By

Ayben TOP

**A Dissertation Submitted to the
Graduate School in Partial Fulfillment of the
Requirements for the Degree of**

MASTER OF SCIENCE

**Department: Chemical Engineering
Major: Chemical Engineering**

**İzmir Institute of Technology
İzmir, Turkey**

September, 2001

We approve the thesis of **Ayben TOP**

Date of Signature

..... **29.09.2001**
Prof. A. Semra ÜLKÜ
Supervisor
Department of Chemical Engineering

..... **29.09.2001**
Asst. Prof. S. Fehime ÖZKAN
Co-Supervisor
Department of Chemical Engineering

..... **29.09.2001**
Asst. Prof. Sacide ALTINKAYA
Co-Supervisor
Department of Chemical Engineering

..... **29.09.2001**
Prof. Devrim BALKÖSE
Department of Chemical Engineering

..... **29.09.2001**
Asst. Prof. Ahmet E. EROĞLU
Department of Chemistry

..... **29.09.2001**
Prof. Devrim BALKÖSE
Head of Chemical Engineering Department

ACKNOWLEDGEMENTS

I would like to express my sincere gratitude to my adviser, Professor A. Semra Ülkü, for her supervision, guidance, support, and encouragement, and for the freedom, she provided me throughout this project. I am also grateful to Professor Devrim Balköse and Assistant Professor S. Fehime Özkan for their valuable suggestions and recommendations. Special thanks to Research Assistant Yelda Akdeniz for her help and support.

I would like to thank research specialists: Filiz Özmıhçı, Özlem Çağlar, Nesrin Gaffaroğulları, and Nesrin Tatlıdil, for their contributions to the characterization studies, Research Assistant Mert Sudağıdan and Department of Biotechnology and Bioengineering for the antibacterial activity tests. I am also indebted to Assistant Professor Ahmet E. Eroğlu and Instructor Huriye Göksungur for their valuable suggestions in the ICP-AES studies, Doctor Noboru Imai and Geological Survey of Japan for the rock standards, and laboratory technicians: Şerife Şahin, Belgin Tunçel, and Tülin Burhanoğlu for their helps in the laboratory work. I would like to appreciate deeply to my roommates, research assistants: Hilal Pehlivan, Semih Elbir, and Dildare Metin for their friendships, supports, and encouragements.

Finally, I would like to thank my family for their supports, encouragements, and understandings.

ABSTRACT

In this study, clinoptilolite, most abundant zeolite present in nature, was proposed as a low cost antibacterial material. As a preliminary work, antibacterial activities of the original, Ag, and Zn forms of the clinoptilolite were investigated against several strains and compared to the commercial antibiotics. No antibacterial action was observed for the original clinoptilolite. Ag loaded clinoptilolite was found to be superior to the Zn-form against *Proteus spp*. and *Pseudomonas aeruginosa*.

The original, Na, Ag, Zn, and Cu forms of the clinoptilolite samples were characterized by FTIR spectroscopy, thermal analyses (TGA, DTA, and DSC), and N_2 physisorption studies. Specific attention was given in to the chemical analysis of the clinoptilolite by ICP-AES. Using the standard addition method, the respective idealized formulas of the original and Na-clinoptilolite based on 72 oxygen atoms in the unit cell were calculated as:

$(Na_{0.816}\ K_{2.070})\ (Ca_{1.060}\ Mg_{0.264})\ (Al_{5.653}\ Fe_{0.390})\ (Si_{30.084})\ O_{72}.\ 20.023\ H_2O$, and

$(Na_{4.763}\ K_{1.057})\ (Ca_{0.076}\ Mg_{0.094})\ (Al_{5.843}\ Fe_{0.221})\ (Si_{29.911})\ O_{72}.17.049\ H_2O$.

In the FTIR spectra of the original and exchanged forms of the clinoptilolite, considerable shifts (from 3460 to 3494.8 cm^{-1}) were observed in the band, which is formed due to the interactions of water molecules with the framework via hydrogen bonds. The positions of the other bands were not affected by cation exchange significantly. From the TGA curves, the water contents ranged between 14.31 and 11.00 % for the original and the cation-exchanged forms of the clinoptilolite. Mainly, two endotherms and one exotherm were obtained in the DTA curves. The first endotherm occurred up to about 150 ^oC, the second endotherm lied between 200 and 700 ^oC, and the exotherm was obtained at about 850 ^oC. Significant differences observed between the shapes of the DSC curves indicated that the cations control the dehydration behavior of the samples. N_2 physisorption isotherms of five samples were all, Type IV with BET surface areas ranging between 34.97 and 46.76 m^2/g.

Ag, Zn and Cu ion exchange equilibria were investigated at 25 ^oC for both the original clinoptilolite and Na-clinoptilolite. In the former case, from the plateau of the isotherms cation exchange capacities were determined as 1.184, 0.439, 0.539 meq/g clinoptilolite for Ag^+, Zn^{2+}, and Cu^{2+} respectively. The major portion of the exchanges was contributed by Na^+ and Ca^{2+}. Distribution coefficient values indicated that at

relatively low initial concentrations, the preference of the clinoptilolite for Zn^{2+} and Cu^{2+} was significant. At higher concentrations, higher distribution coefficients were obtained for Ag^{+} compared to Zn^{2+} and Cu^{2+}. Langmuir and Freundlich models were applied for each equilibrium data. For Zn^{2+} and Cu^{2+} exchanges, Langmuir model gave better correlation and Freundlich model fitted experimental data slightly better in the case of Ag^{+} exchange.

Equilibrium isotherms for Ag^{+}-Na^{+}, Zn^{2+}-Na^{+}, and Cu^{2+}-Na^{+} pairs were investigated. Silver exchange isotherm lied above the diagonal over the whole composition range. For zinc and copper exchanges, the isotherms were above the diagonal up to equivalent fractions of exchanging ion in solution phase (A_s) at about 0.2. While full exchange was attained for silver, partial exchanges were obtained in the case of zinc and copper. The standard free energy of exchange values were found as –6.0, 2.03 and 3.09 kj/equiv for Ag^{+}-Na^{+}, Zn^{2+}-Na^{+}, and Cu^{2+}-Na^{+} pairs respectively. From these values selectivity sequence was obtained as $Ag^{+} > Na^{+} > Zn^{2+} > Cu^{2+}$.

Consequently, by considering the preliminary antibacterial activity results, specific cation exchange capacities, and selectivity sequence of the clinoptilolite, Ag-clinoptilolite seemed to be promising antibacterial material. The results of the current study compared to the literature data pointed out that cation exchange behavior of the clinoptilolite is dependent on its original cationic composition. Therefore, it is necessary to carry out specific studies on representative samples from the deposit before any practical application.

ÖZ

Bu çalışmada, doğada en çok bulunan zeolit olan klinoptilolit, düşük maliyetli antibakteriyel malzeme olarak öngörülmüştür. Yapılan ön çalışmalarda, klinoptilolitin orijinal, Ag ve Zn formlarının birkaç bakteri türüne karşı antibakteriyel aktiviteleri incelenmiş ve ticari antibiyotiklerle karşılaştırılmıştır. Orijinal klinoptilolitin antibakteriyel davranışı gözlenmemiştir. Ag yüklenmiş klinoptilolit, *Proteus spp*. ve *Pseudomonas aeruginosa* türlerine karşı Zn formuna üstünlük sağlamıştır.

Klinoptilolit örneklerinin orijinal, Na, Ag, Zn ve Cu formları FTIR spektroskopisi, termal analizler (TGA, DTA, ve DSC) ve N_2 fiziksel adsorpsiyon çalışmaları ile karakterize edilmiştir. Klinoptilolitin ICP-AES ile kimyasal kompozisyonunun belirlenmesine özel önem verilmiştir. Standart katma metodu kullanılarak, orijinal ve sodyum klinoptilolitinin birim hücrede 72 oksijen atomuna dayalı idealleştirilmiş formülleri sırasıyla:

$(Na_{0.816}\ K_{2.070})\ (Ca_{1.060}\ Mg_{0.264})\ (Al_{5.653}\ Fe_{0.390})\ (Si_{30.084})\ O_{72}.\ 20.023\ H_2O$ ve

$(Na_{4.763}\ K_{1.057})\ (Ca_{0.076}\ Mg_{0.094})\ (Al_{5.843}\ Fe_{0.221})\ (Si_{29.911})\ O_{72}.\ 17.049\ H_2O$

olarak hesaplanmıştır. Klinoptilolitin orijinal ve katyon değiştirilmiş formlarının FTIR spektrumlarında, su moleküllerinin hidrojen bağları aracılığıyla iskeletle etkileşiminden dolayı oluşan bantta 3460'dan 3494.8 cm^{-1}'e varan kaymalar gözlenmiştir. Diğer bantların yerleri katyon değişiminden belirgin olarak etkilenmemiştir. TGA eğrilerinden, klinoptilolitin orijinal ve katyon değiştirilmiş formlarının su içeriklerinin % 14.31 ve % 11.00 arasında değiştiği belirlenmiştir. DTA eğrilerinde başlıca iki endoterm ve bir ekzoterm elde edilmiştir. İlk endoterm 150 ^oC'ye kadar oluşmuştur, ikinci endoterm 200 ile 700 ^oC arasında yer almaktadır, ekzoterm ise, 850 ^oC çevresinde elde edilmiştir. DSC eğrilerinin şekillerinde gözlenen belirgin farklar, örneklerin dehidrasyon davranışlarını katyonların kontrol ettiğini göstermektedir. Bütün örneklerin N_2 fiziksel adsorpsiyon izotermleri Tip IV olmakla birlikte, BET yüzey alanları 34.97 ile 46.76 m^2/g arasında değişmektedir.

Orijinal ve Na-klinoptilolit için 25 ^oC'de Ag, Zn ve Cu iyon değişim dengeleri incelenmiştir. İzotermlerin platolarından, orijinal klinoptilolitin katyon değiştirme kapasitesi, Ag^+, Zn^{2+}, ve Cu^{2+} için sırasıyla 1.184, 0.439, 0.539 meq/g olarak bulunmuştur. Katyon değişimlerinin büyük bir kısmı Na^+ ve Ca^{2+} tarafından gerçekleştirilmiştir. Dağılım katsayısı değerleri, nispeten düşük derişimlerde

klinoptilolitin Zn^{2+} ve Cu^{2+} seçimliliğinin belirginliğini göstermiştir. Daha yüksek derişimlerde ise, Zn^{2+} ve Cu^{2+} ile karşılaştırıldığında, Ag^{+} için daha yüksek dağılım katsayıları elde edilmiştir. Denge verilerine Langmuir ve Freundlich modelleri uygulanmıştır. Zn^{2+} ve Cu^{2+} değişimleri için, Langmuir modeli daha iyi korelasyon vermiştir, Ag^{+} değişiminde ise, Freundlich modeli deneysel verilere biraz daha iyi uyum sağlamıştır.

Ag^{+}-Na^{+}, Zn^{2+}-Na^{+} ve Cu^{2+}-Na^{+} çiftlerinin denge izotermleri incelenmiştir. Gümüş değişim izotermi bütün kompozisyon değerlerinde diyagonalin üzerinde yer almaktadır. Çinko ve bakır değişimlerinde ise; izotermler, zeolit fazına geçen iyonların çözelti fazındaki eşdeğer kesirlerinin (A_s) yaklaşık 0.2'ye kadar olan kısmında diyagonalin üzerindedir. Gümüş, bütün sodyum iyonlarıyla değişirken, çinko ve bakırda kısmi iyon değişimleri elde edilmiştir. Ag^{+}-Na^{+}, Zn^{2+}-Na^{+}, ve Cu^{2+}-Na^{+} çiftleri için iyon değişiminin standart serbest enerjileri sırasıyla –6.0, 2.03 ve 3.09 kj/equiv olarak bulunmuştur. Bu değerlerden seçimlilik sırası $Ag^{+} > Na^{+} > Zn^{2+} > Cu^{2+}$ olarak elde edilmiştir.

Sonuç olarak; antibakteriyel aktivite ön çalışmalarının sonuçları ile klinoptilolitin spesifik katyon değiştirme kapasitesi ve seçimlilik sırası göz önüne alındığında, Ag-klinoptilolit gelecek vadeden bir antibakteriyel malzeme olarak gözükmektedir. Bu çalışmanın sonuçlarının literatürle karşılaştırılması, klinoptilolitin katyon değişim davranışının orijinal katyonik kompozisyonuna bağlı olduğunu işaret etmektedir. Bu nedenle, herhangi bir pratik uygulamadan önce yataktan alınan temsili örnekler üzerine özel çalışmalar yapmak gerekmektedir.

TABLE OF CONTENTS

LIST OF FIGURES

LIST OF TABLES

Chapter 1

INTRODUCTION

Among metallic elements, heavy metals such as silver, zinc, copper, mercury, tin, lead, bismuth, cadmium, chromium, and thallium possess antibacterial properties (Niira et al. 1990). Silver is the mostly used antibacterial metal ion since it has the highest antibacterial activity among metals and it is less toxic (Kawahara et al. 2000, Hotta et al. 1998). In addition to silver, some divalent metal ions, zinc and copper ions, are often employed because these divalent ions have heat resistance, although the antibacterial action is somewhat less than that of a silver ion (Kubota et al. 1993).

Silver ion has been widely utilized as a disinfectant or a germicide in the form of a solution of silver nitrate. However, the use of silver nitrate solution is inconvenient for handling and can be used only for restricted purposes. Then, a polymeric substance holding the antibacterial metal particles that is prepared either by binding or adding fine wires or powder of the metals themselves, or by incorporating compounds of the metals to the polymer was proposed to reduce these disadvantages. Yet, in such methods, in which the metals themselves are used, the metals show poor compatibility because the specific weights and Young's moduli of the metals are usually very high compared with those of the conventional polymers. Additionally, such metals lead to a heavy weight of products and a high cost as they are necessarily used in a large amount. In the method wherein compounds of the metals are used, obtained product can be utilized restrictedly because of the heavy influence of the compounds on polymer properties. Also, it shows poor durability of the antibacterial performance since the metal ions are merely contained or attached to the polymer. Later, a polymer containing organic functional groups that have ion exchange function was suggested to retain the metal ions. However, in this method adverse effect of these functional groups on physical properties of the polymer should not be disregarded (Hagiwara et al. 1990).

Apart from these materials, there have been known inorganic antibiotics such as silver-supporting active carbon and organic antibacterial or antifungus agents like N-(fluorodichloromethylthio)-phthalimide. However, in the former, silver ions are rapidly leached out and, therefore, it is difficult to attain a sustained antibiotic effect. On the other hand, some of the organic antibacterial or antifungus agents have no

antibacterial effect depending on the kinds of bacteria or mold. Furthermore, even those having heat resistance, sometimes may decompose or evaporate at high processing temperatures thereby reducing the antibacterial effect.

To eliminate the disadvantages of these conventional materials, antibacterial zeolites prepared by replacing completely or partially exchangeable ions present in zeolite such as sodium, potassium, and calcium etc. with antibacterial metal ions were proposed. Antibacterial metal loaded zeolite was reported to exhibit a sustained antibacterial action in water and in the air and not to cause the change in the properties during processing. Although it gradually causes discoloration in the course of time, this discoloration exerts no influence on the antibacterial activity of the zeolite (Niira et al. 1990).

Antibacterial zeolite can be applied to a variety of fields. For example, it may be used as a filling material in polymers by imparting antibacterial action to the polymeric items. It can be utilized as anti-algal agent in water cleaner or cooling water systems. In the field of paints, it governs antibiotic, antifungus, and anti-algal properties to coated films. In the paper making process, it may be incorporated into various paper materials such as wet tissue paper, and packaging paper (Niira et al. 1990). Apart from these fields, silver-zeolite was suggested to be a useful vehicle to confer antibacterial activity on dental materials (Kawahara et al. 2000). Thus, antibacterial zeolite may be employed in any field in which the development and proliferation of microorganisms such as general bacteria, and algae must be suppressed (Niira et al. 1990).

There are several studies concerned with the use of synthetic and natural zeolites: A, X, Y, Z, and clinoptilolite supporting metal ions (Ag, Cu, Zn, Hg, Sn, Pb, Bi, Cd, Cr, Ti) as bactericides for water disinfection (Rivera-Garza et al. 2000). In the industry, the Japanese product Zeomic, which is known as silver treated synthetic Zeolite A, has been used as a sterilizing and antibacterial agent in paper, plastic, paint, ceramics, and almost everything else that people touch or come into contact with in their daily lives (Mumpton 1997). Based on these surveys, much less cost of clinoptilolite, most abundant natural zeolite, compared to the synthetic zeolites, gave the idea of the use of the clinoptilolite in this field. In the recent study (Rivera-Garza et al. 2000), Mexican silver clinoptilolite-heulandite mineral was reported to eliminate the pathogenic microorganisms *E. coli* and *S. faecalis* from water, thereby confirming this proposal.

However, variations in purity and composition, and some mineral impurities

present in the clinoptilolite may bring about some differences in cation exchange behavior of the clinoptilolite, as well as the other properties affected by the cation exchange. In the scope of this study, investigations of mostly proposed antibacterial metals: Ag, Zn, and Cu exchange properties of the untreated and Na-clinoptilolite, originated from Gördes, and their characterizations were aimed.

Chapter 2

ZEOLITES

2.1. Definition

Zeolite is the crystalline, hydrated aluminosilicate of alkaline or alkaline earth metals, especially, sodium, potassium, calcium, magnesium, strontium and barium. Structurally, zeolite is the "framework" aluminosilicate composed of infinitely extended three-dimensional network of AlO_4 and SiO_4 tetrahedra that form channels and interconnected voids, which are occupied by cations and water molecules. It may be expressed in two different formulas; oxide formula and idealized formula represented as follows:

- Oxide formula: $M_{2/n}O.Al_2O_3.xSiO_2.yH_2O$
- Idealized formula: $M_{x/n}[(AlO_2)_x(SiO_2)_y]\cdot wH_2O$

In the oxide formula, M represents the cation of valence n as in the idealized formula and x is generally equal to or greater than 2 since AlO_4 tetrahedra can join only to SiO_4 tetrahedra. The structural formula of a zeolite may be best expressed by the idealized formula for the crystallographic unit cell where w is the number of water molecules and the ratio y/x varies between 1 and 5 depending on the structure. The sum (x + y) represents the total number of tetrahedra, while the portion with [ ] defines the framework composition (Breck 1974, Tsitsishvili et al. 1992).

2.2. Structure

The primary building unit of the zeolite framework is the tetrahedron in which the center is occupied by a silicon or aluminum atom with four oxygen atoms at the corners as shown in Figure 2.1. Each oxygen atom is shared between two tetrahedra. Hence, the tetrahedra form a continuous framework. Substitution of Si^{4+} by Al^{3+} defines the negative charge of framework, which is compensated by monovalent or divalent cations located together with water molecules in the channels. Cations in the channels can be substituted easily and therefore, they are termed exchange or extra framework cations, while Si and Al, which are not exchanged under ordinary conditions, are called

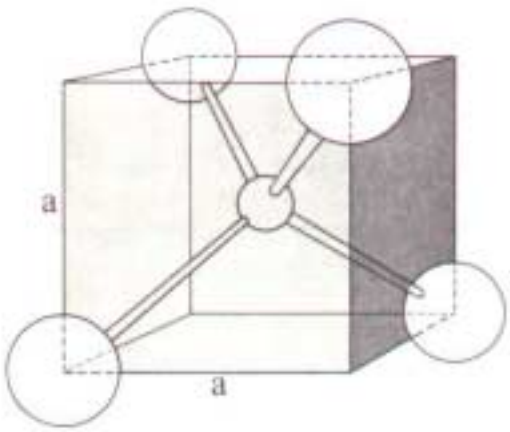

Figure 2.1. $(SiO_4)^{-4}$ or $(AlO_4)^{-5}$ Tetrahedron (Breck 1974).

tetrahedral (T) or framework cations (Tsitsishvili et al. 1992).

Framework topology that forms the basis of the classification of zeolites, can simply be given by the notion of the "secondary building unit" In the SBU, Si-Al distribution is neglected, only the positions of the tetrahedral (T) silicons or aluminums are shown. Oxygen atoms lie near the connecting solid lines, which are not intended to mean bonds. Those structural units: four, six, eight membered ordinary rings, double rings and complexes are represented in Figure 2.2 (Breck 1974, Tsitsishvili et al. 1992).

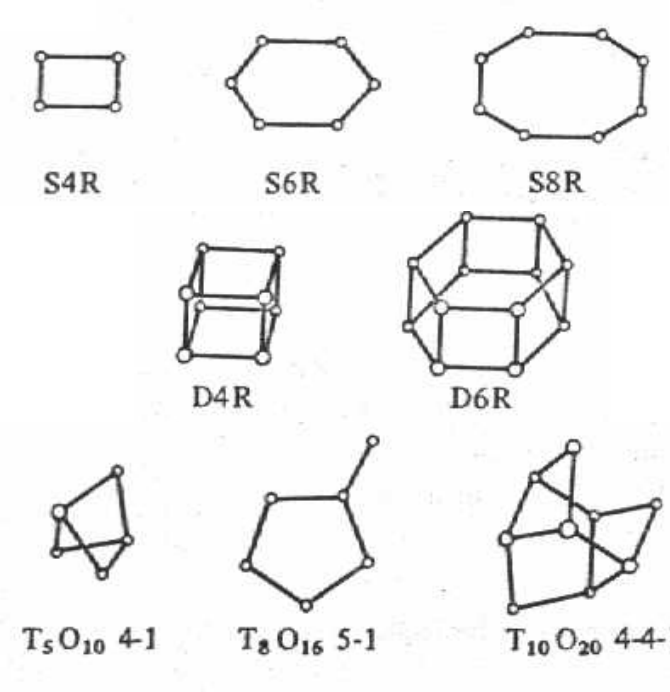

Figure 2.2. Secondary Building Units (SBU) in the Zeolite Structures (Breck 1974, Tsitsishvili et al. 1992).

Thus, zeolite structure can be summarized as aluminosilicate framework, exchangeable cations and zeolitic water. Aluminosilicate framework is the most stable component and defines the structure. Exchangeable cations surrounded with water molecules and oxygen atoms fill the channels and cavities in the zeolite framework and balance framework charge, while water molecules distribute the framework charge hence, act as a stabilizer (Tsitsishvili et al. 1992).

2.3. Characteristics

Zeolites have superior characteristics compared to the other crystalline inorganic oxide-materials. For example; they can separate molecules based on the size and configuration of the molecule relative to the size and geometry of the apertures of the zeolite structure, due to the uniform and microporous pore structure within their crystals. Thus, they act as "molecular sieves". They also adsorb molecules with permanent dipole moment with selectivity not found in other adsorbents (Breck 1974, Moscou 1991). Zeolites are accessible to perform all sorts of ion exchange reactions. They are suitable for catalyzing organic reactions because of their high thermal stability and internal acidity.

Since all metal-oxygen tetrahedra are exposed to the internal zeolite surface, they are in principle all accessible depending on pore dimensions. This makes zeolites appropriate for all sorts of modifications. These modifications are:

a) exchange of extra-framework cations
b) replacement of tetrahedral cations
c) introduction of metal particles.

As each aluminum atom introduces one negative charge to the framework and thus requires one positive counter ion, the zeolite can be thought as a real "stoichiometric inorganic polymer". This stoichiometry in combination with the complete accessibility for smaller molecules and the crystalline and homogeneous nature of the zeolites provide to develop and calibrate characterization techniques such as IR spectroscopy, NMR spectroscopy, NH_3-adsorption and –desorption etc.

Other features include ability to tailor acid site properties such as the average site density and the number of next nearest neighbors (NNN), diversification in composition and structures and their versatile potential for catalytic applications (Moscou 1991).

2.4. Uses

Zeolites may be either obtained from mineral deposits or synthesized. Over 150 species of synthetic zeolite have been synthesized and 7 kinds of mineral zeolites have been found in substantial quantity and purity. However, commercially only twelve basic types listed in Table 2.1 are utilized.

Table 2.1. Zeolite Types in Commercial Applications (Breck 1980).

Mineral Zeolites	**Synthetic Zeolites**
Mordenite	Zeolite A
Chabazite	Zeolite X
Erionite	Zeolite Y
Clinoptilolite	Zeolite omega
	Zeolon, Mordenite
	ZSM
	Zeolite F
	Zeolite W

The major factors that determine commercial use of zeolites are (1) structural chemistry, (2) availability, and (3) cost (Breck 1980).

Zeolites are primarily used as adsorbents, catalysts, and ion exchangers as summarized in Figure 2.3. Substantial amount of the zeolites is consumed as a detergent builder to remove Ca^{2+} and Mg^{2+} ions by ion exchange. Zeolite A is here a suitable substitute to phosphates, which cause environmental problems (Moscou 1991, Townsend 1991). Other ion exchange applications include removal of NH_4^+ and heavy metals from waste waters as well as Cs^+ and Sr^{2+} removal from nuclear effluents (Breck 1980).

Zeolites play an important role in the petroleum and refining industries because of their strong acidity and/or their size selectivity (Armor 1998). In terms of volume, most of the zeolite catalysts are used in oil refining where Zeolite Y is employed on a large scale in catalytic cracking (Maxwell and Stork 1991). Other applications are

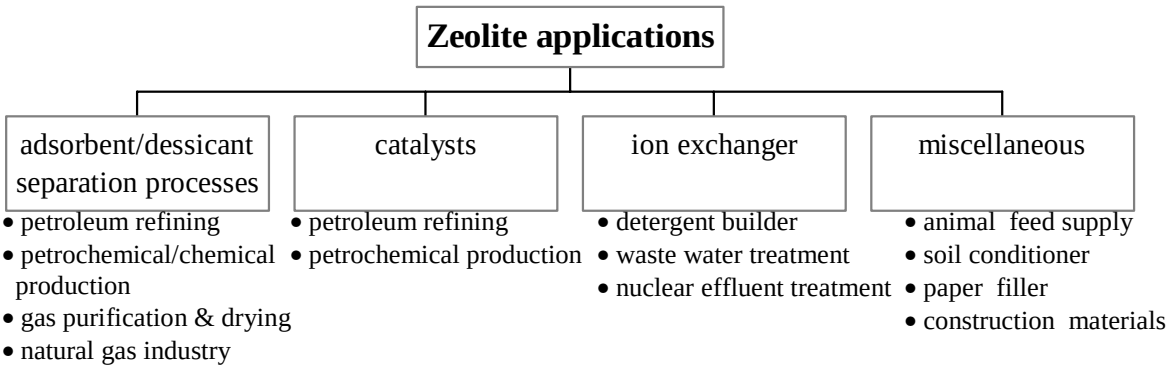

Figure 2.3. Application Fields of Zeolites.

hydrocracking (Zeolite Y, Mordenite), hydro-isomerization and dewaxing (Mordenite and ZSM-5) (Moscou 1991).

Molecular sieving properties combined with high selectivity to polar molecules provide a basis for zeolites as adsorbents. They are widely used in oil refining, chemical and petrochemical industries such as separation of n-paraffins from branched paraffins and p-xylene from its isomers etc., separation or drying of atmospheric gases and natural gas industry (Breck 1974, Moscou 1991). Apart from these application fields, natural zeolites are employed as animal feed supply and soil conditioner in agriculture, paper filler and additive to construction materials (Flenigen 1984, Moscou 1991).

Chapter 3

CHARACTERIZATION OF ZEOLITES

3.1 Introduction

Prior to a specific application, it is necessary to characterize the zeolite to see whether it has desired properties or not (van Booff and Roelofsen 1991). Although there are many characterization techniques, for this study four of them listed in Table 3.1 were considered.

Table 3.1. Characterization Methods with Corresponding Properties.

Characteristic	Method
Structure, Adsorbed species	IR Spectroscopy
Textural properties	Physical Adsorption Measurement
Thermal stability, Dehydration behavior	Thermal Analysis (TGA, DTA, DSC)
Chemical composition	ICP-AES

3.2. IR Spectroscopy

IR Spectroscopy is used for the structural characterization of zeolite, especially in situations where clear X-ray patterns can not be obtained (Lechert 1984). Hence this method of investigation is complementary to X-ray structural analysis (Breck 1974). The spectrum is frequently determined by the KBr pellet technique (Karge 1998). Interpretation of the spectrum is based on assignment of the infrared bands to certain structural groups in the various frameworks (Breck 1974).

In the infrared spectrum of zeolites, the lattice vibrations can be observed in the range of 300-1300 cm^{-1} (van Booff and Roelofsen 1991). These vibrations can be divided into two classes, (1) internal vibrations of the TO_4 tetrahedron which is the primary unit of the structure and which are not sensitive to other structural vibrations, and (2) vibrations which may be related to the linkages between tetrahedra. Class 2

Table 3.2. Zeolite IR Assignments (in cm^{-1}) (Breck 1974).

1. Internal tetrahedra	- Asym. stretch	1250-950
	- Sym. stretch	720-650
	- T-O bend	500-420
2. External linkages	- Double ring	650-500
	- Pore opening	420-500
	- Sym. stretch	750-820
	- Asym. stretch	1150-1050

vibrations are sensitive to the overall structure and the joining of the individual tetrahedra in secondary structural units, as well as their existence in the larger opening Positions of these are represented in Table 3.2.

The association of the water molecules with the cations and/or framework oxygen ions of zeolites can also be determined by IR. The three typical bands are; the broad band characteristic of hydrogen-bonded OH at about 3400 cm^{-1}, the sharp band typical of isolated OH at 3700 cm^{-1}, and the usual bending vibration of water at 1645 cm^{-1}. The isolated OH stretching is due to the interaction of the water hydroxyl with the cation while the other bands are attributed to the hydrogen bonding of the water molecule to the surface oxygen and to the bending mode of water (Breck 1974). It is also possible to characterize zeolite/adsorbate systems other than adsorption and desorption of water by IR. For example, adsorbed or occluded template molecules (or their decomposition products) are detectable by e.g. CH and/or NH vibration bands (Karge 1998).

3.3. Physical Adsorption Measurements

Physical adsorption (physisorption) is a phenomenon, which is resulted from the interactions between the solid (adsorbent) and the adsorbable gas (adsorptive) due to the intermolecular forces, attractive dispersion forces, short range repulsive forces and low degree of specific forces e.g. polarization, field-dipole, gradient-quadrupole

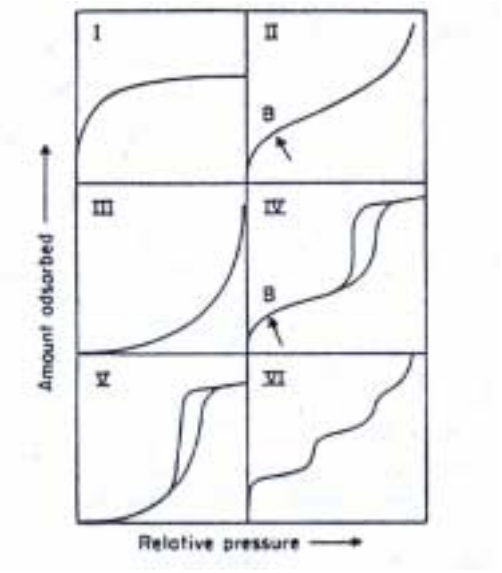

Figure 3.1. Types of Physisorption Isotherms (Sing et al. 1985).

(Sing 1988, Rouquerol et al. 1999). Physical adsorption measurements are widely used to obtain textural properties of materials such as surface area, pore volume and pore size distribution. IUPAC classification of pores with respect to their effective width is as follows:

(i) macropores have widths exceeding about 50 nm
(ii) mesopores have widths between 2 nm and 50 nm
(iii) micropores have widths not exceeding 2 nm.

Characterization is based on the models that use physisorption data, in other words interpretation of adsorption isotherms. Choice of adsorptive, experimental methods and outgassing of adsorbent are key points for the collection of adsorption data, hence construction of the isotherm. The first stage in the interpretation of the physisorption isotherm is to identify the isotherm type that is the nature of adsorption process(es): monolayer-multilayer adsorption, capillary condensation or micropore filling.

The physisorption isotherms may be grouped in six types as shown in Figure 3.1. Type I isotherm is given by a microporous solid (e.g. molecular sieve zeolite or activated carbon) having a relatively small external surface. In contrast, Type II isotherm represents unrestricted monolayer-multilayer adsorption on a non-porous or macroporous adsorbent. The characteristic features of the Type IV isotherm are its hysteresis loop and the limiting uptake at high p/p^o in mesopores. The remaining isotherms are less common: Type VI represents stepwise multilayer adsorption on a

uniform non-porous surface, whereas Types III and V are associated with weak adsorbent-adsorbate interactions (Sing et al. 1988).

3.3.1. Determination of the Surface Area

3.3.1.1. Langmuir Model

Langmuir model can be applied only to Type I isotherms. It was derived from the kinetic theory of gases and is based on the following assumptions:

- Adsorbent surface is pictured as an array of N^s equivalent and independent sites for localized adsorption (one molecule per site)
- Monolayer adsorption
- The probability of desorption of an adsorbed molecule from the surface is independent of the surface coverage (i.e. there are no lateral interactions between the adsorbed molecules)
- Energy of adsorption (E) is constant (Rouquerol et al. 1999).

Langmuir model can be expressed as:

$$\theta = \frac{n}{n_m} = \frac{bp}{1+bp} \qquad (3.1)$$

where b = adsorption coefficient,

n = moles adsorbed at p,

n_m = monolayer capacity.

At low p, $1 + bp \sim 1$, then $\theta = bp$ (Henry's Law) (3.2a)

and at high p, $1 + bp \sim bp$, then $\theta \to 1$. (3.2b)

In the linear form:

$$\frac{p}{n} = \frac{p}{n_m} + \frac{1}{n_m b} \qquad (3.3)$$

Plot of p/n vs. p gives slope = $1/n_m$ and intercept = $1/n_m b$ about in the $0.01 \le p/p^o \le 0.10$ range providing the best correlation coefficient.

Then, the surface area (A) can be calculated as:

$$A = n_m L a_m \qquad (3.4)$$

where L = Avogadro's number

a_m = surface area occupied by one molecule adsorptive (Sing et al. 1985).

3.3.1.2. Brunauer-Emmett-Teller (BET) Model

BET model is the extension of Langmuir kinetic theory to multilayer adsorption. Hence, it is applicable to Type II and Type IV isotherms. Following assumptions are involved:

- Multilayer has infinite thickness at $p/p^o = 1$ ($i = \infty$)
- Adsorbed molecules in one layer act as adsorption sites for molecules in the next layer at any pressure below p^o
- E_i values are independent of adsorbed molecules for each layer
- In the second and higher layers E_i has the same value as liquefaction energy E_L of the adsorptive i.e. $E_2 = E_3$ .....$= E_i = E_L$ (Rouquerol et al. 1999).

BET model can be described as:

$$\frac{n}{n_m} = \frac{Cx}{(1-x)(1-x+Cx)} \tag{3.5}$$

where $x = p/p^o$, $C \approx \exp(\frac{E_1 - E_L}{RT})$ and $E_1 - E_L$= net molar energy of adsorption.

In the linear form:

$$\frac{p}{n(p^o - p)} = \frac{1}{n_m C} + \frac{C-1}{n_m C}\frac{p}{p^o} \tag{3.6}$$

Approximately in the $0.05 \leq p/p^o \leq 0.30$ range, providing the best correlation coefficient, plot of $p/(n\,(p^o-p))$ vs. p/p^o represents a straight line with:

$s = \frac{C-1}{n_m C}$ and $i = \frac{1}{n_m C}$. Finally, surface area is determined by Eq. 3.4.

3.4. Thermal Analyses

Thermoanalytical methods are one of the important tools for the characterization of the zeolites. Thermal analysis is the temperature dependence measurement of the physical properties of a substance.

Thermogravimetric Analysis (TGA) and Differential Thermal Analysis (DTA) measuring the change of weight and the change of heat respectively are the most common techniques for the characterization of zeolite properties (Lechert 1984).

TGA measures weight loss of the sample as it is heated to elevated temperatures.

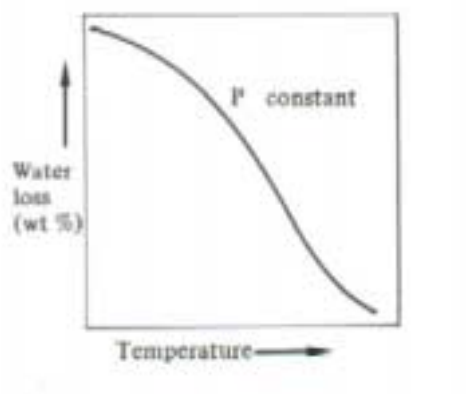

Figure 3.2. Typical TGA Curve of a Stable Zeolite (Breck 1974).

It gives information about the water content and types of water in the zeolite structure (Knowlton et al. 1981, Breck 1974). A typical TGA curve of a stable zeolite is represented in Figure 3.2.

DTA determines the temperatures at which thermal reactions take place in zeolite structure. The typical DTA curve of a zeolite is given in Figure 3.3. The low temperature endotherm indicates the evolution of water and/or possibly other volatile substances in the zeolite cavities, while the higher temperature exotherm represents conversion of the zeolite to another amorphous or crystalline phase (Lechert 1984, Breck 1974).

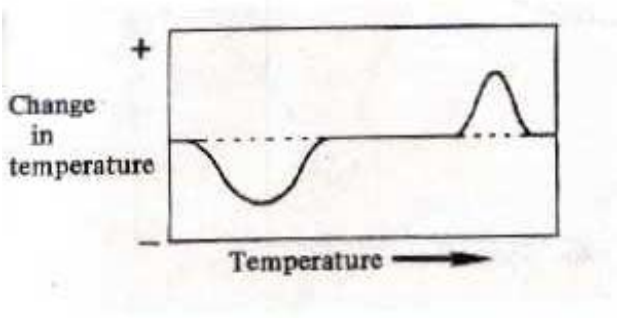

Figure 3.3. Typical DTA Curve of a Zeolite (Breck 1974).

3.5. Determination of the Chemical Composition

Inductively Coupled Plasma Atomic Emission Spectrometer (ICP-AES) is widely used in the determination of the chemical composition of the zeolites. The crucial step in the accurate analysis is to prepare sample properly. Fusion dissolution or acid digestion method may be applied.

In the fusion method, lithium tetraborate and/or lithium metaborate can be used to decompose the samples. Lithium metaborate is a better flux for highly siliceous samples, while lithium tetraborate is better for high iron containing ones. Subsequent to the fusion process, the bead formed is dissolved in 1.6 M nitric acid solution (Liberatore 1993).

In the acid digestion method, the sample is first heated in concentrated HNO_3 until a small volume of acid remains. Then, concentrated HF is added and heated to obtain a clear acid solution. The addition of HF ensures the loss of Si as SiF_6, thus reducing the dissolved solids of the final solution (Liberatore 1994). Then, it is dissolved in the appropriate acid solutions.

The solution formed is introduced to the spectrometer; resulting elemental concentrations are then translated to their oxide formulas to represent the final composition.

Chapter 4

ION EXCHANGE IN ZEOLITES

4.1. Ion Exchange Phenomenon

As its name implies, ion exchange describes a process by which ions are transferred from a solid phase to liquid phase and from liquid phase to solid phase simultaneously. Since ions undergo a phase change, ion exchange can be regarded as a sorption process (JMM Consulting Engineers 1985). However, in contrast to other sorption processes, ion exchange is necessarily stoichiometric. Each ion, which is removed from the solution is replaced by an equivalent amount of ion in the exchanger of the same sign by conserving electroneutrality (Helfferich 1962). Thus, ion exchange can be considered as a stoichiometric sorption process.

Ion exchange phenomenon can be simply explained by "sponge model". In this model, ion exchanger is thought as a sponge with counter ions (exchangeable ions) floating in the pores. When the sponge is immersed in a solution, counter ions can leave the pores and float out. However, to preserve electroneutrality another counter ion from the solution enters the sponge and takes its place in compensating of the framework charge. As described in this picture, ion exchange concept can be given by the "redistribution of ions" (Helfferich 1962).

4.2. Ion Exchange Reactions in Zeolites

Cation exchange ability is one of the important characteristics of zeolites. Ion exchange has been observed to take place under different conditions including in solution at normal pressures and temperatures up to 100 ^{o}C, at elevated temperatures and pressures in aqueous medium (above 400 ^{o}C tetrahedral cations also exchange), in the gas phase (farions), and in molten salts and the solid state (Tsitsishvili et al. 1992).

Cation exchange behavior of zeolites depend on: (1) the nature of the cation species, the cation size, both anhydrous and hydrated, and cation charge; (2) the temperature; (3) the concentration of the cation species in solution; (4) the anion species associated with the cation in solution; (5) the solvent (most exchange has been carried

out in aqueous solutions, although some work has been done in organic solvents); and (6) the structural characteristics of the particular zeolite (Breck 1974).

Main difference in the ion exchange behavior of zeolites and other exchangers (clay minerals and resins) is the microporous crystalline nature of zeolites. Since the microporous channels in the zeolite are comparable size to typical cation size, cations may be excluded from all or part of the internal surface of the zeolite on the basis of their size (Townsend 1991). Also, zeolites have unusual cation selectivity superior to the other exchangers. For example; clinoptilolite has high selectivity to NH_4^+ ions not found in the other exchangers. Because of their three-dimensional framework structure most zeolites do not undergo any structural changes with ion exchange (Breck 1974). Considerable resistances of the zeolites to radiation and thermal damage make them an obvious choice in the removal and storage of radionuclides. Zeolites find application as water softeners in detergents where the relative cheapness of Zeolite A makes it an attractive option in such a "throw- away" application (Townsend 1986). Present and potential ion exchange application fields of zeolites are summarized in Table 4.1.

Cation exchange in zeolites leads to alteration of stability, adsorption behavior, and selectivity, catalytic activity and other important physical properties. Since many of these properties depend on controlled cation exchange with particular cation species, detailed information on the cation exchange equilibria is important (Breck 1974).

4.3. Ion Exchange Equilibrium

When zeolite containing cation B is immersed in a solution including cation A, due to the concentration difference between A and B in zeolite and in solution phase, diffusion is established. Ion exchange process may be described by the following equation:

$$z_A\, B_{(z)}^{z_B^+} + z_B\, A_{(s)}^{z_A^+} \rightleftarrows z_A\, B_{(s)}^{z_B^+} + z_B\, A_{(z)}^{z_A^+} \qquad (4.1)$$

where z_A, z_B are the charges of the exchange cations A and B and the subscripts z and s refer to the zeolite and solution, respectively.

Reaction proceeds until equilibrium is reached (Breck 1974, Helfferich 1962). Equilibrium properties of a system have great importance because it is possible to obtain a measure of selectivity of the zeolite for one ion over either another or a group of other ions. Moreover, various thermodynamic parameters can be obtained

Table 4.1. Ion Exchange Applications of Zeolites (Breck 1980, Flenigen 1984).

Present Applications	**Advantage(s)**
Removal of Cs^+ and Sr^{2+} radioisotopes - Linde AW-500, mordenite, clinoptilolite	Stable to ionisation radiation Low solubility Dimensional stability High selectivity
Removal of NH_4^+ from waste water- Linde F, Linde W, clinoptilolite	NH_4^+ - selective over competing cations
Detergent builder Linde A, Linde X (ZB-100, ZB-300)	Remove Ca^{2+} and Mg^{2+} by selective exchange No environmental problem
Potential applications	**Advantage**
Radioactive waste storage	Same as Cs^+, Sr^{2+} removal
Aquaculture- AW-500, clinoptilolite	NH_4^+ - selective
Regeneration of artificial kidney dialysate solution	NH_4^+ - selective
Feeding NPN to ruminant animals	Reduces NH_4^+ by selective exchange to non-toxic levels
Metals removal and recovery	High selectivities for various metals
Ion exchange fertilizers	Exchange with plant nutrients such as NH_4^+ and K^+ with slow release in soil

from the experimental data using appropriate thermodynamic formulation and accurate activity coefficient data for the dissolved salts in the external solution (Townsend 1991).

To conduct these calculations, the first step is the construction of the isotherm, which characterizes equilibrium. Ion exchange isotherm is a graphical representation that covers the experimental conditions at a given temperature. Usually, it is plotted in terms of equivalent fractions of exchanging ion in solution and in zeolite phase by

keeping total solution normality constant. The equivalent fractions of the exchanging cation in solution, (A_s) and zeolite, (A_z) can be given by:

$$A_s = \frac{z_A m_s^A}{z_A m_s^A + z_B m_s^B} \tag{4.2}$$

$$A_z = \frac{\text{no. equivalents of exchanging cation A}}{\text{total equivalents of cations in the zeolite}} \tag{4.3}$$

where m_s^A and m_s^B are the concentrations of the respective ions in equilibrium solution, also $(A_z + B_z) = 1$ and $(A_s + B_s) = 1$.

Selectivity is the preference of the zeolite for one of two ions at a given equilibrium composition and the temperature. It is expressed by the separation factor, α_B^A, defined by:

$$\alpha_B^A = \frac{A_z B_s}{B_z A_s} \tag{4.4}$$

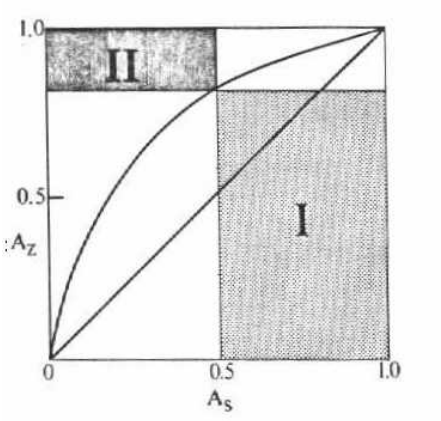

If ion A is preferred, α_B^A is greater than unity. It is possible to derive separation factor from the isotherm. Using the summation terms, separation factor is obtained as the ratio of area I to area II as given in Figure 4.1.

Figure 4.1. Derivation of the Separation Factor from the Isotherm (Breck 1974).

Cation selectivity of zeolites are influenced by the following factors: (1) framework topology; (2) ion size and shape; (3) charge density on the anionic framework; (4) ion valency; and (5) electrolyte concentration in the aqueous phase (Barrer 1978).

The ion exchange isotherms for exchange of cations in zeolites may be classified in five groups as given in Figure 4.2. In curve a, the zeolite exhibits a preference for the entering ion A ($\alpha_B^A > 1$) and the isotherm lies above the diagonal. In curve c, $\alpha_B^A < 1$, and the isotherm lies below the diagonal indicating that B is much preferred. In curve b, selectivity varies with the degree of exchange and resulted isotherm is sigmoidal in

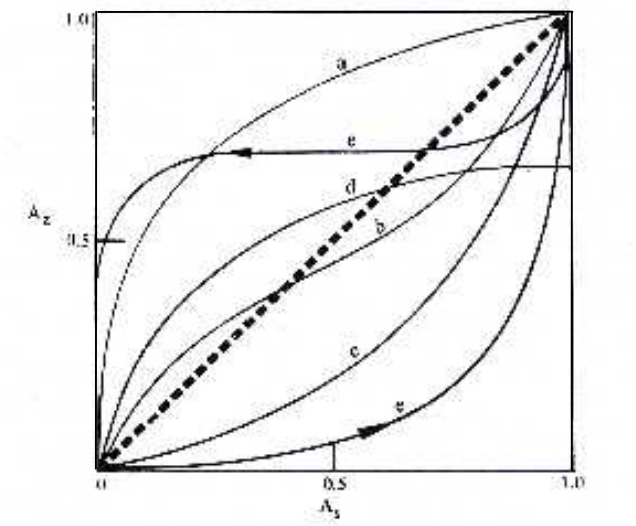

Figure 4.2. Types of Ion Exchange Isotherms (Breck 1974).

shape. Curve d represents that complete exchange is not achieved by the entering ion, due to the ion-sieving effect. Thus, $x_{max} < 1$. In curve e, unusual case is observed where exchange results in two zeolite phases and produces a hysteresis loop.

Various thermodynamic parameters may be obtained from the ion exchange isotherm. Mass action quotient or rational selectivity coefficient includes the charge of the ions, z_A and z_B and can be given as:

$$K_m = \frac{A_z^{z_B} B_s^{z_A}}{B_z^{z_A} A_s^{z_B}} \tag{4.5}$$

It is clear that for uni-univalent exchange mass action coefficient is identical to the separation factor.

The corrected selectivity coefficient contains a correction for the ions in equilibrium solution:

$$K_c = \frac{A_z^{z_B} B_s^{z_A}}{B_z^{z_A} A_s^{z_B}} \frac{\gamma_B^{z_A}}{\gamma_A^{z_B}} = K_m \Gamma \tag{4.6}$$

where γ_A and γ_B are mean ionic activity coefficients of the respective ions in solution, and Γ is the activity ratio. Calculation procedure for the determination of the activity ratios in solution is given in Appendix.

The thermodynamic equilibrium constant is defined by:

$$K_a = K_c \frac{f_A^{z_B}}{f_B^{z_A}} \tag{4.7}$$

where f_A and f_B are the activity coefficients of A and B in the zeolite and obtained from the Gaines and Thomas approach by ignoring salt imbibition and water activity terms as

follows:

$$\ln f_A^{z_B} = (z_B - z_A)B_z - \ln K_{c(A_z)} + A_z \ln K_{c(A_z)} + \int_{A_z}^{1} \ln K_c \, dA_z \tag{4.8}$$

$$\ln f_B^{z_A} = -(z_B - z_A)A_z + A_z \ln K_{c(A_z)} - \int_{0}^{A_z} \ln K_c \, dA_z \tag{4.9}$$

and thus,

$$\ln K_a = (z_B - z_A) + \int_{0}^{1} \ln K_c \, dA_z \tag{4.10}$$

K_a can be determined by either the graphical integration of the plot of ln K_c against A_z which is known as "Kielland plot", or analytically by integrating the polynomial which gives the best fit to the experimental data. If partial exchange is attained, it is necessary to normalize the isotherm. This involves dividing all values of A_z by the maximal value observed experimentally to give normalized A_z^N values as:

$$A_z^N = A_z / A_{z\,(max)} \tag{4.11}$$

Then, normalized parameters should be used. Thus, for example Eq. 4.8 becomes:

$$\ln f_A^{z_B} = (z_B - z_A)B_z^N - \ln K_{c(A_z)}^N + A_z^N \ln K_{c(A_z)}^N + \int_{A_z}^{1} \ln K_c^N \, dA_z^N \tag{4.12}$$

The superscript N refers to normalized values.

The standard free energy per equivalent exchange can then be found as (Breck 1974, Dyer et al. 1981):

$$\Delta G^{\theta} = \frac{-RT \ln K_a}{z_A z_B} \tag{4.13}$$

Chapter 5

GENERAL INFORMATION ON CLINOPTILOLITE

5.1. Definition and Characteristics

Clinoptilolite, a member of heulandite group of natural zeolites, is the most abundant zeolite found in nature (Gottardi and Galli 1985, Tsitsishvili et al. 1992). Its approximate chemical composition may be expressed as follows (Tsitsishvili et al. 1992):

- Oxide formula: $(K, Na, 1/2Ca)_2O.Al_2O_3.10SiO_2.8H_2O$
- Idealized formula: $(K_2, Na_2, Ca)_3[(Al_6\ Si_{30})O_{72}]24\ H_2O$

However, there may be remarkable changes in the composition of framework and exchangeable cations. K^+, Na^+, Ca^{2+}, and Mg^{2+} are the most common charge-balancing cations. Small but measurable amounts of Fe^{3+} may be found in clinoptilolite mineral. Although some of Fe^{3+} may be exchangeable, its major part is considered to be located in the framework tetrahedral sites (Ackley et al. 1992).

Clinoptilolite is isostructural with heulandite i.e. they both have the same XRD patterns. Yet, there exist some differences between them, as followings. Clinoptilolite has Si/Al>4, while heulandite, contains Si/Al<4. As a result of high Si/Al ratio, clinoptilolite is thermally stable to temperatures in excess of 500 ^oC, different from the heulandite which undergoes structural collapse at 350 ^oC, because the bonds between Si and O are much stronger than Al-O bonds (Zhao et al. 1998). On the other hand, lower aluminum content of the clinoptilolite brings about low cation density, 3 bivalent cations or 6 monovalent cations per unit cell at maximum (Tsitsishvili et al. 1992). Clinoptilolite can also be distinguished from heulandite on the basis of cation content, having alkali cations dominant [(Na + K) > Ca], whereas heulandite has Ca > (Na + K). Finally, clinoptilolite generally contains somewhat less water than heulandite (Smyth et al. 1990).

5.2. Structure

Cation exchange, catalytic, and adsorption properties, behavior of zeolitic water,

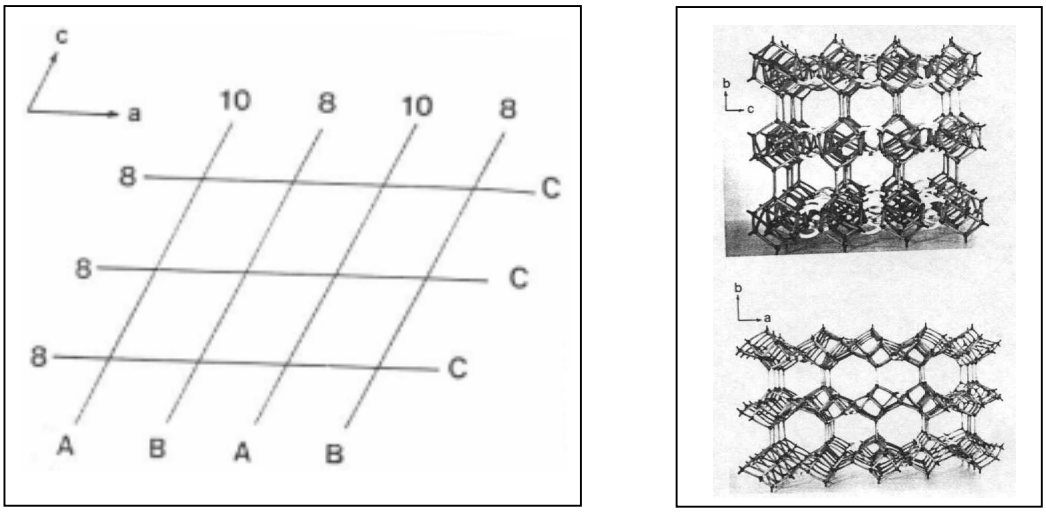

(a) (b)

Figure 5.1. a) Orientation of Clinoptilolite Channel Axis b) Model Framework for the Structure of Clinoptilolite (Ackley and Yang 1991a).

stability as well as various physical properties such as electrical conductivity are strongly based on the structure. Thus, in order to interpret and relate these properties, structural information is essential (Breck 1974).

Table 5.1 Channel Characteristics and Cation Sites in Clinoptilolite (Ackley and Yang, 1991a).

Channel	Tetrahedral ring size/channel axis	Cation Site	Major cations	Approx. Channel dim. (nm x nm)
A	10/c	M(1)	Na, Ca	0.72 x 0.44
B	8/c	M(2)	Ca,Na	0.47 x 0.41
C	8/a	M(3)	K	0.55 x 0.40
A	10/c	M(4)	Mg	0.72 x 0.44

Clinoptilolite has heulandite (HEU) topology, whose secondary building unit can be described by 4-4-1 type (Breck 1974). According to the literature, the structure of clinoptilolite consists of a two dimensional system of three types of channels, A (10-member ring) and B (8-member ring), perpendicularly intersected by channels C (8-member ring) as shown in Figure 5.1. Channel characteristics and cation sites of clinoptilolite are summarized in Table 5.1.

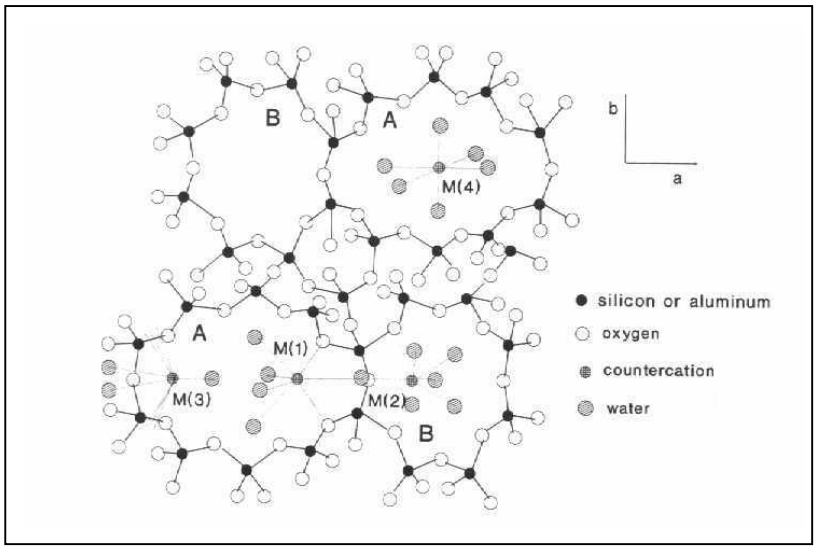

Figure 5.2. The c-Axis Projection of the Structure of Clinoptilolite (Arcoya et al. 1996).

A view of clinoptilolite structure, including the cation sites is represented in Figure 5.2. The main cation positions in this structure are: M(1), in channel A, is coordinated with two framework oxygen and five H_2O molecules. This site is occupied by Ca^{2+} and preferably by Na^{+}. M(2), located in channel B is coordinated by three framework oxygen atoms and five H_2O molecules. M(2) is occupied by Na^{+} and preferably Ca^{2+}. M(3), situated in channel C, is coordinated by six framework oxygen atoms and three H_2O molecules. It is occupied by K^{+} and probably, Ba^{2+}. Because this position is very close to M(1), a simultaneous occupancy of both sites is not possible.

M(4) is located in the center of channel A different from M(1). It is coordinated by six H_2O molecules forming an octahedral system. The occupancy of this site is low, and provided by Mg^{2+} (Arcoya et al. 1996).

5.3. Uses

Uses of natural clinoptilolite can be summarized as bulk mineral applications, adsorption processes and ion exchange separations. Catalytic applications are limited compared to the synthetic zeolites.

Relatively low cost, abundance, and in some cases unavailability of alternatives makes clinoptilolite effective in the bulk applications like paper filler, dietary supplement and soil conditioner. Processed clinoptilolite was reported to be sold as filler materials for groundwood and wood –free paper with the trade names "SGW" and

"HiZ" respectively in Japan (Torii 1978). Addition of 1 to 5 wt. % clinoptilolite to the diet of food animals was demonstrated to improve growth and feed utilization and to reduce diseases in pigs, cattle, sheep, and chickens (Pond 1995). Favorable effects of the use of clinoptilolite- rich tuff on farm animals have also been observed as previous studies (Bartko et al. 1995). Applications of clinoptilolite in agronomy and horticulture have been developing. Clinoptilolite has shown to slow nitrification by 11 %, reduce nitrate leaching by 30 %, increase ammonium and potassium retention, reduce ammonia volatilization, slowly release NH_4^+, K^+ and other plant nutrients and hence to improve fertilizer efficiency. It has also been being used as soil conditioner to improve soil physical properties and to remedy acidic or contaminated soils, due to the its rigid and porous structure, chemical stability in the range of common soil pHs, physical hardness, high cation exchange capacity, and ion selectivity. Thus, these improvements in soil physical and chemical properties may partly explain observed crop-yield increases (Allen and Ming 1995). It was also indicated that NH_4-clinoptilolite could enhance yields thereby supporting the use of NH_4-clinoptilolite in agriculture as effective soil amendments (Eberl et al. 1995).

It is known that dehydrated zeolites have excellent adsorption properties, and synthetic zeolites are widely used in drying and gas separation. Both mordenite-tuff and clinoptilolite-tuff found in Japan were reported to show excellent adsorptive properties compared with the commercial adsorbents, such as synthetic zeolites, silica gel, and activated alumina. Because of its high affinity for water, dehydrated clinoptilolite-tuff has been primarily used as a desiccant, e.g., in the packaging of caking-proof powders (Torii 1978). Other adsorption related applications of clinoptilolite and its ion-exchanged derivatives include natural gas purification and drying (removal of CO_2, H_2S, N_2, and H_2O), air separation (both O_2 and N_2 production), flue gas cleanup (SO_2 removal), and NH_3 removal in coal gasification (Ackley et al. 1992).

Ion exchange applications of clinoptilolite are mainly: treatment of municipal wastewaters- removal of ammonia, removal of cesium and strontium from radioactive wastewaters and heavy metal removal from industrial wastewaters (Kesraoui-Ouki et al. 1994). Uses of clinoptilolite in aquaculture to remove ammonia and in industry for ammonia-nitrogen removal in waste water systems as well as removal of ammonium ions from the wastewater of soap and detergent factory were reported (Torii 1978). Clinoptilolite-rich tuffs were reported to be utilized in Hungary, in two stages of the treatment of municipal wastewater: before the aeration tank and in the removal of

ammonium from treated effluent (Kallo 1995). Another application field of clinoptilolite is RIM-NUT (removal of nutrients) process. It is based on the ion exchange and precipitation processes, which permit selective removal of ammonium and/or phosphate ions from wastewater to recover $MgNH_4PO_4$, a high value fertilizer by-product, different from the classical NH_4^+-removal methods. The process has been technically and economically effective in several pilot plants as well as demonstrative plants in Italy and in the United States (Liberti et al. 1995). Clinoptilolite has been determined as leading candidate for use in municipal sewage treatment plants for ammonia removal and it was also reported to be suitable for separation and purification of cesium-137 from radioactive wastewater stored on the Hanford Reservation (Mercer and Ames 1978). Chelishchev (1995), reported the use of clinoptilolite at Chernobyl for the removal of low-level radioactive waste from contaminated waters and for the containment of radionuclides. The substitution of clinoptilolite for commercial cation-exchange resins has also been emphasized to increase the volume of purified water by 5-10 times. Clinoptilolite has been found to be effective in the treatment of low-level radioactive waste streams containing cesium, strontium, and cobalt from the nuclear processing plant at West Valley, New York (Grant et al. 1987). Zamzow and Murphy (1992), tested the effectiveness of clinoptilolite for the treatment of wastewater from an abandoned copper mine in Nevada. The metal ions Fe^{3+}, Cu^{2+}, and Zn^{2+} in copper mine wastewater were reported to be removed to below drinking water standards, while Mn^{2+} and Ni^{2+} could not be treated effectively. Clinoptilolite was investigated to treat acid mine drainage (AMD) from a closed copper mine in Nevada containing Al^{3+}, Ca^{2+}, Cu^{2+}, Fe^{3+}, Mn^{2+} and Zn^{2+} plus trace amounts of Cd^{2+}, Co^{2+}, and Ni^{2+}. It was reported that with sufficient contact time clinoptilolite could reduce the concentrations of cations in AMD to or less than drinking water standards (Zamzow and Schultze 1995).

Natural zeolites are generally not considered in catalyst production due to their chemical and mineral impurities. Thus, they can only be used for the reactions in which these contaminants do not effect catalytic transformations like hydration of acetylene to acetaldehyde. The Cd-clinoptilolite was reported to be the most active, selective, and stable catalyst over the Cd-exchanged forms of synthetic zeolites, A, X, Y, erionite, mordenite and ZSM-5 and natural chabazite, heulandite and stilbite under the hydration reaction conditions (Onyestyak and Kallo 1995).

Chapter 6

PREVIOUS STUDIES ON CLINOPTILOLITE

6.1. Pretreatment Studies

Conditioning procedure has been found to have considerable influence on the efficiency of the ion exchange process. In order to enhance the cation exchange properties of clinoptilolite, different pretreatment methods have been applied.

Murphy et al. (1976), compared various pretreatment methods in which, clinoptilolite samples exposed to the (1) acid, (2) alkali, (3) alkali followed by NaCl, (4) acid followed by NaOH and then NaCl, for ammonium removal. 20 % increase over untreated sample in the exchange capacity was attained by pretreatment (4), while the other treatments provided 5 % or less improvement. Klieve and Semmens (1980), studied the effects of pretreatment with NaOH, HNO_3, steam and heat (600 ^oC, 1 h) on the performance of ammonium removal as well as the total ammonium capacity. NaOH treated clinoptilolite was observed to have the highest capacity, whereas the heat-treated was the lowest. On the other hand, pretreatment of clinoptilolite with NaOH, HNO_3, and steam did little improvement in the zeolite's performance, while heat treatment improved zeolite's selectivity significantly. Semmens and Seyfard (1978), determined the exchange capacity of clinoptilolite by eluting its ammonium form with 1 N NaCl. Successive capacity tests on the same sample were resulted higher exchange capacity in agreement with Jorgensen (1976), who noted the increase in the capacity with the number of regenerations.

Semmens and Martin (1988), investigated the influence of pretreatment on the capacity and selectivity of clinoptilolite for metal ions. They found that, exposing clinoptilolite to the large volumes of concentrated sodium chloride solution, thereby displacing potassium and calcium ions from the zeolite matrix was resulted in an effective increase in the zeolite capacity and apparent selectivity for heavy metals such as copper and cadmium. In the study of Czaran et al. (1989), it was aimed to establish whether modifications of the original rocks led to a higher efficiency in silver exchange. For this reason, different cationic forms of clinoptilolite were prepared and then, silver exchange capacities were determined. As indicated in Table 6.1, maximum

Table 6.1. Ag^+ Exchange Capacities of Different Cationic Forms of Clinoptilolite (Czaran et al. 1989).

Cationic Form	**Ag^+ Exchange Capacity (mg/g)**
Original rock	74.0
Na-CLI	120.7
K-CLI	86.6
NH_4-CLI	84.3
Ca-CLI	75.0
Mg-CLI	59.3

exchange level was reached in Na-form of clinoptilolite.

Kesraoui-Ouki et al. (1993), studied the effects of treatment and conditioning on the removal of Pb^{2+}, and Cd^{2+} from effluent wastewaters. The results indicated that, converting clinoptilolite and chabazite to a nearly homoionic state in the Na-form by exposing to concentrated NaCl solution, improved their exchange capacity significantly. Conditioned and treated zeolites were observed to have improved exchange capacity and the removal efficiency, when operating at metal concentrations greater than

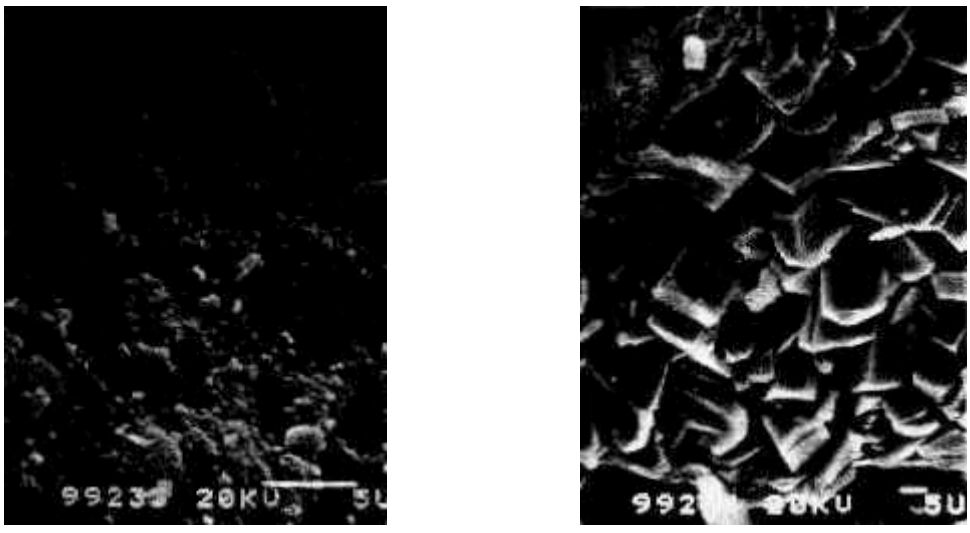

(a) (b)

Figure 6.1. SEM Photomicrographs of Natural Zeolite Clinoptilolite (Size < 150μm) (a) Virgin (As Received), (b) Conditioned with NaCl (Kesraoui-Ouki et al. 1993).

250 mg/L compared with as-received samples, in Pb^{2+}, and Cd^{2+} removal. It was interpreted that, conditioning enhanced the crystal structure and cleaned up the zeolite surface as shown in Figure 6.1 and this would probably improve exchange capacity.

6.2. Characterization Studies

6.2.1. IR Spectroscopy

Infrared spectrum has been found to be useful for the quantitative determination of clinoptilolite content of zeolitic tuffs. Goryainov et al. (1993), obtained several calibration curves for the 610 and 1212 cm^{-1} clinoptilolite IR bands. They observed that, the results of IR and XRD quantitative analyses correlated well, if there was no interference from absorption bands of admixed non-zeolitic minerals. The accuracy of the IR quantitative method was found to be about ± 5 %. Krivacsy and Hlasav (1995), developed a method for the quantitative determination of clinoptilolite in natural zeolites based on diffuse reflectance FTIR spectroscopy (DRIFTS). In this technique, using three calibration curves based on the intensities of the 1214, 1063, and 609 cm^{-1} absorption bands of clinoptilolite, a simple and time-saving analysis was provided compared with the powder XRD method and/or the conventional pellet preparation IR technique.

Rodriguez-Fuentes et al. (1998), investigated the thermal and cation influence on IR spectra of clinoptilolite in the range of 400 to 1700 cm^{-1}. The 450 cm^{-1} band assigned to T-O bending, 1205 cm^{-1} band of T-O internal stretching, and 1640 cm^{-1} band of OH bending were found to be most affected by the cation exchange and thermal history of the sample. In this study, a linear relation between the relative transmittances and Sanderson's electronegativities of various cationic forms of clinoptilolite was determined.

6.2.2. Physical Adsorption Measurements

Hernandez et al. (2000a), determined nitrogen and argon sorption properties of some natural zeolites from Mexico and their acid modified forms at 76 K. N_2 sorption isotherm of natural clinoptilolite was Type IV, while both N_2 and Ar isotherms of its modified form were obtained as Type IV with a significant Type I contribution.

Table 6.2. Sorption Properties of the Clinoptilolite from Mexico (Hernandez et al. 2000a).

Sample	Surface Area ($m^2 g^{-1}$)		Micropore Volume ($cm^3 g^{-1}$)		
	BET	t-plot	t-plot	DR corrected	DR original
CLIN[a]	13.60	15.47	0.0000	0.0000	0.0048
CLIM[b]	381.4	119.5	0.1236	0.1575	0.1614
CLIMAr[c]	230.2	95.45	0.0631	0.0673	0.0851

a = natural clinoptilolite, b = HCl modified clinoptilolite, c = Ar sorption on HCl modified clinoptilolite

Sorption results involved in this study are given in Table 6.2.

Hernandez et al. (2000b), studied the N_2 sorption behavior of a series of natural and modified (dealuminated) clinoptilolite at 76 K. Sing's α_s plots, de Boer's t-plots, Lee and Newnham's direct comparison plots, and Dubinin's classical methods were used to assess the microporosity of the samples. They introduced difference isotherm method to evaluate the accessible volume of micropores as follows:

- First, the N_2 uptake (at a given relative pressure) of the reference (i.e. natural) zeolite is multiplied by the ratio between the external surface area of test sample and the surface area of the reference
- The latter quantity is then subtracted from the corresponding uptake (i.e. at the same p/p^o) of the modified zeolite
- These differences are calculated along whole p/p^o range to obtain the difference isotherm from which pore analysis can be performed.

The surface area values calculated from BET model, Langmuir equation, and the t-plot as well as the other important parameters such as C of the BET equation and the total pore volume V_Σ calculated according to Gurvitsch rule (applied at $p/p^o = 0.95$) for Etla clinoptilolite and its modified forms are shown in Table 6.3 and micropore volumes, W_o ($cm^3 g^{-1}$) of the same samples calculated by different methods (A: α_s plot, B: t-plot, C: direct comparison method, D: difference isotherm method, and DA: Dubinin-Astakhov plot with n=3) are represented in Table 6.4.

6.2.3. Thermal Analyses

Knowlton et al. (1981), used TGA, and DSC techniques to study the types of water associated with clinoptilolite. They classified water in clinoptilolite as externally

Table 6.3. Textural Parameters of Etla Clinoptilolite and its Acid Treated Forms (Hernandez et al. 2000b).

Sample	surface area (m^2 g^{-1})			C	p/p^o BET plot	V_Σ (cm^3 g^{-1})
	BET	Langmuir	t-plot			
N[a]	10.70	14.87	10.70	55	0.10-0.31	0.028
H[b](1)[c]	11.81	10.88	11.81	77	0.10-0.31	0.028
H(2)	20.56	27.25	15.29	-115	0.10-0.31	0.036
H(3)	44.10	63.95	31.95	-106	0.10-0.31	0.057
H(4)	89.94	134.80	33.25	-39	0.10-0.31	0.079
H(5)	109.6	158.7	51.97	-91	0.10-0.31	0.106

a = natural sample, b = H represents HCl modified sample c = the number in parenthesis designates the quantity of acid leaching process

Table 6.4. Micropore Volumes of Modified Forms of Etla Clinoptilolite with Different Methods (Hernandez et al. 2000b).

Sample	A	B	C	D	DA	Average
H(2)	0.005	0.003	0.005	0.005	0.012	0.006
H(3)	0.017	0.023	0.017	0.017	0.026	0.020
H(4)	0.041	0.032	0.042	0.041	0.063	0.044
H(5)	0.054	0.031	0.055	0.054	0.066	0.052

adsorbed water, loosely bound zeolitic water and tightly bound zeolitic water. In this study, it was found that inflection points on thermogravimetric curves at approximately 80 ^oC and 170 ^oC corresponded to changes in the proportions of externally adsorbed water to loosely bound water and loosely bound water to tightly bound water, respectively. The temperatures and heats of dehydration obtained from differential scanning calorimetry agreed these three types of water. These temperatures and heats of dehydration were given as 75 ± 10 ^oC and 59.2 ± 5.9 kJ/mole H_2O, 171 ± 2 ^oC and 58.7 ± 6.1 kJ/mole H_2O, 271 ± 4 ^oC and 78.7 ± 7.0 kJ/mole H_2O for external water, loosely bound water and tightly bound water respectively. Bish (1988), examined the

dehydration behavior of Na, K, Li, Cs, Mg, Sr, and Ba exchanged clinoptilolites. The amount of water lost below 800 ^{o}C was obtained to vary from 7.8 % for Cs-clinoptilolite to about 15.5 % for Mg-, Li-, and Sr-clinoptilolites. In this study, all of zeolites studied, dehydrated in a stepwise manner, as an evidence for water held with different bond strengths in every sample. It was concluded that, the amounts of water associated with these zeolites depended strongly on the exchangeable cations. Stepwise water lost was also indicated for parent and modified clinoptilolites (K- and H/NH_4^+ forms) in the study of Kasture et al. (1998).

Akdeniz (1999), investigated TGA and DTA curves of clinoptilolite samples from different regions of Western Anatolia. Weight losses of the samples are tabulated in Table 6.5. In the DTA curves two endotherms at around 60 ^{o}C and 550 ^{o}C and one exotherm at about 830 – 840 ^{o}C were observed for Gördes and Bigadiç clinoptilolites.

Esenli and Kumbasar (1994), studied the dehydration behavior of Western Anatolian clinoptilolites related to their chemical compositions. They indicated that, thermal stabilities of clinoptilolites decrease with increasing divalent cation content. They also observed that, divalent cation rich clinoptilolites showed an endotherm at 230 ^{o}C, while clinoptilolites rich in univalent cations (mainly K) did not have this reaction on their DTA curves.

Table 6.5. Percentage Weight Losses of Western Anatolian Clinoptilolites (Akdeniz 1999).

Sample	**< 85 ^{o}C external water**	**85 – 285 ^{o}C loosely b. water**	**285 – 500 ^{o}C tightly b. water**	**> 500 ^{o}C**	**total**
Gördes 1	3.66	5.17	2.27	1.09	12.19
Gördes 2	4.27	6.07	1.72	1.50	13.50
Bigadiç	3.28	6.07	2.68	1.46	13.51

6.2.4. Chemical Composition

Ackley and Yang (1991b), modified fusion dissolution method for clinoptilolite. The procedure proposed is as follows:

- A 100-mg sample of zeolite is combined with 0.6 g of a 1:2 lithium

Table 6.6. Results of ICP Analyses of Natural and Modified Clinoptilolites by Different Authors (Ackley and Yang 1991b, Pabalan 1994).

Component (w/w %)	Ackley and Yang (1991b)			Pabalan (1994)		
	Untreated	Purified	Na-form	Untreated	Purified	Na-form
SiO_2	62.74	68.48	61.74	67.26 ± 0.36	69.13 ± 0.34	68.28 ± 0.57
Al_2O_3	10.15	11.40	9.97	11.10 ± 0.12	11.38 ± 0.06	11.28 ± 0.09
TiO_2	0.15	0.11	0.26	0.10 ± 0.00	0.06 ± 0.03	0.04 ± 0.03
Fe_2O_3	0.95	0.87	0.55	0.84 ± 0.01	0.47 ± 0.01	0.40 ± 0.02
MgO	0.62	0.75	0.11	0.36 ± 0.01	0.27 ± 0.02	0.16 ± 0.03
CaO	1.22	1.56	0.03	0.73 ± 0.04	0.09 ± 0.02	0.02 ± 0.01
Na_2O	3.37	3.48	6.38	3.47 ± 0.08	4.83 ± 0.02	6.36 ± 0.04
K_2O	2.26	2.03	0.53	3.51 ± 0.06	2.77 ± 0.05	0.66 ± 0.05
MnO	0.02	0.01	0.01	n. d.	n. d.	n. d.
P_2O_5	0.06	0.0	0.05	n. d.	n. d.	n. d.
H_2O	18.5	11.3	20.4	n. d.	n. d.	15.21 ± 0.18

n. d. = not determined

metaborate/lithium tetraborate fluxing mixture

- The dry powder mixture is then placed in an oven at 1000 ^oC for approximately 1h
- After cooling, the fused glass bead is dissolved in a hot aqueous solution (250-ml) containing 10 ml of 1:1 HNO_3
- The solution is then presented to the nebulizer in the ICP instrument at a flowrate of 0.86 ml/min, whereupon it is introduced to the plasma by argon carrier
- The resultant elemental compositions are then translated to their oxide forms
- Finally, moisture content is determined by difference.

Pabalan (1994), used ICP-AES to analyze untreated, purified, and sodium forms of the clinoptilolite. In this study, the samples were dissolved in HCl/HNO_3 matrix subsequent to lithium metaborate fusion. The water content of Na-clinoptilolite samples were determined by weighing three samples in self-sealing quartz crucibles before and after heating at 900 ^oC for two hours. The results of two studies are represented in Table 6.6.

6.3. Ion Exchange Studies

Each zeolite provides a different pattern of ion exchange selectivity. The selectivity series of increasing preference for clinoptilolite reported by different authors are represented in Table 6.7 (Sherman 1978).

Table 6.7. Ion Exchange Selectivity Patterns of Clinoptilolite (Sherman 1978).

Selectivity Series	Author(s)
$nC_4H_9NH_3 < nC_3H_7NH_3 < NH_4 < C_2H_9NH_3$	Barrer, Papadopoulos, and Rees
Li<Na<Rb<K<Cs	Sherry
Li<Ca<Sr<Ba<Na<K<Rb	Filizova
Na<K<Cs	Ames
Na<NH_4<Cs	Howery and Thomas
Cu<Zn<Cd<Pb<Ba	Semmens and Seyforth
Zn<Cu<Cd<Pb	Fujimori and Moriya
Mg<Ca<Na<NH_4<K	Sherman and Ross
Li<Na< NH_4<K<Rb<Cs Mg<Ca<Sr<Ba	Ames
Na<Ag<Pb At low loadings: Na<Cu≈Zn<Cd<Ag<Pb	Chelishchev et al.

Langella et al. (2000), obtained the isotherms of NH_4^+, Cu^{2+}, Zn^{2+}, Cd^{2+}, and Pb^{2+} exchange for Na^+ at 25 ^oC and 0.1 total normality. Exchange isotherms describing $Cu^{2+}$and Na^+, Zn^{2+} and Na^+ equilibria are given in Figure 6.2. As it can be seen from the isotherms, combination of c and d type isotherms i.e. nonselective behavior with partial exchange were observed. Maximal exchange levels (x_{max}) were obtained as less than unity for all cases as summarized in Table 6.8 with the thermodynamic parameters computed. From these data the selectivity sequence was derived as: $NH_4^+ > Pb^{2+} > Na^+ > Cd^{2+} > Cu^{2+} \cong Zn^{2+}$.

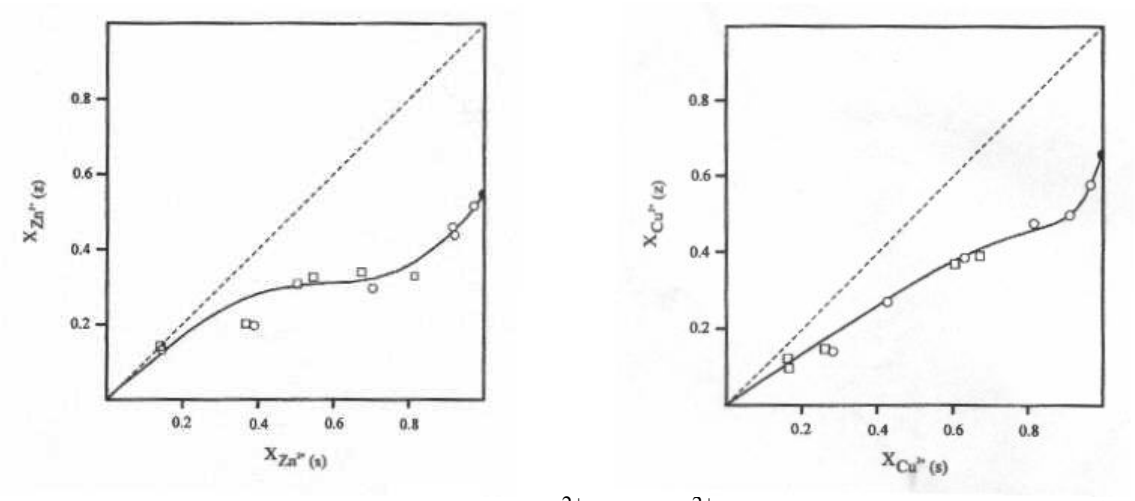

Figure 6.2. Isotherms for Exchanges of Zn^{2+} and Cu^{2+} into Na-Clinoptilolite at 25 ^{o}C (Langella et al. 2000).

Table 6.8. Maximum Exchange Levels and Thermodynamic Parameters for Na-Clinoptilolite at 25 ^{o}C (Langella et al. 2000).

Cation pair	$\mathbf{x_{max}}$	$\mathbf{K_a}$	$\mathbf{\Delta G^{\theta}}$ **(kJ/equiv)**
NH_4^+ - Na^+	0.901	10.21	-5.72
Cu^{2+} - Na^+	0.663	0.11	2.71
Zn^{2+} - Na^+	0.538	0.10	2.83
Cd^{2+} - Na^+	0.373	0.61	0.61
Pb^{2+} - Na^+	0.745	4.40	-1.82

Chapter 7

EXPERIMENTAL

7.1 Materials

In this study, Gördes clinoptilolite mineral, supplied from Enli Madencilik Company was used. In the preliminary experiments, clinoptilolite particles with 1.7-3.5 mm dimensions were utilized for the determination of antibacterial activities of modified clinoptilolites. Powder form was prepared by crushing clinoptilolite bearing rocks and then grinding them into two different mesh sizes: 38-75 μm (400-200 mesh) and below 38μm (-400 mesh). All ion exchange equilibrium and characterization studies were carried out using the former portion. In the first group of the ion exchange equilibrium experiments, $AgNO_3$, $Zn(NO_3)_2.5H_2O$ and $CuSO_4.5H_2O$ were used as metal sources. NaCl was used to prepare near homoionic Na-form of clinoptilolite prior to binary exchange equilibrium studies, in which nitrate salt of each cation was utilized. In the determination of the chemical composition of the clinoptilolite samples, three different Japanese Reference Rock Standards (JRRS), JSd-1, JSd-3, and JR-3 were used. The standards were supplied by Geological Survey of Japan, which certified the chemical compositions of them as well. All other concentration measurements were carried out using ICP standards.

7.2. Methods

Experimental work can be summarized in three groups:

- Preliminary preparation and testing of antibacterial metal loaded clinoptilolite
- Ion exchange equilibrium studies
- Characterization.

7.2.1. Preparation and Testing of Antibacterial Metal Loaded Clinoptilolite

Clinoptilolite particles were heated in deionized water up to 90 ^{o}C to remove water-soluble impurities. Washed samples were dried in oven at 110 ^{o}C. Then, they

were treated with 0.05 M of antibacterial metal salt solution in the shaker maintained at 35 ^{o}C, for two days. The solid to solution ratio was provided as 1 g: 20 ml. Cation exchanged forms of clinoptilolite were washed with deionized water to remove nitrates. Exchange process was repeated one more time for increasing the amount of antibacterial metal loaded to clinoptilolite.

Antibacterial actions of the untreated, silver and zinc forms of clinoptilolite against *Enterobacter spp*., *S. aureus*, *Pseudomonas aeruginosa*, *Streptococcus pyogenes*, *Proteus spp*., and *E. coli* were determined by the disk-diffusion (Kirby-Bauer) method. Firstly, bacterial cultures were grown on Mueller-Hinton agar or blood agar medium depending on the type of strain at 37 ^{o}C for overnight. One colony was picked up and dissolved in 1ml of distilled water. Then, the turbidity was adjusted to McFarland no:1 (10^{9} CFU). After placing a sterile cotton swab in the bacterial suspension, the swab is streaked in at two directions over the surface of the Mueller-Hinton agar to obtain uniform growth. 0.05 g of clinoptilolite powder with commercial antibiotics (10 μg of Meropenem or 30 μg of Vancomycin) for positive control, were incorporated to the plate. The plates were incubated at 37 ^{o}C over 5 % CO_2 medium. Finally, radius of inhibition zone of each sample in the plate was measured at the end of the first day.

7.2.2. Ion Exchange Equilibrium Studies

Ion exchange equilibrium studies were investigated in two groups: a) Ag^{+}, Zn^{2+}, and Cu^{2+} exchanges of the untreated clinoptilolite, b) Ag^{+}-Na^{+}, Zn^{2+}-Na^{+}, Cu^{2+}-Na^{+} binary exchange equilibrium studies. All ion exchange reactions were carried out in polyethylene bottles placed in a shaker at 25 ^{o}C for 2 days. Solid and solution phases were separated with a centrifuge at 4000 rpm. Concentrations of exchanging metal along with sodium potassium, calcium, and magnesium in the initial and final solutions were determined using Varian ICP 96 model Inductively Coupled Plasma Atomic Emission Spectrometer (ICP-AES) after making appropriate dilutions. Cation exchanged forms of the clinoptilolite were washed with deionized water, and then equilibrated with water vapor over saturated NH_4Cl solution to ensure constant water content prior to characterization.

In the first part of experiments initial metal concentration was varied between 5×10^{-4} N and 0.1 N and the solid to solution ratio was adjusted between 1:100

and 1:200.

In the latter case, near homoionic Na-clinoptilolite was prepared by stirring 125 g of sample with 1250 ml of 1 N NaCl at 500 rpm in a 2000 ml closed beaker placed in a constant temperature water bath maintained at 60 ^{o}C for a week. NaCl solution was replaced every day. Then, treated clinoptilolite was washed with deionized water several times and dried in oven at 110 ^{o}C. Later, it was placed over saturated NH_4Cl solution prior to the ion exchange experiments and characterizations. Binary ion exchange experiments were conducted by equilibrating weighed amounts of Na-clinoptilolite with a series of solutions containing the two competing cations, at different concentration ratios, but at a constant normality equal to 0.1 N. The masses of clinoptilolite were varied between 0.1 and 1g, while the solution volumes were changed from 5 to 25 ml. Zeolite mass to solution ratio were adjusted both to obtain significant differences in the initial and final concentrations of the cations in the solutions and an evenly-spaced distribution of points along the ion exchange isotherm.

7.2.3. Characterization

Original and Na, Ag, Zn, and Cu exchanged forms of the clinoptilolite were characterized using ICP-AES, FTIR, thermal analyses (TGA, DTA, DSC), and physisorption techniques. Ag, Zn, and Cu exchanged forms of the clinoptilolite were obtained in the first group of the equilibrium studies with 0.1 N initial concentration of appropriate salt of metal. Near homoionic form of Na-clinoptilolite, prepared prior to binary exchange experiments, was used in the characterization studies.

It is necessary to digest the samples before being introduced to ICP-AES. In this study, fusion dissolution method summarized as follows was used:

- Approximately 0.2 g of sample was mixed with 2 g of lithium tetraborate
- Mixture was fused in furnace at 1000 ^{o}C for 45 minutes and allowed to cool
- Formed glass bead was dissolved in 1.6 M HNO_3 solution on a magnetic stirrer
- Solution was completed to 250 ml by ensuring 5 v/v % of 65 % HNO_3 and diluted if necessary
- Blank was obtained by fusing only 2 g of lithium tetraborate and following the same procedure.

In the measurement section, two analytical procedures: the direct calibration

and the standard addition method were applied. In both techniques, calibration curves were constructed by the instrument. Sample calibration curves of the direct calibration method and the standard addition method are given in Figure A.13 and Figure A.14 respectively. For the direct calibration technique, Japanese Reference Rock Standards, which were prepared according to the sample preparation method described above, were used as the standards and concentration of any species in the sample was obtained directly from the calibration curve, plotted intensity vs. concentration specified. Standard addition method involved adding several increments of a standard solution (ICP standards) to the sample solution. Measurements were made on the original sample and on the sample plus the standard after each addition.

IR characterizations were carried out between 400 and 4000 cm^{-1} with Shimadzu FTIR-8201 model Fourier Transformed Infra-red Spectrometer using KBr pellet technique. KBr pellets were prepared by pressing 4 mg sample and 200 mg KBr.

TGA, DTA and DSC analyses were conducted using Shimadzu TGA-51/51H, Shimadzu DTA50, and Shimadzu DSC50 types of instruments respectively. Approximately 10 mg sample was heated at 10 ^{o}C/min under 40 ml/min nitrogen purge stream up to 1000 ^{o}C in the TGA and DTA studies. DSC runs were carried out up to 500 ^{o}C at the same heating rate and nitrogen flowrate with 3-4 mg of sample.

Nitrogen physisorption studies were performed at 77.45 K using Micromeritics ASAP 2010 model static volumetric adsorption instrument. The samples were dried in oven at 200 ^{o}C for 3 hours prior to degassing and degas conditions were adjusted as 350 ^{o}C and 24 hours.

Chapter 8

RESULTS AND DISCUSSION

8.1. Preliminary Antibacterial Activity Tests

Antibacterial activities of untreated, Ag, and Zn forms of clinoptilolite were determined using disk diffusion method. Commercial antibiotics (Meropenem or Vancomycin) were used for positive control. Antibacterial action was not observed for untreated clinoptilolite.

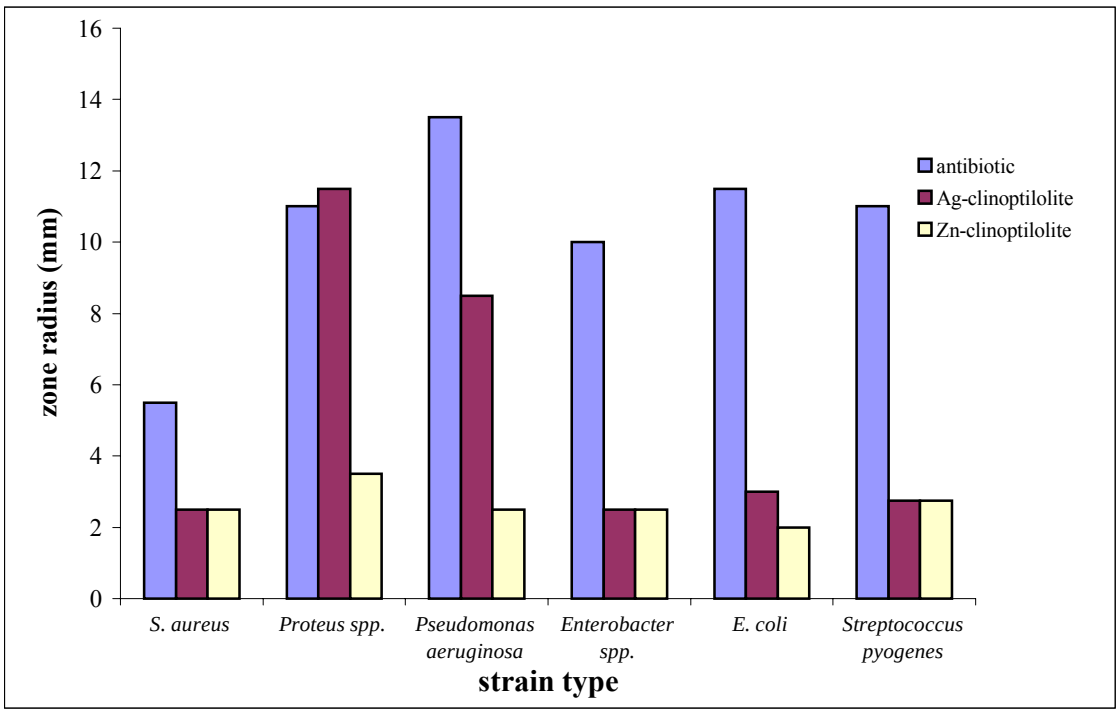

Figure 8.1. Zone Radii of Test Samples against Different Strains.

Zone radii of Ag and Zn forms of clinoptilolite and the commercial antibiotics, measured at the end of the first day, are given in Figure 8.1. Although Zn form of clinoptilolite possesses antibiotic action, it is not significant compared to commercial antibiotics in all cases. However, antibacterial activity of Ag-clinoptilolite against *Proteus spp*. and *Pseudomonas aeruginosa* is competitive to commercial antibiotics. For the other strains, Ag-clinoptilolite showed the same behavior as Zn-form.

8.2. Characterization Studies

8.2.1. Determination of the Chemical Composition by ICP-AES

Chemical compositions of the original and the cation-exchanged forms of the clinoptilolite were determined by following the steps given below:

- Comparison of the results of the direct calibration method and the standard addition method applied to the analyses of Japanese Reference Rock Standards (JRRS)
- Comparison of the results of the different standards used in the standard addition method
- Consistency analysis of Japanese Reference Rock Standards
- Determination of the chemical compositions of the original and Na-clinoptilolite by the direct calibration (using Japanese Reference Rocks as standards) and the standard addition method and then evaluation of these results considering different aspects
- Determination of the chemical compositions of the other cationic forms of clinoptilolite using mass balances.

Table 8.1. Analyses of Japanese Reference Rock Standards with the Direct Calibration Method.

sample / ***species***	**JSd-1**		**JSd-3**		**JR-3**	
	measured (w/w %)	**certified (w/w %)**	**measured (w/w %)**	**certified (w/w %)**	**measured (w/w %)**	**certified (w/w %)**
SiO_2	64.2	66.55	77.3	76	77.69	72.76
Al_2O_3	15.72	14.65	10.378	9.908	12.59	11.9
Fe_2O_3	6.098	5.059	4.963	4.368	5.608	4.72
K_2O	3.585	2.183	3.277	1.917	6.731	4.29
Na_2O	4.504	2.727	2.190	0.411	7.230	4.69
CaO	3.874	3.034	0.607	0.56	0.058	0.093
MgO	2.072	1.813	1.288	1.17	0.049	0.05

In Table 8.1, analysis results of Japanese Reference Rock Standards obtained by using the direct calibration method are presented and these results are compared with the certified values. There appeared no significant difference between the measured

and the certified values of SiO_2, Al_2O_3, CaO, and MgO, while there existed considerable differences in Fe_2O_3, K_2O, and Na_2O. This is attributed to the "matrix effect", which was reported as the major problem in the analyses of rocks and arose as a possible result of the change of ionization in plasma, and various interferences due to the polyatomic or doubly charged ions (Imai 1990). In the literature, following methods were proposed for the correction of the matrix effect (Ujiie and Imai 1995): (1) internal standardization, (2) standard addition, (3) addition of the major elements to the calibration standard (matrix matching), (4) use of a geological standard rock as a calibration standard, (5) separation of major elements by ion-exchange and extraction method.

In this study, method (2) and method (4) were applied for the elimination of the matrix effect. Comparisons of the results of the direct calibration method with those of the standard addition method for each reference rock standard are given in Table 8.2 to Table 8.4. Since the major portion of the matrix is formed by SiO_2, it was measured only by the direct calibration method, even though it was listed in the standard addition column. Consistencies of the values obtained by both the direct calibration and the standard addition method indicated that Al_2O_3, CaO, and MgO were not affected by the matrix significantly. On the other hand, higher values of Fe_2O_3, K_2O, and Na_2O obtained from direct calibration emphasized that the signals of these species were increased by the matrix. Standard addition method seemed to be successful for the suppression of matrix effect in the case of Fe_2O_3, and K_2O. However, even though it gave considerably better results than the direct calibration method, percentages of Na_2O determined by the standard addition method still deviated from the certified values. For checking whether the standards used affected the results, the sample JR-3 was measured by the standard addition method, but using different standards prepared according to the following procedures:

- A1 was measured by the addition of combination of Na, K, Mg, Al, Fe, and Ca matrix as standard
- A2 was determined by the addition of these elements separately
- A3 was obtained by addition of multi-element standard containing 23 elements.

Results of each measurement are given in Table 8.5. Consistency of each measurement indicated that standards were not different from each other significantly and there still exists a missing point in the measurement of Na.

Table 8.2. Comparison of the Standard Addition with the Direct Calibration Method for JSd-1.

species (w/w %)	measured standard add.	measured direct cal.	certified values	% difference standard add.	% difference direct cal.
SiO_2	64.797*	64.2	66.55	2.635	3.531
Al_2O_3	14.020	15.72	14.65	4.298	7.304
Fe_2O_3	5.117	6.098	5.059	1.154	20.538
K_2O	2.286	3.585	2.183	4.701	64.224
Na_2O	3.380	4.504	2.727	23.959	65.163
CaO	3.363	3.874	3.034	10.853	27.686
MgO	2.003	2.072	1.813	10.504	14.286

* measured by the direct calibration method

Table 8.3. Comparison of the Standard Addition with the Direct Calibration Method for JSd-3.

species (w/w %)	measured standard add.	measured direct cal.	certified values	% difference standard add.	% difference direct cal.
SiO_2	75.833*	77.3	76	0.220	1.711
Al_2O_3	10.719	10.378	9.908	8.182	4.744
Fe_2O_3	4.797	4.963	4.368	9.817	13.622
K_2O	1.812	3.277	1.971	8.046	66.261
Na_2O	0.483	2.19	0.411	17.601	432.847
CaO	0.671	0.607	0.56	19.805	8.393
MgO	1.201	1.288	1.17	2.618	10.085

* measured by the direct calibration method

Table 8.4. Comparison of the Standard Addition with the Direct Calibration Method for JR-3.

species (w/w %)	measured standard add.	measured direct cal.	certified values	% difference standard add.	% difference direct cal.
SiO_2	74.228*	77.69	72.76	2.018	6.776
Al_2O_3	12.342	12.59	11.9	3.717	5.798
Fe_2O_3	5.126	5.608	4.72	8.594	18.814
K_2O	4.269	6.731	4.29	0.495	56.900
Na_2O	5.591	7.23	4.69	19.219	54.158
CaO	0.161	0.058	0.093	103.7	37.634
MgO	0.074	0.049	0.05	48.125	2.000

* measured by the direct calibration method

Table 8.5. Comparison of Different Standards Used in the Analysis of JR-3

species (w/w %)	measured values			certified values	% difference		
	A1	A2	A3		A1	A2	A3
SiO_2	n. d.*	74.876	74.228	72.76	n. d.	2.908	2.018
Al_2O_3	11.241	11.417	12.342	11.9	5.537	4.058	3.717
Fe_2O_3	4.832	4.443	5.126	4.677	3.319	5.008	8.594
K_2O	4.465	4.540	4.269	4.29	4.077	5.823	0.495
Na_2O	5.864	5.887	5.591	4.69	25.022	25.514	19.219
CaO	n. d.	0.189	0.161	0.093	n. d.	103.7	73.01
MgO	0.098	0.085	0.074	0.05	95.831	70.582	48.125

* n.d. = not determined

For the consistency analysis of Japanese Reference Rock Standards, intensity values of each sample (after making appropriate dilutions) were used to construct calibration curves. All calibration curve data are given in Appendix. As shown in Figure A.6 to Figure A.12, and in Table A.5 to Table A.11, these standards seem to be consistent with each other. Although percentages of errors in the case of CaO and MgO were obtained to be high, in fact the absolute values of certified and calculated values are quite close.

Analyses of the original and Na-clinoptilolite were carried out with both the direct calibration method, using Japanese Reference Rocks as standards, and the standard addition method. As given in Table 8.6, no significant differences obtained except calcium in Na-CLI and sodium in both the original and Na-forms as obtained in the early analyses of Japanese Reference Rocks. According to the total percentages, direct calibration method with the JRRS gave almost perfect results. However, it is clear that deviations from 100 %, in the case of the standard addition method, were most probably resulted from overestimated SiO_2 values. On the other hand, by considering the cation balance, the error in the standard addition method was found to be within the acceptable range of error percentage whose maximum value was stated as 10 %, by Gotardi and Galli (1985). From these considerations, it may be concluded that, the direct calibration using the JRRS is better for the determination of SiO_2, while the performance of the standard addition method is higher in the case of the other cations.

The number of atoms based on 72 oxygen atoms per unit cell is represented in Table 8.7. Therefore, respective idealized chemical formulas of the original and Na-clinoptilolite were obtained as $(Na_{0.816}\,K_{2.070})$ $(Ca_{1.060}\,Mg_{0.264})$ $(Al_{5.653}\,Fe_{0.390})$

Table 8.6. Compositions of the Original and Na-Clinoptilolite with Different Methods.

species (w/w %)	Standard addition		JRRS	
	Org-CLI	Na-CLI	Org-CLI	Na-CLI
SiO_2	71.27*	70.74*	66.36	68.36
Al_2O_3	11.36	11.73	11.39	11.36
Fe_2O_3	1.227	0.694	1.173	0.633
K_2O	3.844	1.959	3.719	1.856
Na_2O	0.998	5.810	0.798	4.894
CaO	2.344	0.169	2.111	0.042
MgO	0.420	0.150	0.443	0.132
H_2O	14.22	12.09	14.22	12.09
Total	105.69	103.70	100.22	99.72

* measured by the direct calibration method using Silicon standard

Table 8.7. The Number of Each Atom per Unit Cell with Different Methods.

species	Standard addition		JRRS	
	Org-CLI	Na-CLI	Org-CLI	Na-CLI
Si	30.084	29.911	29.817	30.068
Al	5.653	5.843	6.029	5.890
Fe	0.390	0.221	0.396	0.209
K	2.070	1.057	2.132	1.042
Na	0.816	4.763	0.695	4.173
Ca	1.060	0.076	1.017	0.020
Mg	0.264	0.094	0.297	0.086
H_2O	20.023	17.049	21.316	17.736
% cation balance error**	8.397	1.599	15.130	11.109

** cation balance error = $[(Al^{3+} + Fe^{3+}) - (Na^{+} + K^{+} + 2\,Ca^{2+} + 2\,Mg^{2+})] / [Al^{3+} + Fe^{3+}] \times 100$ %

$(Si_{30.084})\ O_{72}.\ 20.023\ H_2O$ and $(Na_{4.763}\ K_{1.057})\ (Ca_{0.076}\ Mg_{0.094})\ (Al_{5.843}\ Fe_{0.221})\ (Si_{29.911})\ O_{72}.\ 17.049\ H_2O$. The idealized form of Na-clinoptilolite was given as $Na_6\ Al_6\ Si_{30}\ O_{72}.\ 24\ H_2O$ in the literature (Tsitsishvili et al. 1992).

Chemical compositions of the Ag, Zn, and Cu forms of clinoptilolite, obtained from the equilibrium studies of the untreated clinoptilolite at 0.1 N initial metal concentrations, could not be measured due to the limitation of the fusion method. Since at high temperatures, as high as fusion temperature of the sample, some cations like Ag, Zn, and Cu will be vaporizing easily, it will be unreasonable to measure them. Hence, the chemical compositions of these cationic forms were estimated, using the equivalents

of sodium, potassium, calcium, and magnesium released during the ion exchange process. Calculated idealized formula of each cationic form is as follows:

Ag-form: $(Ag_{3.114}\ Na_{0.212}\ K_{1.34})\ (Ca_{0.237}\ Mg_{0.197})\ (Al_{5.653}\ Fe_{0.390})\ (Si_{30.084})\ O_{72.}\ 15.40\ H_2O$

Zn-form: $(Zn_{0.555}\ Ca_{0.814}\ Mg_{0.229})\ (Na_{0.468}\ K_{1.871})\ (Al_{5.653}\ Fe_{0.390})\ (Si_{30.084})\ O_{72}.\ 18.98\ H_2O$

Cu-form: $(Cu_{0.728}\ Ca_{0.723}\ Mg_{0.229})\ (Na_{0.386}\ K_{1.789})\ (Al_{5.653}\ Fe_{0.390})\ (Si_{30.084})\ O_{72}.\ 17.79\ H_2O.$

8.2.2. FTIR Investigations

FTIR spectra of the original and exchanged forms of the clinoptilolite were investigated between 400 and 4000 cm^{-1} region. As shown in Figure 8.2, no significant changes in the IR patterns were determined in the lattice vibrations region (up to 1300 cm^{-1}) except a shoulder at 520 cm^{-1} which vanished almost completely in the case of monovalent exchange, while it appeared for the original, zinc and copper forms. In the water vibration bands, the band at about 3460 cm^{-1} was observed to broaden for the cases of silver, zinc, and copper forms.

Table 8.8. Assignments of Vibration Bands of the Original and Cation Exchanged Forms of the Clinoptilolite.

Vibration modes	Symbol	Frequency (cm^{-1})				
		Org-CLI	**Na-CLI**	**Ag-CLI**	**Zn-CLI**	**Cu-CLI**
Internal T-O bending	A1	468.7	466.7	461	464.8	464.8
External double ring	A2	605.6	607.5	605.6	605.6	607.5
Internal symmetric stretch	A3	721.3	719.4	723.3	721.3	719.4
External asymmetric stretch	A4	792.7	790.8	788.8	790.8	790.8
External symmetric stretch	A5	1050	1058.9	1056.9	1051.1	1053
Internal asymmetric stretch	A6	1215	1215	1215	1215	1215
OH bending	A7	1639.4	1639.4	1641.3	1637.4	1645.2
H-bonded OH stretching	A8	3460	3481.3	3494.8	3467.7	3479.3
Isolated OH stretching	A9	3633.6	3629.8	3633.6	3629.8	3625.9

Vibration band assignments of the samples are summarized in Table 8.8. No considerable variations were noticed in A2, A3, A4, and A6 bands. However, A1 and A5 bands shifted with cation exchange, thereby indicating the interactions between cations and zeolite framework. Frequencies of water bending and stretching were also altered. Surprisingly, A8 band, which is formed due to the interactions of water

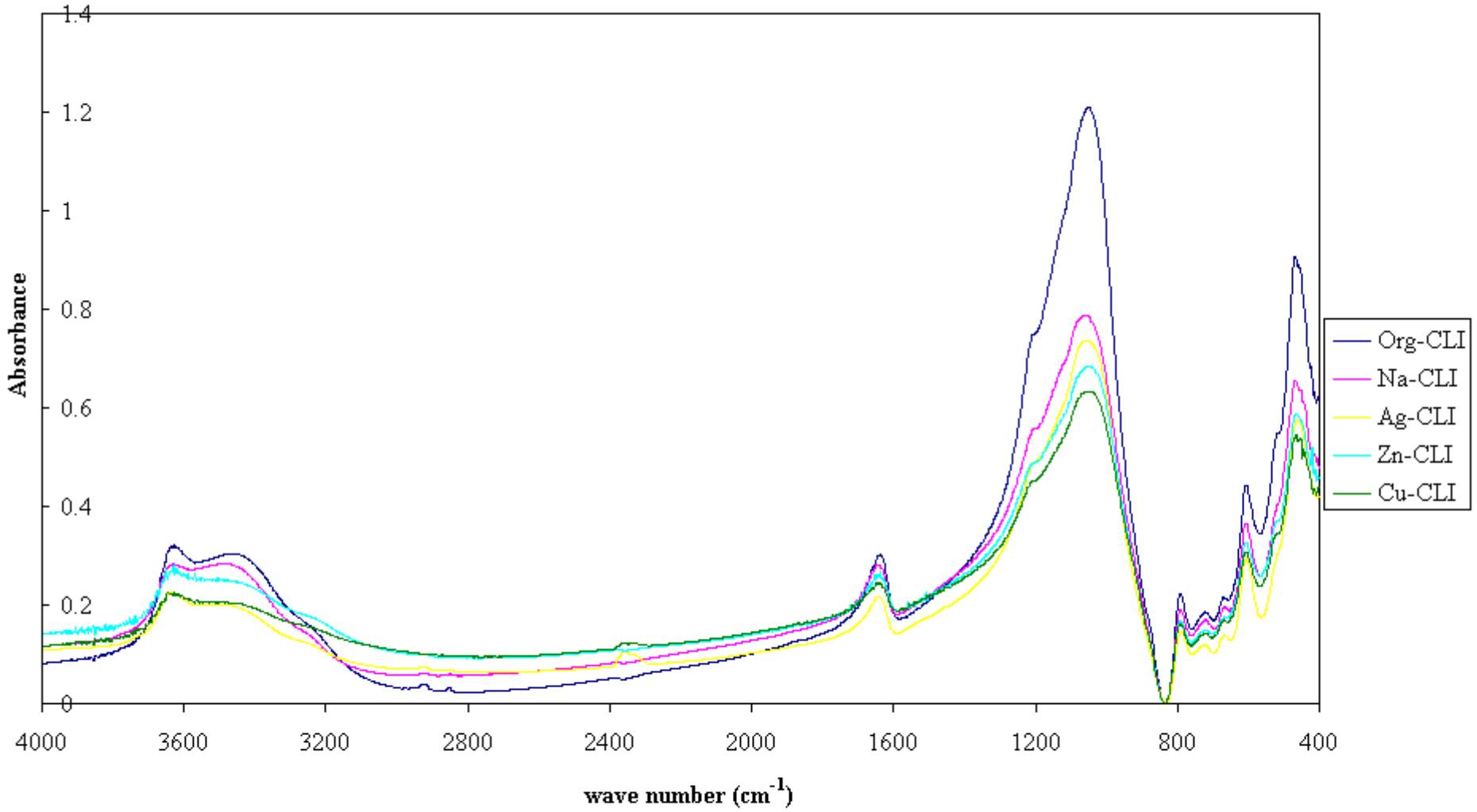

Figure 8.2. FTIR Spectra of the Original and Exchanged Forms of the Clinoptilolite.

molecules with the framework via hydrogen bonds, were affected more significantly than the A9 band that occurs owing to the interactions of water hydroxyl with the cations. Modification of the interactions between water and framework with the presence of different extra framework cations may be the explanation of this phenomenon. For the same reason, the use of the A7 band, for quantitative estimation of water content may be unrealistic. The strength of H-bond varies with the frequency adversely. In other words, a strong H- bond, tends to lower the wave number. Therefore, the shifts of the vibration band of A8 indicated how strong extra framework cations affect the interactions between water molecules and framework.

8.2.3. Thermal Analyses

8.2.3.1 Thermal Gravimetric Analysis (TGA)

TGA curves of the original and cation-exchanged forms of the clinoptilolite are shown in Figure 8.3. Total amount of water lost below 800 ^{o}C in each form is represented in Table 8.9.

Table 8.9. Total Amount of Water Lost up to 800 ^{o}C for Each Form.

Sample	% Weight loss up to 800 ^{o}C
Org-CLI	14.31
Na-CLI	12.26
Ag-CLI	11.00
Zn-CLI	13.59
Cu-CLI	13.02

The water loss values between 14.31 % and 11.00 % indicated the dependence of water content of clinoptilolite on the exchangeable cation composition as given in earlier studies (Akdeniz 1999, Bish 1988).

The change of weight percentage of water with ionic potential (charge / ionic radius) is given in Figure 8.4. The ionic potential was calculated by considering the other exchangeable cations present in the structure. Increasing trend of percentage of water with ionic potential was obtained for monovalent cations in the study of Bish.

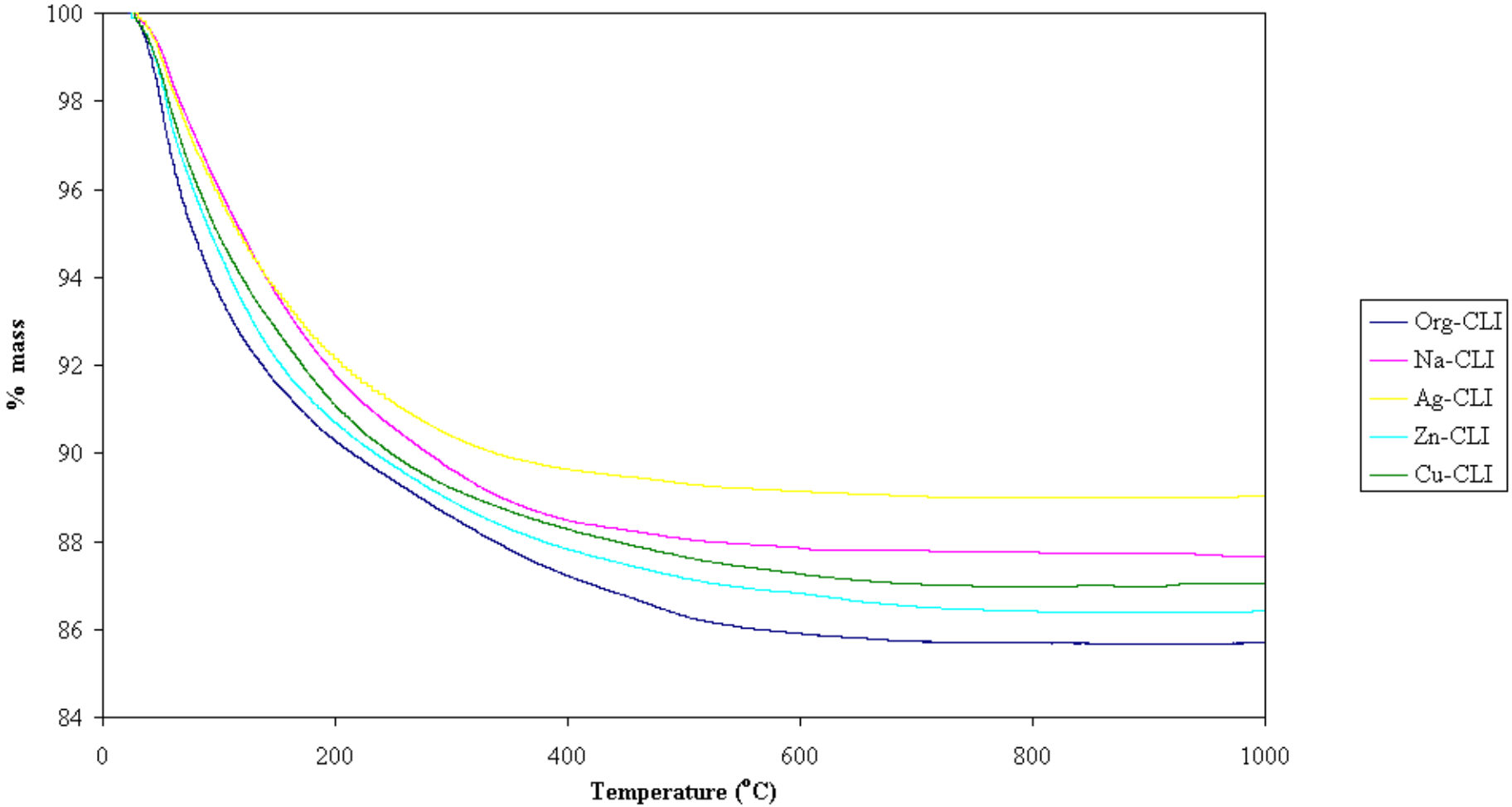

Figure 8.3. TGA Curves of the Original and Exchanged Forms of the Clinoptilolite.

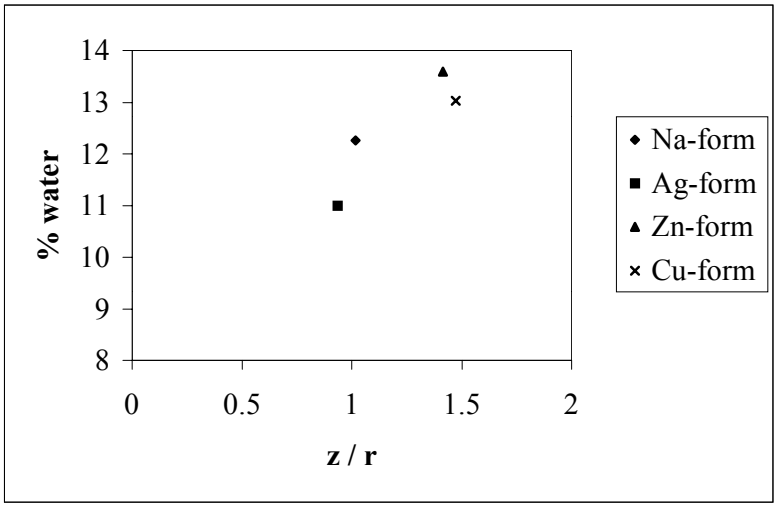

Figure 8.4. Weight Percentage of Water versus Ionic Potential.

However, random distribution was determined in the case of divalent cations (Bish 1988). Similar tendencies were obtained in the current study.

Knowlton et al. (1981), studied the types of water in untreated clinoptilolite and adopted their results to clinoptilolite in general. They concluded that the nature of water in clinoptilolite is predominantly dependent on the interactions of water molecules with the Si, Al framework. Using their assumption for each form of clinoptilolite, percentage of each type of water was determined roughly, as given in Table 8.10.

Table 8.10. Percentages of External, Loosely Bound, and Tightly Bound Water.

Sample	**External Water (< 85 ^{o}C)**	**Loosely Bound Water (85 ^{o}C -285 ^{o}C)**	**Tightly Bound Water (285 ^{o}C-500 ^{o}C)**	**(> 500 ^{o}C)**	**Total**
Org-CLI	5.50	5.71	2.48	0.62	14.31
Na-CLI	3.13	6.97	1.85	0.31	12.26
Ag-CLI	3.38	6.02	1.28	0.32	11.00
Zn-CLI	4.50	6.36	1.97	0.76	13.59
Cu-CLI	4.14	6.46	1.76	0.66	13.02

Derivative TGA curves are shown in Figure 8.5. They are useful for the determination of steps of water loss. The differences in stepwise mechanisms indicated

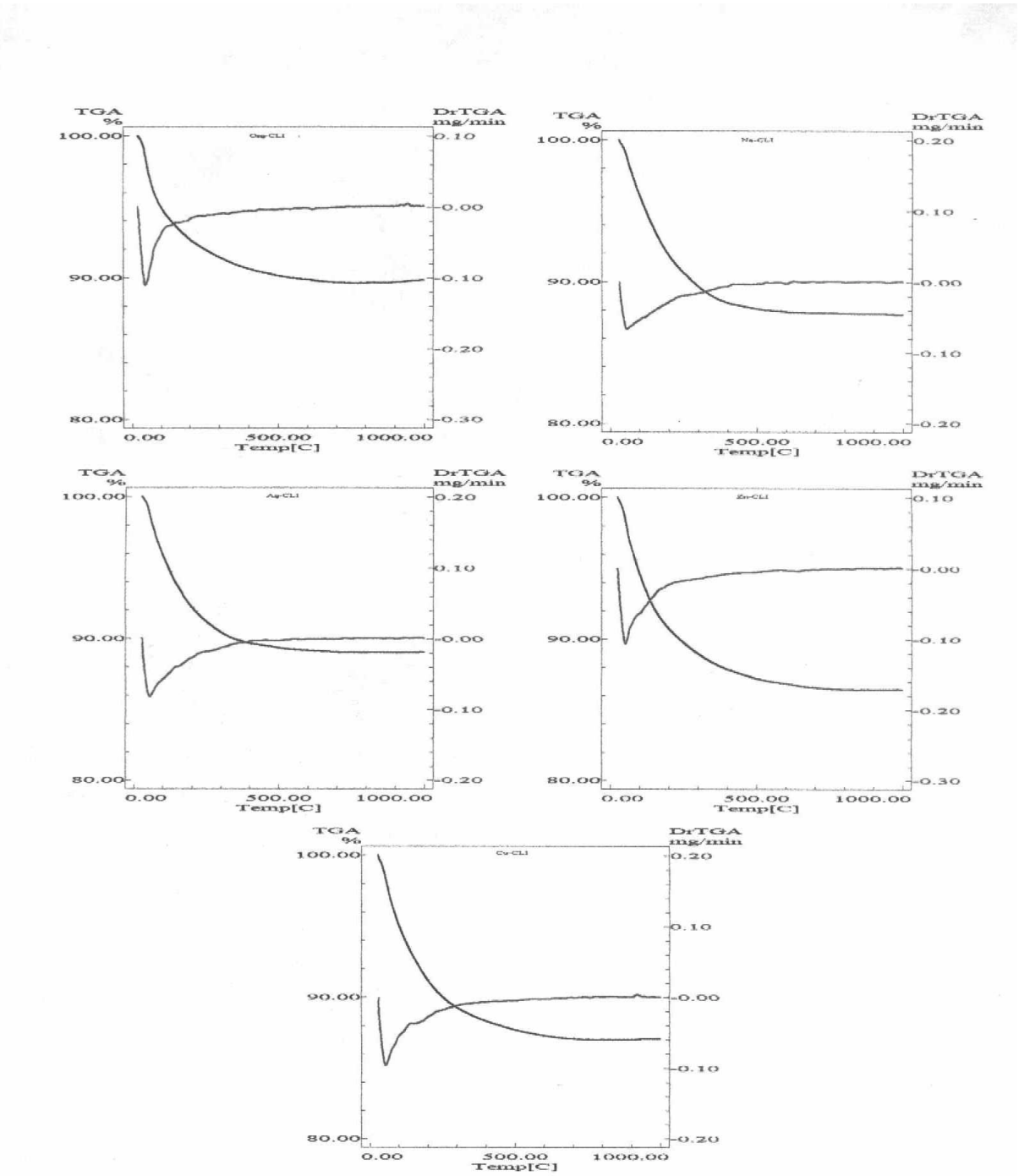

Figure 8.5. DTGA Curves of the Original and Exchanged Forms of the Clinoptilolite.

that water held with different bond strength, varied with composition. Original clinoptilolite dehydrated in two steps, a sharp step up to 110 ^{o}C (6.90 %), and a broad one between 110 and 570 ^{o}C (7.11 %). Na-form lost its water in two steps, one up to 240 ^{o}C (9.21 %) and the other one between 240 and 620 ^{o}C (2.98 %). Ag-form dehydrated in one broad step up to 600 ^{o}C (10.87 %). Zn-form had losses up to 95 ^{o}C (5.14 %) and between 95 and 600 ^{o}C (8.04 %), and Cu-form had losses up to 145 ^{o}C (6.84 %) with between 145 and 600 ^{o}C (5.90 %). Mechanisms of water losses agreed with Bish. However, Gördes clinoptilolite had losses up to higher temperatures than the sample used in Bish's study (clinoptilolite from Castle Creek, Idaho, U.S.).

8.2.3.2 Differential Thermal Analysis (DTA)

DTA curve of each sample is shown in Figure 8.6. Mainly, two endotherms and one exotherm were obtained in all samples. Peak minimum and peak maximum temperatures are summarized in Table 8.11.

Table 8.11. DTA Peak Minimum and Peak Maximum Temperatures.

Sample	1st Endotherm Temperature (^{o}C)	2nd Endotherm Temperature (^{o}C)	Exotherm Temperature (^{o}C)
Org-CLI	44.38	576.4	845.3
Na-CLI	87.57	578.1	844.6
Ag-CLI	82.39	650.0	851.1
Zn-CLI	94.14	592.0	842.5
Cu-CLI	55.57	590.0	832.9

The first endotherm, which is more certain for original and zinc forms, occurred up to about 150 ^{o}C. The insignificant nature of this peak along with its low formation temperature indicated that the endotherm, most probably occurred due to the release of the external water and/or loosely bound water. Shifts in the peak minimum temperatures observed in the different cationic forms of clinoptilolite indicated the dependence of bond strength of water to the composition.

The second endotherm that occurred between 200 and 700 ^{o}C, possibly shows the dehydration of water with higher bond strength. However, in the study of

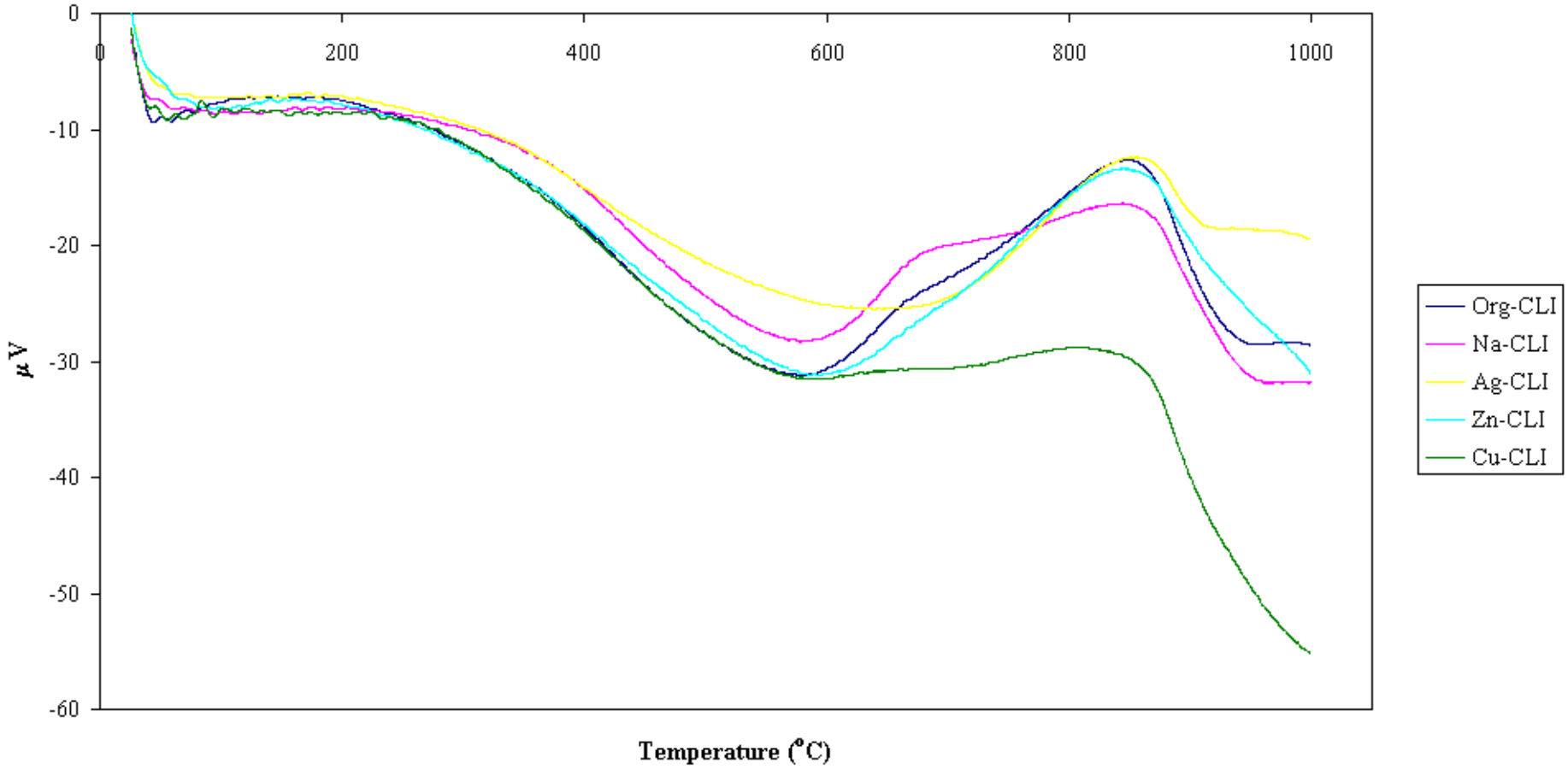

Figure 8.6. DTA Curves of the Original and Exchanged Forms of the Clinoptilolite.

Mumpton (1960), it was reported that aside from a broad endotherm up to 400 ^{o}C, clinoptilolite exhibits no thermal reaction up to about 1000 ^{o}C. Conversely, Esenli and Kumbasar (1994), obtained three endotherms at 120, 230, and 730 ^{o}C. Similarly, small endotherms were observed between 300 and 600 ^{o}C in addition to the first one centered about 100 ^{o}C, by Yücel and Çulfaz (1985), and they explained these endotherms with the existence of at least two different types of water. These differences indicated that, the nature of the DTA curve is strongly dependent on composition. The high peak minimum temperature of the second endotherm may cause some doubts about whether the endotherm occurred due to the dehydration of water or phase transition. Although the existence of no breaks in TGA curves weakens the probability of structural change, all these possibilities should be supported with XRD studies. No significant differences were obtained in the peak minimum temperatures of the original, sodium, zinc, and copper forms but that of silver form is somewhat much higher. The exotherm at about 850 ^{o}C, definitely indicated the collapse in the structure. Small shifts in the peak maximum temperature of the samples emphasized that the exchanges with these cations did not alter the stability of clinoptilolite so much.

8.2.3.3 Differential Scanning Calorimetry (DSC)

DSC curve of each sample is shown in Figure 8.7. There appeared significant differences between the shapes of the curves. Mainly, Na-form has one endotherm, the original sample has two endotherms, Zn and Cu-forms have three endotherms, and Ag-form has a small exotherm at about 327 ^{o}C, in addition to two endotherms. Peak minimum temperatures are summarized in Table 8.12.

Table 8.12. DSC Peak Minimum Temperatures.

Sample	1st Endotherm Temp. (^{o}C)	2nd Endotherm Temp. (^{o}C)	3rd Endotherm Temp. (^{o}C)
Org-CLI	65.71	310	-
Na-CLI	58.18	-	-
Ag-CLI	64.14	165	-
Zn-CLI	70.35	133.5	361.8

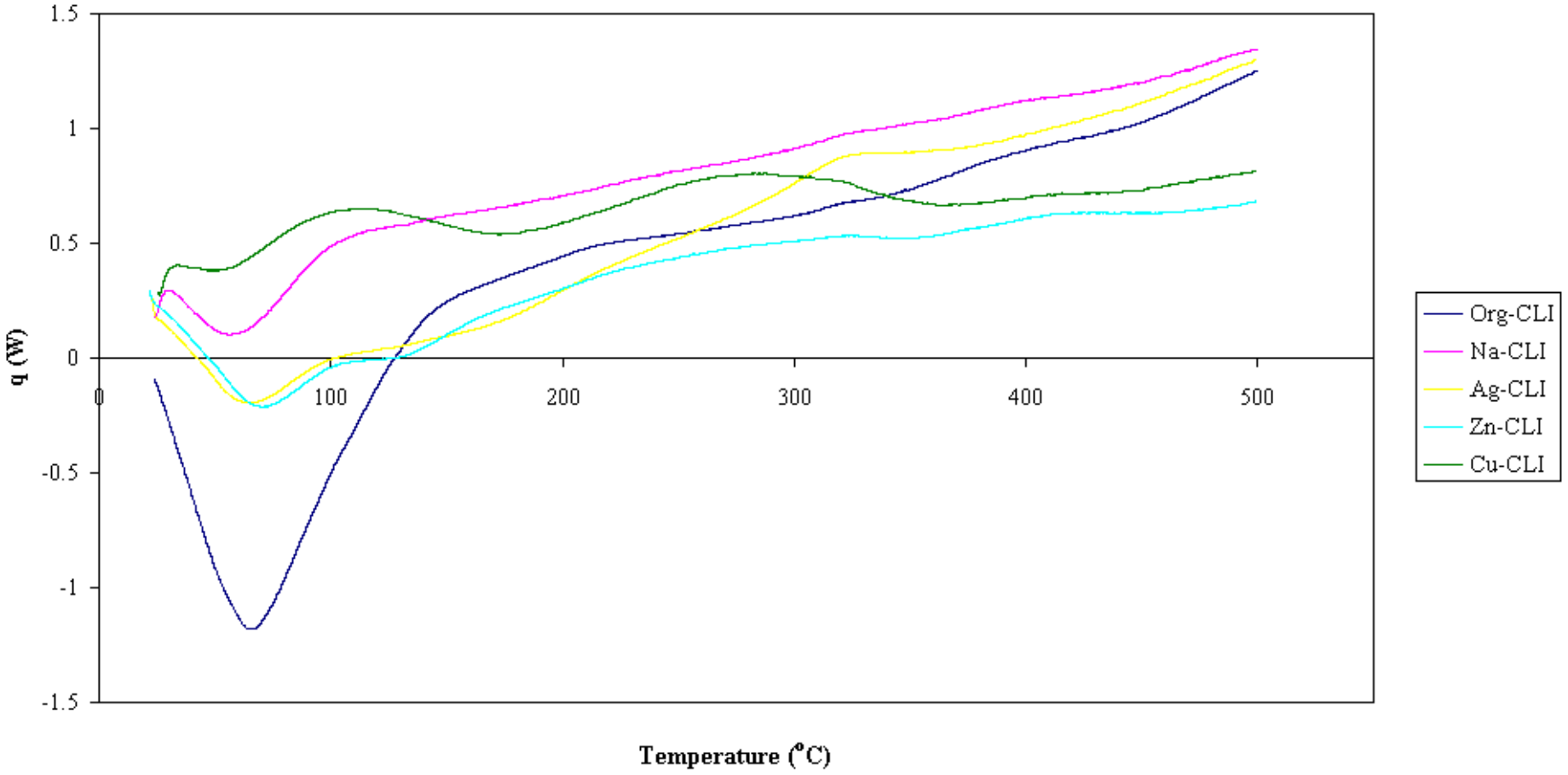

Figure 8.7. DSC Curves of the Original and Exchanged Forms of the Clinoptilolite.

DSC analyses indicated that modifications with Na, Ag, Zn, and Cu exchanges lowered the amount of heat absorbed. Especially, Cu-form showed a very different energy absorption-temperature behavior. The endotherm observed at about 60-70 ^{o}C for the other samples, tended to vanish for Cu-form. However, TGA analyses indicated that Cu-form lost approximately the same amount of water with the other samples. Thus, the disappearance of the endotherm may be explained with a simultaneous exothermic phenomena occurred with water desorption or the strength of the bond between the cation and water molecules.

The changes in the DSC patterns of each sample can be attributed to the distribution of cation-water molecule distances. Since the framework structure and charge should be identical for all the samples, the exchangeable cation and the sites occupied by the cation must control the dehydration behavior of the samples (Bish 1988).

8.2.4. Adsorption Related Properties

Physisorption experiments were carried out using N_2 at 77.4 K as adsorptive. The physisorption isotherms of five samples are all, Type IV. As an example of adsorption-desorption behavior of the samples, forward and reverse points are shown only for the original sample in Figure 8.8. Adsorption isotherms of the original and cation exchanged forms of the clinoptilolite are represented in Figure 8.9.

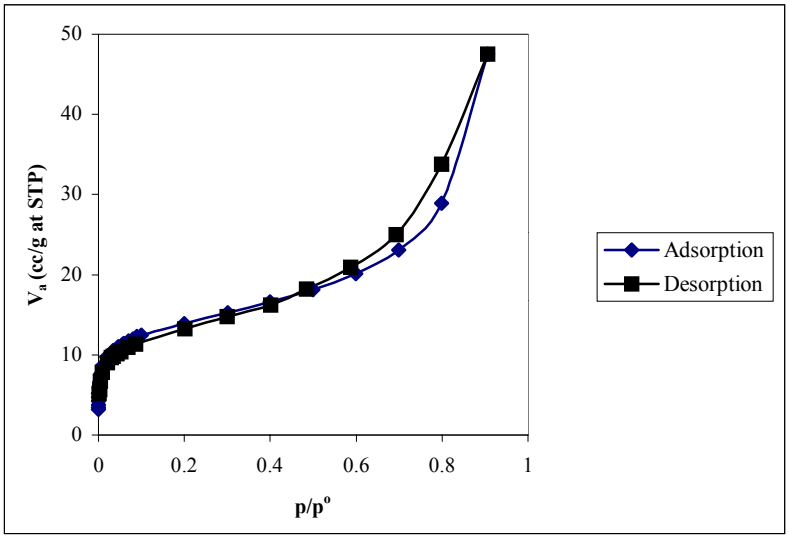

Figure 8.8. Adsorption-Desorption Behavior of the Original Clinoptilolite.

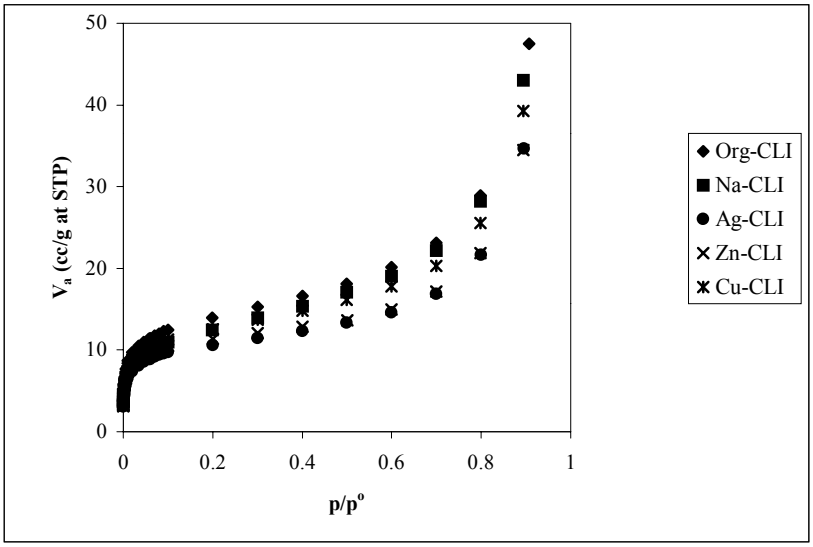

Figure 8.9. Adsorption Isotherms of the Original and Cation Exchanged Forms of the Clinoptilolite.

For comparison purposes, BET and Langmuir surface areas and parameters of each model for each sample are summarized in Table 8.13. Although, BET model seemed to fit experimental data better, high or negative C values are indicative of the micropores, and their measurements is not amenable to analysis by BET method without modification (Webb and Clyde 1997). For this reason, maximum adsorption capacities (V_a at $p/p^o \approx 0.9$) were considered to investigate the effect of cation exchange on sorption behavior rather than the surface area measurements.

Table 8.13. BET and Langmuir Surface Areas with Model Parameters for Each Sample.

Sample	BET Model			Langmuir Model		
	S. Area (m^2/g)	C	V_m (cc/g STP)	S. Area (m^2/g)	b	V_m (cc/g STP)
Org-CLI	46.76	-465.5	10.741	57.36	0.0079	13.175
Na-CLI	43.06	337	9.8912	50.80	0.0093	11.669
Ag-CLI	34.97	-177.9	8.0321	45.21	0.0083	10.384
Zn-CLI	36.71	-131.8	8.4326	48.42	0.0078	11.123
Cu-CLI	41.98	-345.7	9.6432	52.26	0.0084	12.005

As a first glance, sorption capacity may be thought to be proportional to ionic potential, in other words an enhancement may be expected in sorption properties as a

result of the exchange with divalent cation or cation with smaller ionic radius. However, channel characteristics of the adsorbent and the dimensions of the adsorptive were also found to be effective. Ackley and Yang (1991), devised a channel blockage matrix for clinoptilolite. They found that cation location is far more important to channel blocking than size or number. Using the nitrogen gas as adsorptive, the change in the microporous structure of the clinoptilolite will not reflect to its sorption capacity, if radii of cations exchanged, and channel characteristics of the clinoptilolite are considered. Therefore, the relatively low values of sorption capacity are due to the fact that N_2 can not enter into all the micropores of the samples and it is mainly adsorbed on the external surface, macropores and mesopores of the solid (Arcoya et al. 1993). Özkan (1996), investigated the sorption behavior of Bigadiç clinoptilolite with different adsorptives. Maximum adsorption capacities of the clinoptilolite were determined as 162.59, 51.73, and 30 cc STP/g for H_2O, CO_2, and N_2 respectively by confirming the effect of the dimensions of the adsorptive.

However, as given in Figure 8.9, there appeared some differences in the sorption capacities of the samples. These differences may be related to the change in the adsorption affinity of the clinoptilolite, since the type, size and location of the cation alter the local electric field as well as adsorbate polarization (Breck, 1974). Hence, modification of the energy of interaction terms between nitrogen and clinoptilolite by cation exchange is the chief reason for the change in the sorption capacity of the samples. Similar behavior was reported by Tsitsishvili et al. (1992). In the case of oxygen enrichment of air process, within the different cationic forms of the clinoptilolite, K-clinoptilolite was reported to enhance oxygen productivity, and this notable efficiency was thought to be due to the greater interaction between the quadrupole moment of the nitrogen molecule and depolarized electrostatic fields generated by the potassium ions.

8.3. Ion Exchange Equilibrium Studies

8.3.1. Ag^+, Zn^{2+}, and Cu^{2+} Exchange Properties of the Untreated Clinoptilolite

Sodium, potassium, calcium, and magnesium are the major exchangeable cations in clinoptilolite. Therefore, in any ion exchange reaction, total equivalents of the major exchangeable cations released to the solution should be equal to those of the

Table 8.14. Exchanged Amounts of Ag^+, Zn^{2+}, and Cu^{2+} from Different Measurements.

Ag^+			Zn^{2+}			Cu^{2+}		
q_{eq}^a (meq /g)	q_{eq}^b (meq /g)	% difference	q_{eq}^a (meq /g)	q_{eq}^b (meq /g)	% difference	q_{eq}^a (meq /g)	q_{eq}^b (meq /g)	% difference
0.0909	0.0931	2.43	0.106	0.0971	8.37	0.1859	0.1677	9.81
0.164	0.1596	2.70	0.1798	0.153	14.91	0.2299	0.2060	10.38
0.1931	0.2035	5.42	0.2907	0.2527	13.06	0.3033	0.2688	11.38
0.3115	0.3077	1.23	0.365	0.3183	12.78	0.3515	0.3704	5.37
0.5065	0.51	0.69	0.3767	0.3807	1.06			

a=from Ag^+, Zn^{2+}, or Cu^{2+} measurements directly
b=from Na^++ Ca^{2+} + K^++ Mg^{2+} measurements

cation sorbed. In this study, amount of ingoing cation was determined by the difference in the concentration of that cation directly as well as from the summation of the equivalents of the major exchangeable cations transferred into solution phase using the principle of conservation of electroneutrality.

As given in Table 8.14, maximum error was obtained as 14.91 %, which is in the limits of the most of analytical instruments. From this observation, it can be concluded that the contribution of the other cations to Ag^+, Zn^{2+}, and Cu^{2+} exchanges is low. Therefore, major portion of the exchange is due to sodium, potassium, calcium, and magnesium ions.

From Table 8.15 to Table 8.17, Ag^+, Zn^{2+}, and Cu^{2+} exchange equilibrium data at 25 ^oC obtained from the summation of the equivalents of the major exchangeable cations of the clinoptilolite are given. Ion exchange isotherms as well as contribution of each major exchangeable cation to the equilibrium isotherms are given from Figure 8.10 to Figure 8.12.

From the plateau of the isotherms maximum exchange capacities were determined as 1.184, 0.439, 0.539 meq/g clinoptilolite for Ag^+, Zn^{2+}, and Cu^{2+} respectively. As given in Table 8.18, the major portion of each exchange was contributed by Na^+ and Ca^+. However, the tenacity with which K^+ and Mg^{2+} were held in the clinoptilolite is significant. Low exchange level of K^+ compared to Na^+ and Ca^{2+} can be explained with the location of potassium ions in the structure of clinoptilolite. As stated in literature, potassium is situated in M(3) site, which has the highest coordination number among all the cation sites in the unit cell. Since K^+ is coordinated by six framework oxygen atoms and three water molecules, the strong bonding of K^+ at this site may be effective in its lower exchange ability.

Table 8.15. Equilibrium Data for Ag^+ Exchange of the Untreated Clinoptilolite at 25 ^oC.

C_o (meq Ag^+/L)	Na^+ (meq/g)	Ca^{2+} (meq/g)	K^+ (meq/g)	Mg^{2+} (meq/g)	C_{eq} (meq Ag^+/L)	q_{eq} (meq Ag^+/g)
0.5	0.0568	0.0173	0.0142	0.0049	0.0342	0.0931
1	0.0903	0.0370	0.0266	0.0056	0.2025	0.1596
2	0.1042	0.0606	0.0322	0.0064	0.6430	0.2035
5	0.1234	0.1291	0.0442	0.0110	1.9230	0.3077
10	0.1539	0.2592	0.0746	0.0223	4.8993	0.5100
25	0.1926	0.4345	0.1321	0.0348	17.0642	0.7934
40	0.2099	0.4785	0.1781	0.0436	30.8964	0.9106
50	0.2241	0.5419	0.1970	0.0466	39.9077	1.0092
60	0.2247	0.5726	0.2264	0.0486	49.2777	1.0722
80	0.2334	0.6178	0.2602	0.0512	68.3743	1.1626
90	0.2297	0.6132	0.2690	0.0509	78.3718	1.1628
100	0.2383	0.6491	0.2878	0.0527	87.7212	1.2279

Table 8.16. Equilibrium Data for Zn^{2+} Exchange of the Untreated Clinoptilolite at 25 ^oC.

C_o (meq Zn^{2+}/L)	Na^+ (meq/g)	Ca^{2+} (meq/g)	K^+ (meq/g)	Mg^{2+} (meq/g)	C_{eq} (meq Zn^{2+}/L)	q_{eq} (meq Zn^{2+}/g)
1	0.0574	0.0194	0.0150	0.0053	0.0291	0.0971
2	0.0801	0.0418	0.0237	0.0075	0.4697	0.1530
5	0.1060	0.0940	0.0386	0.0141	2.4728	0.2527
10	0.1168	0.1328	0.0484	0.0203	6.8167	0.3183
25	0.1290	0.1658	0.0618	0.0240	21.1932	0.3807
40	0.1279	0.1706	0.0662	0.0246	36.1062	0.3894
50	0.1312	0.1761	0.0698	0.0253	45.9767	0.4023
60	0.1302	0.1836	0.0720	0.0271	55.8721	0.4128
80	0.1381	0.1943	0.0791	0.0284	75.6014	0.4398
100	0.1374	0.1940	0.0785	0.0280	95.6210	0.4379

Table 8.17. Equilibrium Data for Cu^{2+} Exchange of the Untreated Clinoptilolite at 25 ^{o}C.

C_o (meq Cu^{2+}/L)	Na^+ (meq/g)	Ca^{2+} (meq/g)	K^+ (meq/g)	Mg^{2+} (meq/g)	C_{eq} (meq Cu^{2+}/L)	q_{eq} (meq Cu^{2+}/g)
1	0.0927	0.0432	0.0273	0.0044	0.1620	0.1677
2	0.1318	0.0921	0.0411	0.0094	0.6266	0.2060
5	0.1631	0.1699	0.0532	0.0173	2.3118	0.2688
10	0.1289	0.1744	0.0487	0.0185	6.2957	0.3704
25	0.1410	0.2143	0.0603	0.0222	20.6220	0.4377
40	0.1544	0.2392	0.0707	0.0248	35.1076	0.4894
50	0.1552	0.2372	0.0741	0.0250	45.0808	0.4919
60	0.1591	0.2553	0.0957	0.0267	54.6332	0.5367
80	0.1647	0.2601	0.1025	0.0273	74.4510	0.5549
90	0.1673	0.2606	0.1070	0.0276	84.3766	0.5623
100	0.1696	0.2658	0.1107	0.0281	94.2577	0.5742

Table 8.18. Exchange Percentages of Exchangeable Cations Present in the Clinoptilolite with Ag^+, Zn^{2+}, and Cu^{2+} at C_o = 0.1 N.

species	% exchange		
	Ag^+	Zn^{2+}	Cu^{2+}
K^+	35.26	9.62	13.56
Na^+	74.03	42.68	52.69
Ca^{2+}	77.64	23.20	31.79
Mg^{2+}	25.29	13.44	13.48

In Figure 8.13, distribution coefficient, R_d, is given as a function of initial concentration. As indicated, at relatively low initial concentrations, the preference of clinoptilolite for Zn^{2+} and Cu^{2+} is significant. This observation agrees with Barrer (1978), who reported that selectivity became progressively greater for the ion of higher valence in the more dilute exchanging solution. This effect was explained by Helfferich (1962), in terms of Donnan potential. The Donnan potential attracts counter ions into the ion exchanger and thus balances their tendency to diffuse out into the solution. The force with which the Donnan potential acts on an ion is proportional to the ionic charge.

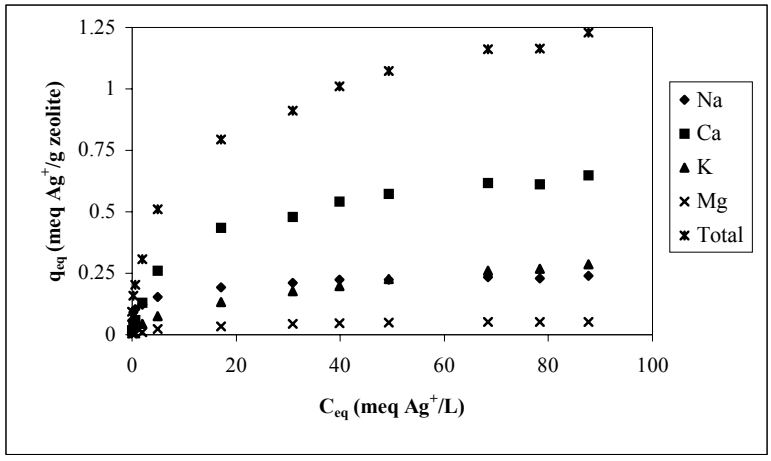

Figure 8.10. Silver Sorption Isotherm for Clinoptilolite at 25 ^oC with the Contribution of Each Cation.

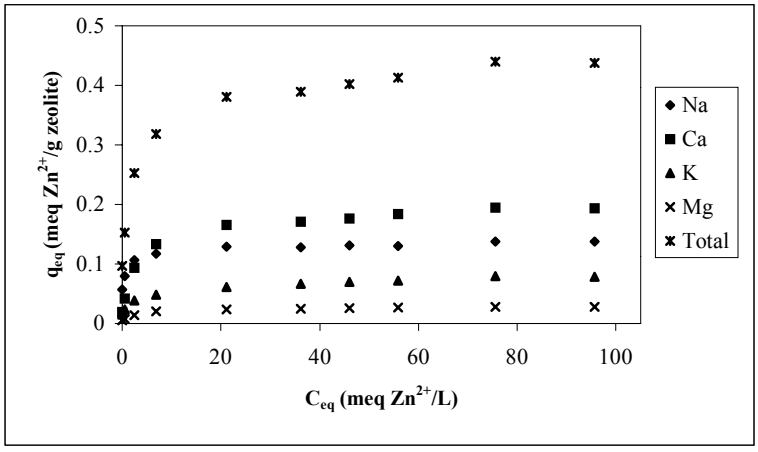

Figure 8.11. Zinc Sorption Isotherm for Clinoptilolite at 25 ^oC with the Contribution of Each Cation.

Hence the counter ion of higher charge is more strongly attracted and preferred by the ion exchanger. The absolute value of the Donnan potential increases with dilution. Consequently, the ion exchanger tends to prefer the counter ion of higher valence at low concentrations. Thus, high distribution coefficients of zinc and copper are not questionable in dilute solutions. However, at higher concentrations higher distribution coefficients were obtained for Ag^+ compared to Zn^{2+} and Cu^{2+}. This may be explained with the actual preference of clinoptilolite towards Ag^+. Barrer (1978), demonstrated that larger ion was preferred by siliceous (low charge) zeolites. Ionic radii of Ag^+, Zn^{2+} and Cu^{2+} are 1.26, 0.83, and 0.82 A^o respectively (Semmens and

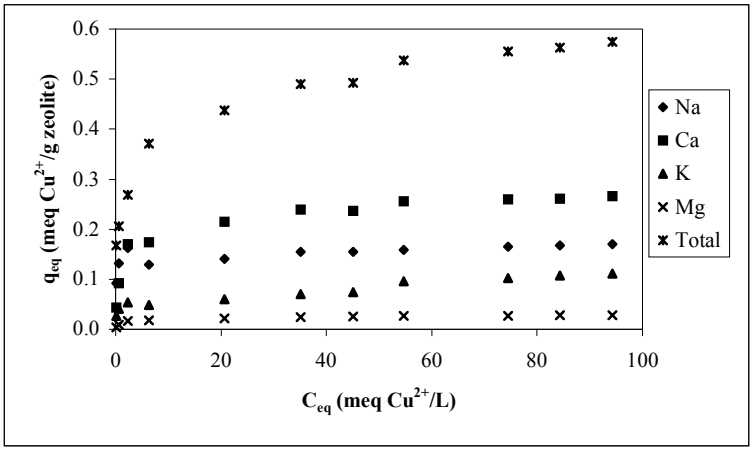

Figure 8.12. Copper Sorption Isotherm for Clinoptilolite at 25 ^{o}C with the Contribution of Each Cation.

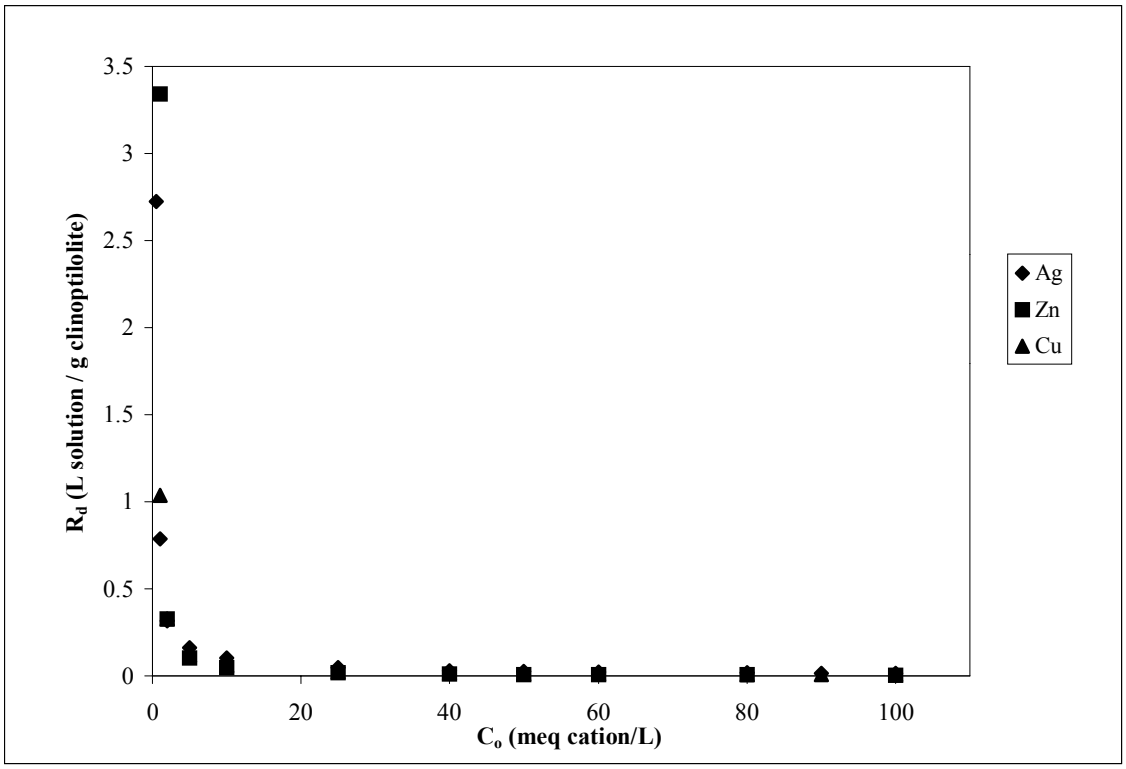

Figure 8.13. Variation of Distribution Coefficients with Initial Concentrations of Solutions for Each Ingoing Cation.

Table 8.19. Langmuir and Freundlich Model Parameters.

Langmuir Model				**Freundlich model**			
	Ag	**Zn**	**Cu**		**Ag**	**Zn**	**Cu**
slope	0.8068	2.265	1.7281	**slope**	0.3435	0.1931	0.1993
Intercept	4.4335	5.2312	6.1872	**Intercept**	-0.5626	-0.7084	-0.6262
R	0.9941	0.9986	0.9974	**R**	0.9966	0.9907	0.9965
b	0.1819	0.433	0.2738	**n**	0.3435	0.1931	0.1993
$\mathbf{n_m}$	1.2395	0.4415	0.5787	**F**	0.2738	0.1957	0.2365

Seyfard 1978, Sherry and Walton 1967). In addition to its higher ion size, higher polarizibility of Ag^+ may also be effective in its preference by the clinoptilolite.

Langmuir and Freundlich models were applied to each equilibrium data. Parameters of each model are given in Table 8.19. As indicated from Figure 8.14 to Figure 8.16, as well as from regression coefficient values, the models showed no considerable superiority to each other. However, for Zn^{2+} and Cu^{2+} exchange Langmuir model gave better correlation, while Freundich model fitted experimental data slightly better in the case of Ag^+ exchange.

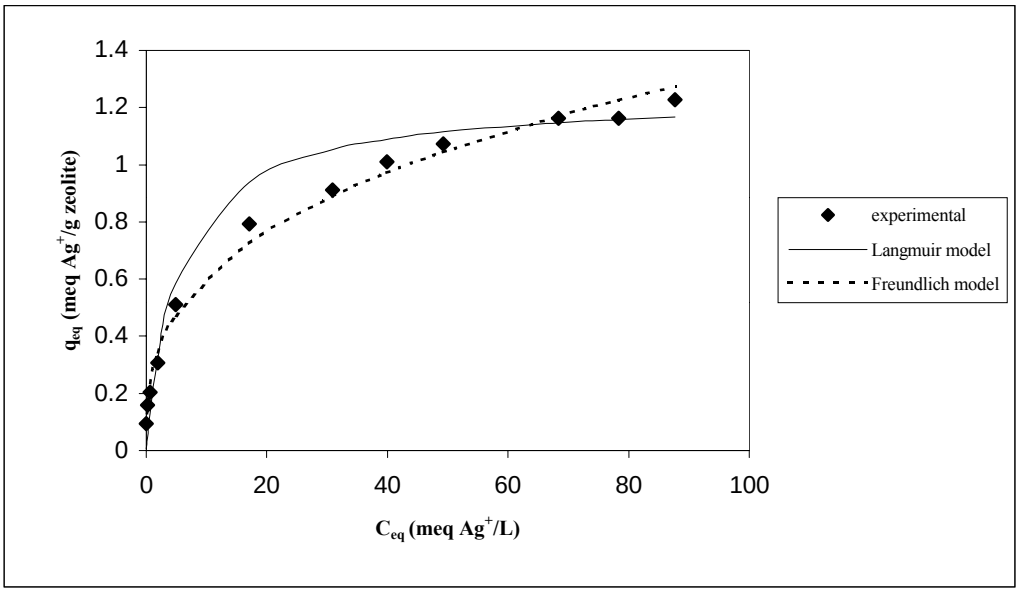

Figure 8.14. Comparisons of Langmuir and Freundlich Models with the Experimental Data for Silver Exchange.

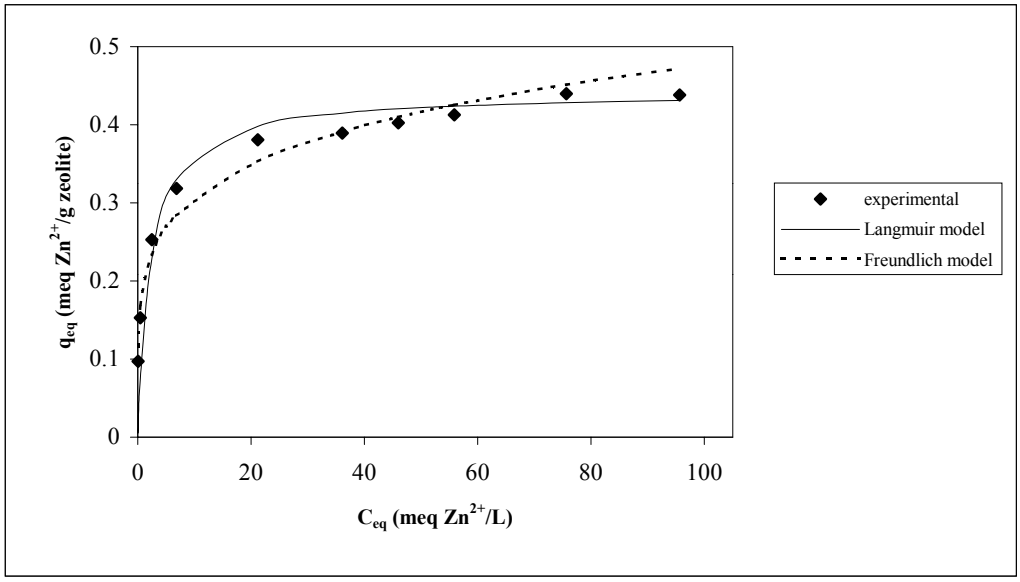

Figure 8.15. Comparisons of Langmuir and Freundlich Models with the Experimental Data for Zinc Exchange.

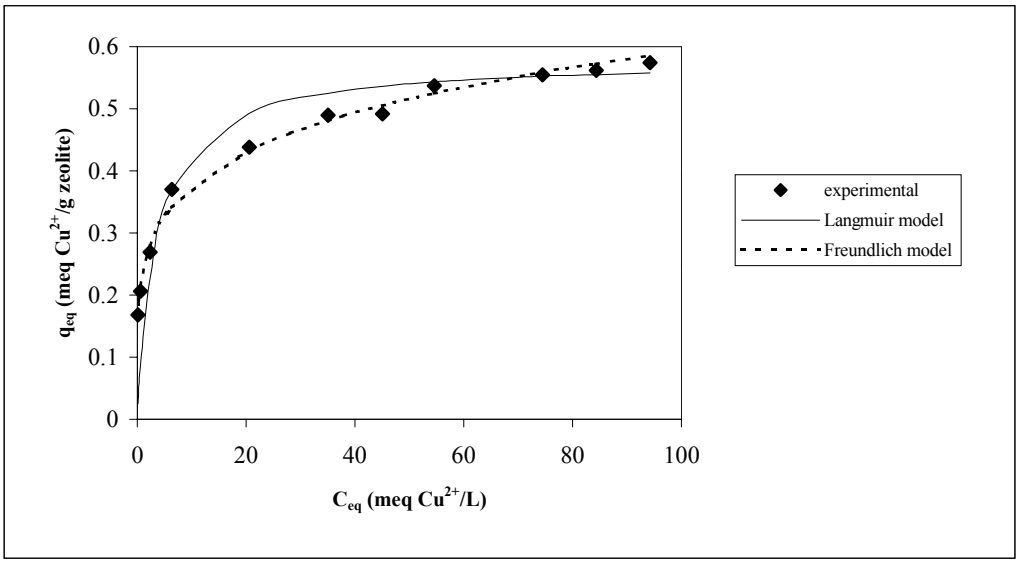

Figure 8.16. Comparisons of Langmuir and Freundlich Models with the Experimental Data for Copper Exchange.

8.3.2. Ag^{+}-Na^{+}, Zn^{2+}-Na^{+}, Cu^{2+}-Na^{+} Exchange Properties of Na-Clinoptilolite

Equilibrium distributions of Ag^{+}-Na^{+}, Zn^{2+}-Na^{+}, and Cu^{2+}-Na^{+} pairs between clinoptilolite and aqueous phases were investigated at 25 ^{o} C. The total normality of the exchange solutions was kept as 0.1 N by varying proportions of the competing ions. Measured initial and final concentrations of the ions along with the zeolite masses and

solution volumes used in the experiments are given in Tables A.12 to A.14 in Appendix.

Ion exchange equilibrium isotherms were plotted in terms of the equivalent fraction of the ingoing ion in solution (A_s) against that in the solid phase (A_z). A_s and A_z were calculated using the equations given below:

$$A_s = z_A M_{A,f} / TN \quad (8.1)$$

$$A_z = z_A (M_{A,i} - M_{A,f}) V / (W . CEC) \quad (8.2)$$

where

$M_{A,i}$ and $M_{A,f}$ = initial and final molar concentrations of ingoing cation, respectively

V = the solution volume

W = the zeolite mass

CEC = cation exchange capacity

TN = total normality = 0.1 N.

Since, potassium, calcium, and magnesium present in Na-clinoptilolite were assumed to be in inaccessible ion exchange sites and not to participate in the ion exchange process, CEC was taken as total equivalents of sodium in clinoptilolite, which corresponds to 1.87 meq / g (Pabalan 1994).

The isotherms of Ag^+-Na^+, Zn^{2+}-Na^+, and Cu^{2+}-Na^+ exchanges are shown in Figure 8.17. to 8.19. Silver exchange isotherm lies above the diagonal over the whole composition range thereby indicating the selectivity of clinoptilolite towards silver. On the other hand, for zinc and copper exchanges, the isotherms are above the diagonal

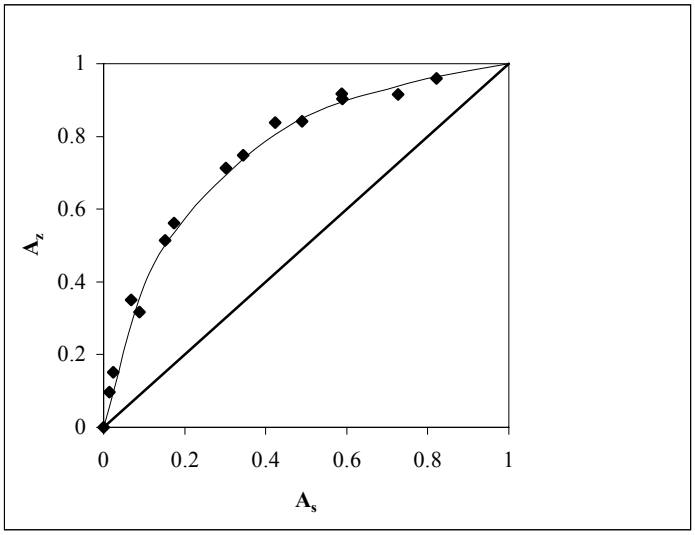

Figure 8.17. Ag^+ - Na^+ Exchange Isotherm at 25 ^oC.

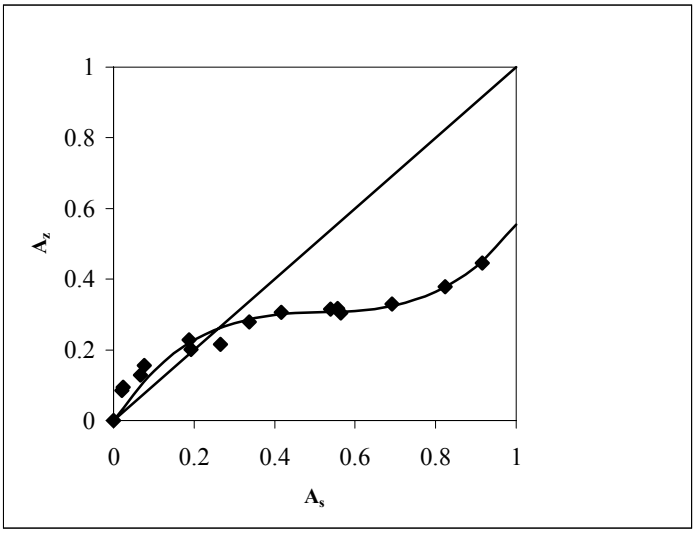

Figure 8.18. Zn^{2+} - Na^{+} Exchange Isotherm at 25 ^{o}C.

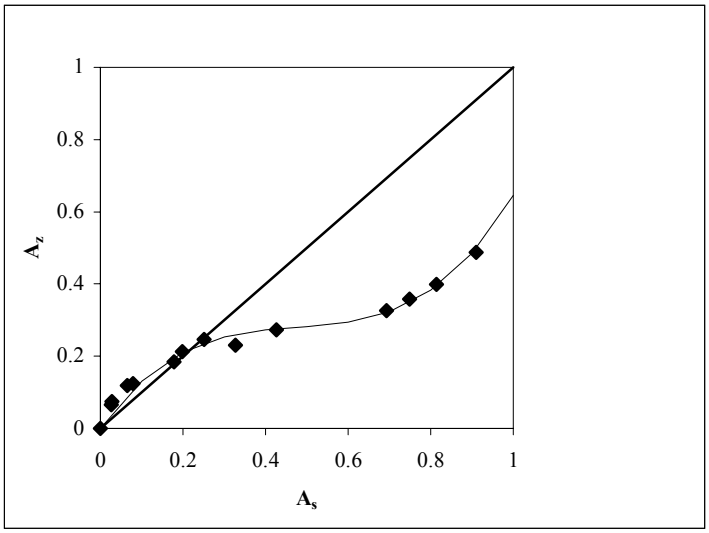

Figure 8.19. Cu^{2+} - Na^{+} Exchange Isotherm at 25 ^{o}C.

only for low concentrations. Therefore, the preferences of clinoptilolite for zinc and copper depend strongly on the concentration. While full exchange was attained for silver, partial exchanges were obtained in the case of zinc and copper.

Thermodynamic properties, obtained from each equilibrium data, were summarized in Table 8.20 to 8.22. Formulations of separation factor, mass action quotient, and corrected selectivity coefficient are given in Chapter 4. Activity ratios of solutions were calculated by combining Pitzer Model with Glueckauf extension of Guggenheim's original theory. The details of the calculation procedure and computer

program along with specific constants of electrolytes, comparisons of experimental and model activity coefficients of each electrolyte and activity ratios of mixed electrolytes are presented in Appendix. In the Pitzer model, mean activity coefficient is in terms of molality scale. Since solutions used in the experiments were prepared as based on molarity, mean activity coefficients should be converted to molar concentration scale. The required equation is given below (Pitzer 1991):

$$\gamma_{\pm} = \frac{c}{m d_o} y_{\pm} \qquad (8.3)$$

where $\gamma_{\pm}$ = mean molal activity coefficient,

$y_{\pm}$ = mean molar activity coefficient

d_o = the density of the pure solvent

and c / m = (molarity / molality) = density of the solution.

For this reason, solution densities were measured as a function of equivalent fractions of the ingoing cation. As given in Figure A.1, densities of the solutions were measured as 1± 0.007 g / ml. Therefore, solution densities were assumed to be constant and conversion between molality and molarity scale was discarded.

Table 8.20. Thermodynamic Properties Related to Ag^+ - Na^+ Exchange Equilibrium.

A_s	A_z	α_B^A	K_m	Γ	K_c
0.0144	0.0966	7.3294	7.3294	1.0403	7.6246
0.0231	0.1513	7.5523	7.5523	1.0403	7.8565
0.0677	0.3503	7.4236	7.4236	1.0403	7.7225
0.0882	0.3170	4.7964	4.7964	1.0403	4.9896
0.1517	0.5148	5.9330	5.9330	1.0403	6.1719
0.1742	0.5612	6.0620	6.0620	1.0403	6.3061
0.3021	0.7129	5.7358	5.7358	1.0403	5.9668
0.3447	0.7479	5.6377	5.6377	1.0403	5.8647
0.4236	0.8377	7.0207	7.0207	1.0403	7.3035
0.4894	0.8416	5.5459	5.5459	1.0403	5.7692
0.5899	0.9033	6.4986	6.4986	1.0403	6.7604
0.5880	0.9178	7.8260	7.8260	1.0403	8.1412
0.7262	0.9155	4.0836	4.0836	1.0403	4.2481
0.8208	0.9596	5.1888	5.1888	1.0403	5.3978

Table 8.21. Thermodynamic Properties Related to Zn^{2+} - Na^{+} Exchange Equilibrium.

A_s	A_z	α_B^A	K_m	Γ	K_c
0.0209	0.0845	4.3189	4.6189	1.4724	6.8009
0.0242	0.0946	4.2134	4.5411	1.4730	6.6891
0.0664	0.1295	2.0929	2.2447	1.4802	3.3226
0.0761	0.1557	2.2374	2.4482	1.4819	3.6279
0.1923	0.2008	1.0554	1.0667	1.5014	1.6015
0.1880	0.2274	1.2713	1.3361	1.5007	2.0051
0.2658	0.2157	0.7596	0.7111	1.5134	1.0762
0.3372	0.2787	0.7594	0.6977	1.5250	1.0640
0.4170	0.3065	0.6179	0.5194	1.5377	0.7987
0.5393	0.3147	0.3923	0.2638	1.5567	0.4106
0.5639	0.3039	0.3376	0.2115	1.5605	0.3301
0.5564	0.3163	0.3689	0.2393	1.5594	0.3732
0.6915	0.3300	0.2197	0.1012	1.5798	0.1598
0.8233	0.3782	0.1306	0.0371	1.5993	0.0593
0.9165	0.4464	0.0734	0.0111	1.6128	0.0179

Table 8.22. Thermodynamic Properties Related to Cu^{2+} - Na^{+} Exchange Equilibrium.

A_s	A_z	α_B^A	K_m	Γ	K_c
0.0259	0.0656	2.6390	2.7511	1.4860	4.0883
0.0286	0.0739	2.7078	2.8402	1.4730	4.1836
0.0645	0.1189	1.9568	2.0776	1.4802	3.0753
0.0794	0.1237	1.6370	1.7199	1.4819	2.5486
0.1777	0.1839	1.0426	1.0504	1.5014	1.5771
0.1990	0.2129	1.0888	1.1081	1.5007	1.6628
0.2515	0.2468	0.9751	0.9690	1.5134	1.4665
0.3269	0.2296	0.6137	0.5362	1.5250	0.8178
0.4261	0.2727	0.5052	0.3987	1.5377	0.6130
0.7481	0.3585	0.1881	0.0739	1.5605	0.1153
0.6937	0.3234	0.2110	0.0955	1.5594	0.1490
0.8133	0.3933	0.1487	0.0458	1.5798	0.0723
0.9096	0.4750	0.0899	0.0155	1.5993	0.0247

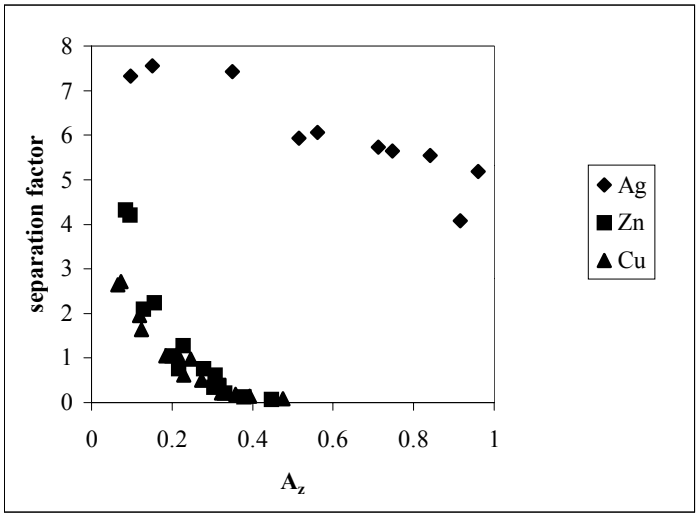

Figure 8.20. Variation of Separation Factors with Equivalent Fractions of Ingoing Cation in Zeolite Phase for Each Exchange.

In Figure 8.20, separation factors (α_B^A) for each exchange are presented. It was indicated that the separation factors of the investigated exchanges decreased as the equivalent fraction of the ingoing cation in zeolite increased. The good selectivity obtained for silver was confirmed with separation factors, substantially greater than unity. In the case of zinc and copper exchanges, above the equivalent fraction in solution phase at about 0.2, unselective behaviors were observed.

The thermodynamic equilibrium constants K_a were determined by the area under the curve ln K_c vs. A_z, known as Kielland plot. Kielland plots of observed equilbria are shown from Figure 8.21 to 8.23. Since partial exchanges are involved for zinc and copper exchanges, normalized forms of Kielland plots were used.

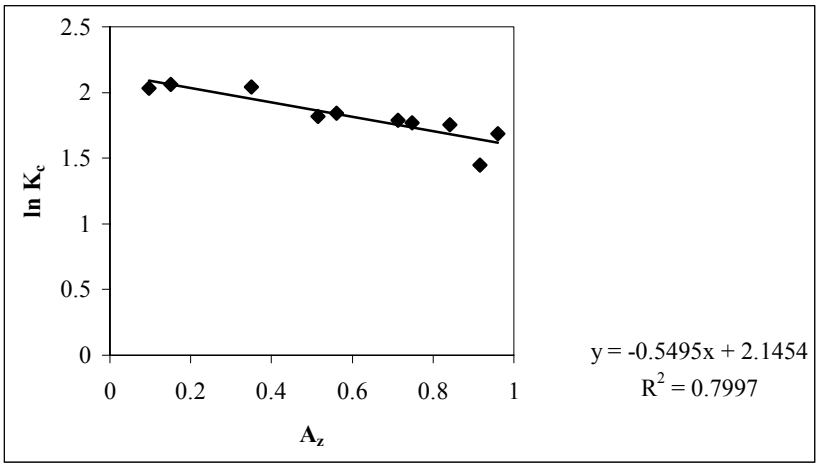

Figure 8.21. Kielland Plot of Ag^+ - Na^+ Exchange.

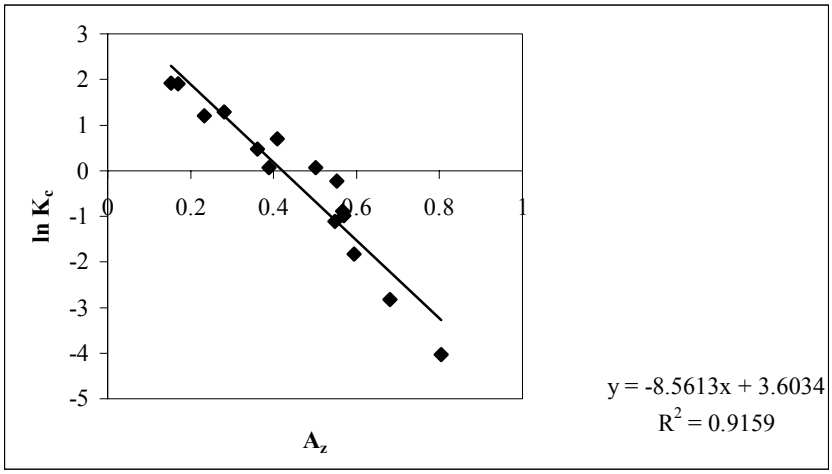

Figure 8.22. Normalized Kielland Plot of Zn^{2+} - Na^{+} Exchange.

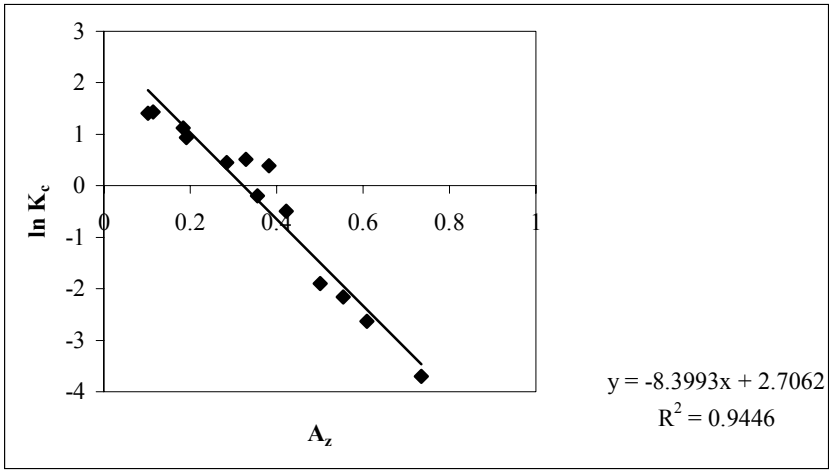

Figure 8.23. Normalized Kielland Plot of Cu^{2+} - Na^{+} Exchange.

Thermodynamic equilibrium constants, the standard free energies of exchanges calculated, and maximum exchange levels are given in Table 8.23. From the data in Table 8.23, following selectivity sequence was obtained: $Ag^{+} > Na^{+} > Zn^{2+} > Cu^{2+}$. Eisenmann theory may be used for the interpretation of this sequence. According to this theory, high Si/Al ratio of clinoptilolite brings about low anionic field that gives good selectivity towards cations of lower charge e.g. Ag^{+} and poor selectivity towards cations of higher charge, e.g. divalent cations (Langella et al. 2000). Higher polarizibility and ionic radius of silver may be another explanations of its preference by clinoptilolite.

Table 8.23. Maximum Exchange Levels, K_a, and ΔG^{θ} Values of Investigated Equilibria.

Cation Pair	x_{max}	K_a	ΔG^{θ} **(kJ/equiv)**
Ag^{+} - Na^{+}	1	11.25	-6.00
Zn^{2+} - Na^{+}	0.555	0.187	2.03
Cu^{2+} - Na^{+}	0.646	0.083	3.09

Poor selectivity of clinoptilolite towards copper may also be resulted from its higher hydration energy (Semmens and Seyfard 1978).

There is scarce of data concerned with Ag^{+} - Na^{+}, Zn^{2+} - Na^{+} and Cu^{2+} - Na^{+} exchange equilibria behavior of clinoptilolite. Langella et al. (2000), obtained the standard free energy of exchange values as 2.83 and 2.71 kj / equiv. for Zn^{2+} - Na^{+} and Cu^{2+} - Na^{+} pairs at the same experimental conditions. Therefore, the differences between the literature data and current study indicated that the cation exchange behavior of clinoptilolite depends on its original cationic composition.

Chapter 9

CONCLUSIONS

Ag, Zn, and Cu cation exchange properties of the original and sodium form of the clinoptilolite were investigated related to the possible utilization of Ag, Zn, and Cu exchanged form of the clinoptilolite as a low cost antibacterial material. The original, Na, Ag, Zn, and Cu forms of the clinoptilolite samples were characterized by FTIR spectroscopy, thermal analyses (TGA, DTA, and DSC), and N_2 physisorption studies. Chemical compositions of the original and Na form of the clinoptilolite were determined by ICP-AES using fusion dissolution method.

FTIR studies indicated that the band, which is formed due to the interactions of water molecules with the framework via hydrogen bonds, was mostly affected by cation exchange. From the thermal analyses results, it was obtained that water content and dehydration behavior of the clinoptilolite are dependent on composition. Adsorption affinity of the clinoptilolite was found to be another parameter affected by the cation composition. By considering radii of cations exchanged and nitrogen molecule and channel characteristics of the clinoptilolite, measured sorption capacity values showed N_2 adsorbed mainly on the external surface, macropores and mesopores of the solid. In the determination of the chemical compositions of the original and Na-clinoptilolite, standard addition method, gave better results according to the cation balance. However, this method suffered from the overestimated values of the total percentages. The comparisons of the results of the standard addition method and the direct calibration method with JRRS pointed out that there is a missing point in the determinations of sodium and silicon.

In the ion exchange studies, higher exchange capacity and good selectivity of clinoptilolite were obtained towards silver. Additionally, preliminary antibacterial tests showed that Ag- clinoptilolite has significant antibacterial activity against *Proteus spp*. and *Pseudomonas aeruginosa*. From these observations, Ag-clinoptilolite seemed to be promising antibacterial material. However, the differences in the results of the current study and the literature indicated that different cationic compositions of the minerals affected both cation exchange capacity and selectivity. Therefore, before any practical utilization of clinoptilolite mineral as a cation exchanger, specific studies on

representative samples should be carried out.

REFERENCES

1) Ackley, M, and Yang, R. T., "Diffusion in Ion-Exchanged Clinoptilolites", AIChE Journal, 37(11), 1991a, pp. 1645-1656.

2) Ackley, M, and Yang, R. T., "Adsorption Characteristics of High-Exchange Clinoptilolites", Industrial Engineering Chemistry Research, 30, 1991b, pp. 2523-2530.

3) Ackley, M., Giese, R. F., Yang, R. T., "Clinoptilolite: Untapped Potential for Kinetic Gas Separations", Zeolites, 12 (September/October), 1992, pp. 780-788.

4) Akdeniz, Y., Cation Exchange in Zeolite, Structure Modification by Using Microwave, M. S. Thesis, İzmir Institute of Technology, İzmir, 1999.

5) Allen, E. R., and Ming, D. W., "Recent Progress in the Use of Natural Zeolites in Agronomy and Horticulture", Natural Zeolites 93: Occurrence, Properties, Use, Ming, D. W., and Mumpton, F. A., International Committee on Natural Zeolites, New York, 1995, pp. 477- 490.

6) Arcoya, A., Gonzalez, J. A., Travieso, N., Seoane, X. L., "Physicochemical and Catalytic Properties of a Modified Natural Clinoptilolite", Clays and Clay Minerals, 29, 1994, pp. 123-131.

7) Arcoya, A., Gonzalez, J. A., Llabre, g., Seoane, X. L., Travieso, N., "Role of Countercations on the Molecular Sieve Properties of a Clinoptilolite", Microporous Materials, 7, 1996, pp. 1-13.

8) Armor, J. N., "Metal-Exchanged Zeolites as Catalysts", Microporous and Mesoporous Materials, 22, 1998, pp. 451-456.

9) Barrer, R. M., "Cation-Exchange Equilibria in Zeolites and Feldspathoids", Natural Zeolites: Occurrence, Properties and Use, Sand, L. B., and Mumpton, F. A., Pergamon, New York, 1978, pp. 385-395.

10) Bartko, P., Seidel, H., Kováč, "Use of Clinoptilolite from Slovakia in Animal Production: A Review", Natural Zeolites 93: Occurrence, Properties, Use, Ming, D. W., and Mumpton, F. A., International Committee on Natural Zeolites, New York, 1995, pp. 467-475.

11) Bish, D. L., "Effects of Composition on the Dehydration Behavior of Clinoptilolite and Heulandite", Occurrence, Properties and Utilization of Natural Zeolites, Kallo, D., and Sherry, H. S., 1988.

12) Breck, D. W., Zeolite Molecular Sieves Structure, Chemistry and Use, Wiley-

Interscience, New York, 1974.

13) Breck, D. W., "Potential Uses of Natural and Synthetic Zeolites in Industry", The Properties and Applications of Zeolites, Townsend, R. P., The Chemical Society, London, 1980, pp. 391-422.

14) Chelishchev, N. F., "Use of Natural Zeolites at Chernobyl", Natural Zeolites 93: Occurrence, Properties, Use, Ming, D. W., and Mumpton, F. A., International Committee on Natural Zeolites, New York, 1995, pp. 525-532.

15) CRC Handbook of Chemistry and Physics 1913-1995, edited by Lide D. R., Frederikse, H. P. R., CRC Press, Boca Raton, 1994.

16) Czaran, E., Papp, J., Meszaros-Kis, A., Domokos, E., "Ag-Ion Exchange by Natural Mordenite and Clinoptilolite", Acta Chimica Hungarica, 126(5), 1989, pp. 673-683.

17) Dyer, A., Enamy, H., Townsend, R. P., "The Plotting and Interpretation of Ion-Exchange Isotherms in Zeolite Systems", Separation Science and Technology, 16(2), 1981, pp. 173-181.

18) Eberl, D. D., Barbarick, K. A., Lai, T. M., "Influence of NH_4-Exchanged Clinoptilolite on Nutrient Concentrations in Sorgham-Sudangrass", Natural Zeolites 93: Occurrence, Properties, Use, Ming, D. W., and Mumpton, F. A., International Committee on Natural Zeolites, New York, 1995, pp. 491-513.

19) Esenli, F., and Kumbasar, I., "Thermal Behavior of Heulandites and Clinoptilolites of Western Anatolia", Zeolites and Related Microporous Materials: State of Art, Weitkamp, J., Karge, H., Hölderich, W., Elsevier, Amsterdam, 1994.

20) Flenigen, E. M., "Molecular Sieve Zeolite Technology: The First Twenty-Five Years", Zeolites: Science and Technology Nato ASI Series No:80, Ribeiro, F. R., Rodrigues, A. E., Rollman, L. D., Naccache, C., Martinus Nijhoff Publishers, The Hague, 1984, pp. 3-34.

21) Goryainov, S. V., Stolpovskaya, V. N., Likhacheva, A. Y., Belitsky, I. A., Fursenko, B. A., "Determination of Clinoptilolite and Heulandite in Tuffaceous Deposits by Infrared Spectroscopy", Natural Zeolites 93: Occurrence, Properties, Use, Ming, D. W., and Mumpton, F. A., International Committee on Natural Zeolites, New York, 1995, pp. 245-255.

22) Gotardi, G., and Galli, E., Natural Zeolites, Springer-Verlag, Berlin, 1985.

23) Grant, D. C., Skriba, M. C., Saha, A. K., "Removal of Radioactive Contaminants from West Valley Waste Streams Using Natural Zeolites", Environmental Progress, 6(2), 1987, pp. 104-109.

24) Hagiwara, Z., Hoshino, S., Ishirin, H., Nohara, S., Tagawa, K., Yamanaka, K., "Zeolite Particles Retaining Silver Ions Having Antibacterial Properties", U. S. Patent, 4911898, 1990.

25) Helfferich, F., Ion Exchange, McGraw-Hill, New York, 1962.

26) Hernandez, M. A., Corona, L., Rojas, F., "Adsorption Characteristics of Natural Erionite, Clinoptilolite and Mordenite Zeolites from Mexico", Adsorption, 6, 2000a, pp. 33-45.

27) Hernandez, M. A., Rojas, F., Lara, V. H., "Nitrogen-Sorption Characterization of the Microporous Structure of Clinoptilolite- Type Zeolites", Journal of Porous Materials, 7, 2000b, pp. 443-454.

28) Hotta, M., Nakajima, H., Yamamoto, K., Aono, M., "Antibacterial Temporary Filling Materials: The Effect of Adding Various Ratios of Ag-Zn-Zeolite", Journal of Oral Rehabilitation, 25, 1998, pp. 485-489.

29) James M. Montgomery Consulting Engineers, Water Treatment Principles and Design, John Wiley & Sons, New York, 1985.

30) Jorgensen, S. E., "Ammonia Removal by Use of Clinoptilolite", Water Research, 10, 1976, pp. 213-224.

31) Kalló, D., "Wastewater Purification in Hungary Using Natural Zeolites", Natural Zeolites 93: Occurrence, Properties, Use, Ming, D. W., and Mumpton, F. A., International Committee on Natural Zeolites, New York, 1995, pp. 341-350.

32) Karge, H. G., " Characterization by Infrared Spectroscopy", Microporous Materials, 22, 1998, pp. 547-549.

33) Kasture, M. W., Joshi, P. N., Soni, H. S., Joshi, V. V., Choudhari, A. L., Shirall, V. P., "Sorption Properties of the Natural, K and Partially Deammoniated (H/NH_4) Forms of Clinoptilolite", Adsorption Science & Technology, 16(2), 1998, pp. 135-151.

34) Kawahara, K., Tsuruda, K., Morishita, M., Uchida, M., "Antibacterial Effect of Silver-Zeolite on Oral Bacteria under Anaerobic Conditions", Dental Materials, 16, 2000, pp. 452-455.

35) Kesraoui-Ouki, S., Cheeseman, C. R., Perry, R., "Effects of Conditioning and Treatment of Chabazite and Clinoptilolite Prior to Lead and Cadmium Removal", Environmental Science and Technology, 27, 1993, pp. 1108-1116.

36) Kesraoui-Ouki, S., Cheeseman, C. R., Perry, R., "Natural Zeolite Utilisation in Pollution Control: A Review of Application to Metals' Effluents", Journal of Chemical Technology & Biotechnology, 59, 1994, pp. 121-126.

37) Klieve, J. R., and Semmens, M. J., "An Evaluation of Pretreated Natural Zeolites for Ammonium Removal", Water Research, 14, 1980, pp. 161-168.
38) Knowlton, G. D., White, T. R., McKague, H., L., "Thermal Study of Types of Water Associated with Clinoptilolite", Clays and Clay Minerals, 29(5), 1981, pp. 403-411.
39) Krivacsy, Z., Hlavay, J., "A Simple Method for the Determination of Clinoptilolite in Natural Zeolite Rocks", Zeolites, 15, 1995, pp. 551-555.
40) Kubota, K., Katoh, T., Hirata, M., Hayashi, K., "Dyed Synthetic Fiber Comprising Silver-Substituted Zeolite and Copper Compound and Process for Preparing Same", U. S. Patent, 5180402, 1993.
41) Langella, A., Pansini, M., Cappelletti, P., de Gennaro, B., de Gennaro, M., Colella, C., "NH_4^+, Cu^{2+}, Zn^{2+}, Cd^{2+}, and Pb^{2+} Exchange for Na^+ in a Sedimentary Clinoptilolite, North Sardinia, Italy", Microporous and Mesoporous Materials, 37, 2000, pp. 337-343.
42) Lechert, H., "The Physical Characterization of Zeolites", Zeolites: Science and Technology Nato ASI Series No:80, Ribeiro, F. R., Rodrigues, A. E., Rollman, L. D., Naccache, C., Martinus Nijhoff Publishers, The Hague, 1984, pp. 151-192.
43) Liberatore, P. A., "Determination of Majors in Geological Samples by ICP-AES", Varian Instruments, ICP-12, 1993.
44) Liberatore, P. A. "Determination of Trace Elements in Geological Samples by ICP-AES", Varian Instruments, ICP-16, 1994.
45) Liberti, L., Lopez, A., Amicarelli, V., Boghetich, G., "Pollution-Abatement Technologies by Natural Zeolites: The Rim-Nut Process", Natural Zeolites 93: Occurrence, Properties, Use, Ming, D. W., and Mumpton, F. A., International Committee on Natural Zeolites, New York, 1995, pp. 351-362.
46) Maxwell, I. E., and Stork, W. H. J., "Hydrocarbon Processing with Zeolites", Introduction to Zeolite Science and Practice, van Bekkum, H., Flenigen, E. M., Jansen, J. C., Elsevier, Amsterdam, 1991.
47) Mercer, B. W., and Ames, L. L., "Zeolite Ion Exchange in Radioactive and Municipal Wastewater Treatment", Natural Zeolites: Occurrence, Properties and Use, Sand, L. B., and Mumpton, F. A., Pergamon, New York, 1978, pp. 451- 460.
48) Moscou, L., "The Zeolite Scene", Introduction to Zeolite Science and Practice, van Bekkum, H., Flenigen, E. M., Jansen, J. C., Elsevier, Amsterdam, 1991, pp. 1-11.
49) Mumpton, F. A., "Natural Zeolites: Where have We been? Where are We Going?", 4th FEZA Euroworkshop on Zeolites, Natural Zeolites: Occurrence, Properties and Use, Italy, 1997.

50) Murphy, C. B., Hrycyk, O., Gleason, W. T., "Natural Zeolites: Novel Uses and Regeneration in Wastewater Treatment", Zeolite 1976 Conference, Arizona.

51) Niira, R., Yamamoto, T., Uchida, M., "Antibiotic Zeolite", U. S. Patent, 4938958, 1990.

52) Onyestyák, G., Kalló D., "Cd-Clinoptilolite as a Catalyst for the Hydration of Acetylene to Acetaldehyde", Natural Zeolites 93: Occurrence, Properties, Use, Ming, D. W., and Mumpton, F. A., International Committee on Natural Zeolites, New York, 1995, pp. 437-445.

53) Özkan, S. F., Adsorbent Dolgulu Kolonların Dinamik Davranışının Deneysel ve Teorik Olarak İncelenmesi, Ph D. Thesis, Ege University, İzmir, 1996.

54) Pabalan, R. T., "Thermodynamics of Ion Exchange Between Clinoptilolite and Aqueous Solutions of Na^+/K^+ and Na^+/Ca^{2+}", Geochimica et Cosmochimica Acta, 58(21), 1994, pp. 4573-4590.

55) Pond, W. G., "Zeolites in Animal Nutrition and Health: A Review", Natural Zeolites 93: Occurrence, Properties, Use, Ming, D. W., and Mumpton, F. A., International Committee on Natural Zeolites, New York, 1995, pp. 449-457.

56) Rivera-Garza, M., Olguin, M. T., Garcia-Sosa, I., Alcantara, D., and Rodriguez-Fuentes, G., "Silver Supported on Natural Mexican Zeolite as an Antibacterial Material", Microporous and Mesoporous Materials, 39, 2000, pp. 431-444.

57) Rodriguez- Fuentes, G., Ruiz-Salvador, A. R., Mir, M., Picazo, O., Quintana, G., Delgado, M., "Thermal and Cation Influence on IR Vibrations of Modified Natural Clinoptilolite", Microporous and Mesoporous Materials, 20, 1998, pp. 269-281.

58) Rouquerol, F., Rouquerol, J., Sing, K. S. W., Adsorption by Powders and Porous Solids: Principles, Methodology and Applications, Academic Press, San Diego, 1999.

59) Semmens, M. J., and Martin, W. P., "The Influence of Pretreatment on the Capacity and Selectivity of Clinoptilolite for Metal Ions", Water Research, 22(5), 1988, pp. 537-542.

60) Semmens, M. J., and Seyfard, M., "The Selectivity of Clinoptilolite for Certain Heavy Metals", Natural Zeolites: Occurrence, Properties and Use, Sand, L. B., and Mumpton, F. A., Pergamon, New York, 1978, pp. 517-526.

61) Sherman, J. D., "Ion Exchange Separations with Molecular Sieve Zeolites", Adsorption and Ion Exchange Separations, AIChE Symposium Series No: 179, The American Institute of Chemical Engineers, 1978, pp. 98-116.

62) Sherry, H. S., and Walton, H. F., "The Ion Exchange Properties of Zeolites II. Ion

Exchange in the Synthetic Zeolite Linde 4-A", Ion Exchange Properties of Zeolites, Vol: 71, No:5, 1967.

63) Sing, K. S. W., Everett, D. H., Haul, R. A. W., Moscou, L., Pierutti, R. A., Rouquerol, J., Sieminiewski, T., "Reporting Physisorption Data for Gas/Solid Systems with Special Reference to the Determination of Surface Area and Porosity", Pure & Applied Chemistry, 57(4), 1985, pp. 603-619.

64) Sing, K. S. W., "Characterization of Adsorbents", Adsorption Science and Technology, NATO ASI Series Vol: 158, Rodrigues, A. E., Le Van, M. D., 1988.

65) Smyth, J. R., Spaid, A. T., Bish, D. L., "Crystal Structures of a Natural and a Cs-Exchanged Clinoptilolite", American Mineralogist, 75, 1990, pp. 522-528.

66) Torii, K., "Utilization of Natural Zeolites in Japan", Natural Zeolites: Occurrence, Properties and Use, Sand, L. B., and Mumpton, F. A., Pergamon, New York, 1978, pp. 441-450.

67) Townsend, R. P., "Ion Exchange in Zeolites: Some Recent Developments in Theory and Practice", Pure & Applied Chemistry, 58(10), 1986, pp. 1359-1366.

68) Townsend, R. P., "Ion Exchange in Zeolites", Introduction to Zeolite Science and Practice, van Bekkum, H., Flenigen, E. M., Jansen, J. C., Elsevier, Amsterdam, 1991, pp. 359-389.

69) Tsitsishvili G. V., Andronikashvili, T. G., Kirov, G. N., Filizova, L., D., Natural Zeolites, Ellis Horwood, New York, 1992.

70) Van Hooff, J. H. C., and Roelofsen, J. W., "Techniques of Zeolite Characterization", Introduction to Zeolite Science and Practice, van Bekkum, H., Flenigen, E. M., Jansen, J. C., Elsevier, Amsterdam, 1991, pp. 241-283.

71) Webb P. A., and Clyde, O., Analytical Methods in Fine Particle Technology, Micromeritics Instrument Corporation, USA, 1997.

72) Yücel, H., and Çulfaz, A., "Yerel ve Doğal Klinoptilolit Zeolitinin Fiziksel ve Kimyasal Özellikleri", Doğa Bilim Dergisi, 9(3), 1985, pp. 288-296.

73) Zamzow, M. J., and Murphy, J. E., "Removal of Metal Cations from Water Using Zeolites", Separation Science and Technology, 27(14), 1992, pp. 1969-1984.

74) Zamzow, M. J., and Schultze, L. E., "Treatment of Acid Mine Drainage Using Natural Zeolites", Natural Zeolites 93: Occurrence, Properties, Use, Ming, D. W., and Mumpton, F. A., International Committee on Natural Zeolites, New York, 1995, pp. 405-413.

75) Zhao, D., Cleare, K, Oliver, C., Ingram, C., Cook, D. , Szostak, R., Kevan, L.,

“Characteristics of the Synthetic Heulandite-Clinoptilolite Family of Zeolites”, Microporous and Mesoporous Materials, 21, 1998, pp. 371-379.

APPENDIX

A.1. Determination of the Activity Ratios in Solution Phase

A.1.1. Theory

The activity of a component provides a basis to describe its chemical potential, which is the measure of thermodynamic properties of the system when matter enters or leaves represented as follows:

$$\mu_i = \mu_i^o + RT \ln (a_i/a_i^o) \quad (A.1)$$

where μ_i^o = standard chemical potential of component i

a_i = activity of component i

a_i^o = standard activity with a value of unity

There is no restriction for the choice of the standard state. For example, when the composition of the solution is given in terms of molality scale, the standard state is "hypothetical one-molal solution" of the ion. The ratio a_i/m_i, defined as the molal activity coefficient γ_i, represents the nonidealities in the solution phase and it takes the value of unity in the ideal case. Hence, chemical potential of individual ionic species can be written as (Pitzer 1991) :

$$\mu_i = \mu_{i(m)}^o + RT \ln (m_i \gamma_i) \quad (A.2)$$

Activity ratio, Γ can be described by single ion activity coefficients as follows:

$$\Gamma = \gamma_B^{z_A} / \gamma_A^{z_B} \quad (A.3)$$

where $\gamma_{A,B}$ = single ion activity coefficients in the solution of the ions $A^{z_A^+}$ and $B^{z_B^+}$ respectively (Dyer et al. 1981).

However, it is not possible to measure activity coefficients of the individual ions directly. Therefore, thermodynamic properties of the electrolytes as a whole are required to determine properties of the individual ions (Pitzer 1991). For the salt with the general formula of $A_{\nu_A}X_{\nu_X}$ where X is the anion and ν_A, ν_X refer to salt stoichiometry, the mean salt activity coefficient is (Dyer et al. 1981):

$$\gamma_{\pm(A_{\nu_A}X_{\nu_X})} = \left[\gamma_A^{z_X} \cdot \gamma_X^{z_A}\right]^{(1/(z_A+z_X))} \quad (A.4)$$

and

$$\Gamma = \gamma_B^{z_A} / \gamma_A^{z_B} = \left[\gamma_{\pm(BX)}\right]^{z_A (z_B + z_X)/z_X} \left[\gamma_{\pm(AX)}\right]^{-z_B (z_A + z_X)/z_X} \quad \text{(A.5)}$$

For a single salt the mean molal activity coefficient (up to 2 M) can be presented by the following model (Pitzer 1991):

$$f^{\gamma} = -A_{\varphi}\left[I^{1/2}/(1 + b\, I^{1/2}) + (2/b) \ln (1 + b\, I^{1/2})\right] \quad \text{(A.6)}$$

$$B_{AX}^{\varphi} = \beta_{AX}^{(0)} + \beta_{AX}^{(1)} \exp(-\alpha\, I^{1/2}) \quad \text{(A.7)}$$

$$B_{AX} = \beta_{AX}^{(0)} + \beta_{AX}^{(1)}\, g(\alpha\, I^{1/2}) \quad \text{(A.8)}$$

$$g(x) = 2\left[1 - (1 + x)\exp(-x)\right]/x^2 \quad \text{(A.9)}$$

$$B_{AX}^{\gamma} = B_{AX} + B_{AX}^{\varphi} \quad \text{(A.10)}$$

$$\ln \gamma_{\pm} = \left|z_A\, z_X\right| f^{\gamma} + m\,(2\nu_A\, \nu_X/\nu)\, B_{AX}^{\nu} \quad \text{(A.11)}$$

where m = molality of the salt (mol / kg)

$$I = \text{ionic strength} = \frac{1}{2}\sum_i m_i\, z_i^2 \quad \text{(A.12)}$$

$$m_i = \nu_i\, m \quad \text{(A.13)}$$

A_ϕ = Debye-Hückel parameter (0.3915 (kg / mol)$^{1/2}$ at 25 ^{o}C)

b = universal parameter (1.2 (kg / mol)$^{1/2}$)

α = constant (2.0 (kg / mol)$^{1/2}$ for 1-1-, 1-2-, and 2-1- type salts at 25 ^{o}C)

$\beta_{AX}^{(0)}, \beta_{AX}^{(1)}$ = constants specific to each salt

However, Γ is described in terms of pure and separate solutions of two salts ($A_{\nu_A}X_{\nu_X}$ and $B_{\nu_B}X_{\nu_X}$) rather than for the salts in mixed solutions in Eq. (5). Required expression of activity coefficients of the salts in mixed is Glueckauf extension of

Guggenheim's original theory expressed as follows:

$$\log \gamma_{(\pm AX)}^{(BX)} = \log \gamma_{\pm(AX)} - \left(\frac{m_B}{4I}\right)\left\{k_1 \log \gamma_{\pm(AX)} - k_2 \log \gamma_{\pm(BX)} - \frac{k_3}{(1 + I^{-1/2})}\right\} \quad \text{(A.14)}$$

$$\log \gamma_{(\pm BX)}^{(AX)} = \log \gamma_{\pm(BX)} - \left(\frac{m_A}{4I}\right)\left\{k_4 \log \gamma_{\pm(BX)} - k_5 \log \gamma_{\pm(AX)} - \frac{k_6}{(1 + I^{-1/2})}\right\} \quad \text{(A.15)}$$

where

$$k_1 = z_B\,(2\, z_B - z_A + z_X) \quad \text{(A.16)}$$

$$k_2 = z_A\,(z_B + z_X)^2\,(z_A + z_X)^{-1} \quad \text{(A.17)}$$

$$k_3 = 0.5\left[z_A\, z_B\, z_X\,(z_A - z_B)^2\,(z_A + z_X)^{-1}\right] \quad \text{(A.18)}$$

$$k_4 = z_A\,(2\,z_A - z_B + z_X) \tag{A.19}$$

$$k_5 = z_B\,(z_A + z_X)^2\,(z_B + z_X)^{-1} \tag{A.20}$$

$$k_6 = 0.5\left[z_A\,z_B\,z_X\,(z_B - z_A)^2\,(z_B + z_X)^{-1}\right] \tag{A.21}$$

Note: a) equations are given in decadic logarithms

b) values of the mean activity coefficients for pure salts $\gamma_{\pm(AX)}$ and $\gamma_{\pm(BX)}$ to be inserted are those that are found for the relevant pure salts at the same ionic strength as the mixed solution of interest. If the exchange is not uni-univalent, I will change with A_s so the values of $\gamma_{\pm(AX)}$ and $\gamma_{\pm(BX)}$ that are inserted

c) in the calculation of I summation should be carried out <u>all</u> the ions present.

Calculation procedure for the solution activity correction can be summarized as follows:

(1) The ionic strength of each solution should be calculated as a function of A_s

(2) For each solution values $\gamma_{\pm(AX)}$ and $\gamma_{\pm(BX)}$ should be obtained from the literature or the model given for that ionic strength

(3) These should be inserted to Eqs. A.14 and A.15 to obtain values of the mean activity coefficients in the mixed solutions

(4) Finally, Γ for each solution (i.e. at each point on isotherm) may be calculated from Eq. A.5 (Dyer et al. 1981).

A.1.2. Model Requirements

Table A.1. Constants Specific to Each Salt for Pitzer Model (Pitzer 1991).

Salt	$\beta^{(0)}$	$\beta^{(1)}$
$NaNO_3$	0.0068	0.1783
$AgNO_3$	-0.0856	0.0025
$Zn(NO_3)_2$	0.3481	1.6913
$Cu(NO_3)_2$	0.2807	1.7325

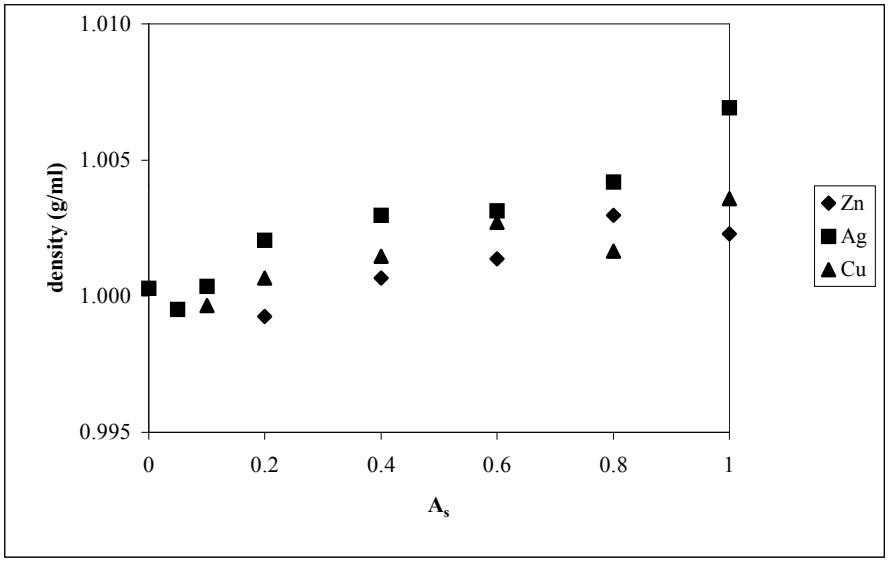

Figure A.1. Variations of the Solution Densities Determined Experimentally at 25 ^{o}C, as a Function of Equivalent Fractions of Ingoing Cation.

A.1.3. Activity Coefficients of Pure Salts

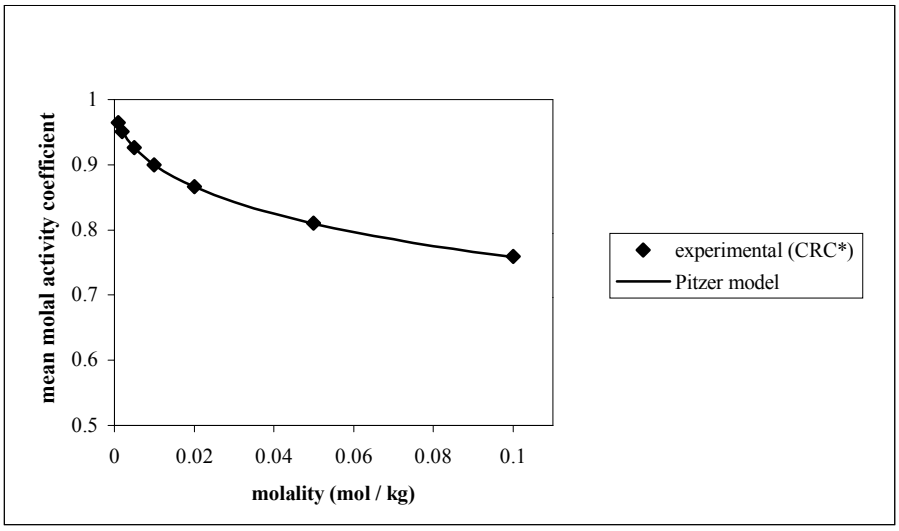

Figure A.2. Comparison of the Experimental and Model Mean Molal Activity Coefficient Values for Pure $NaNO_3$ Solutions.(*CRC Handbook of Chemistry and Physics 1913-1995 (1994))

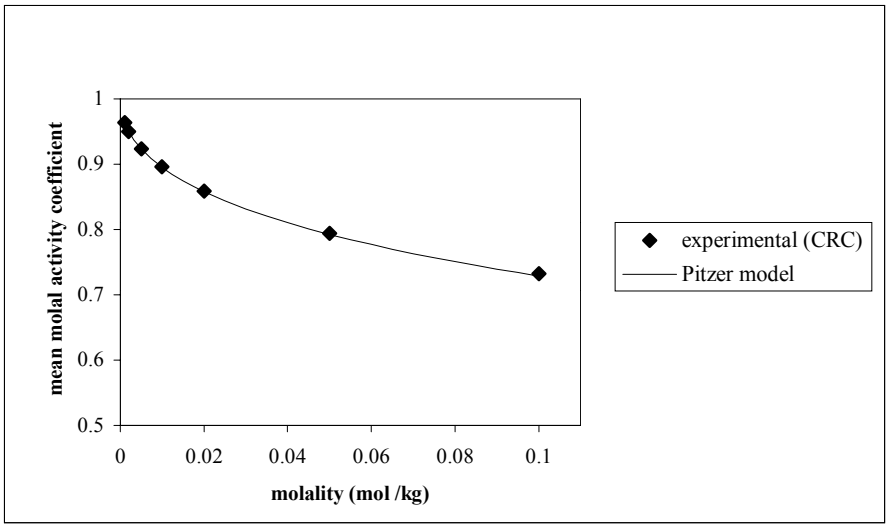

Figure A.3. Comparison of the Experimental and Model Mean Molal Activity Coefficient Values for Pure $AgNO_3$ Solutions.

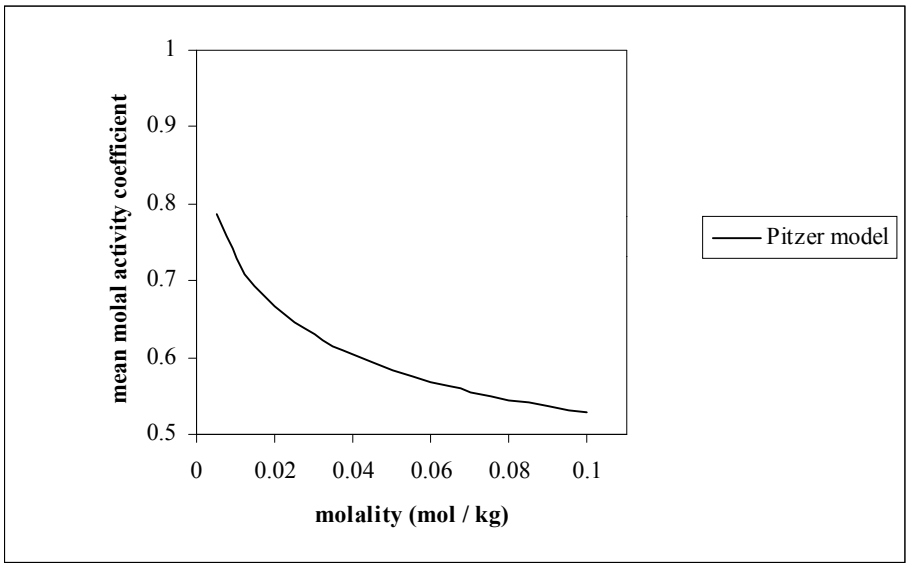

Figure A.4. Model Mean Molal Activity Coefficient Values for Pure $Zn(NO_3)_2$ Solutions (Experimental data is not available).

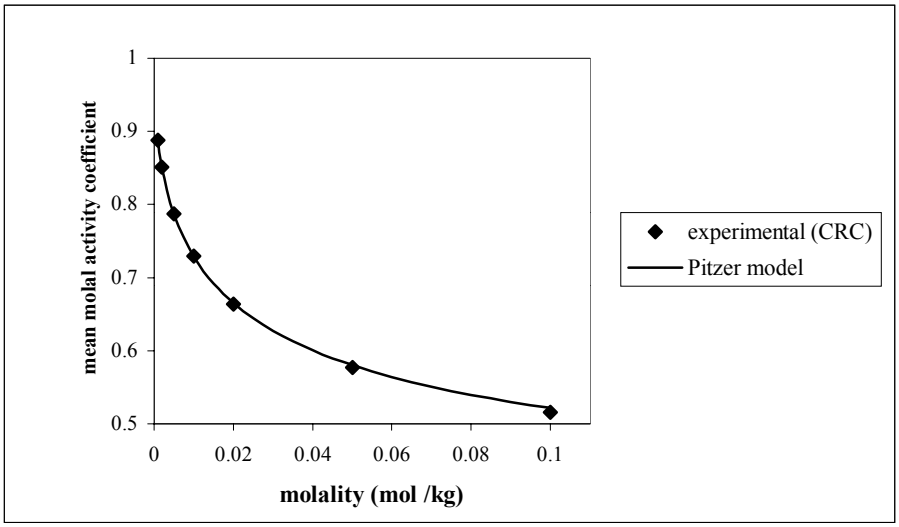

Figure A.5. Comparison of the Experimental and Model Mean Molal Activity Coefficient Values for Pure $Cu(NO_3)_2$ Solutions.

A.1.4. Sample Program in Q-Basic Language

```
      CLS
      REM ***************************************************************
      REM *   THIS PROGRAM CALCULATES SOLUTION ACTIVITY RATIOS           *
      REM *   AS A FUNCTION OF EQUIVALENT FRACTIONS. IT DETERMINES       *
      REM *   ACTIVITY COEFFICIENTS OF THE PURE ELECTROLYTES, THEN       *
      REM *   USES GLUECKAUF METHOD FOR THE ACTIVTY COEFFICIENTS         *
      REM *   OF THE MIXED SOLUTION                                      *
      REM ***************************************************************
      REM PARAMETERS OF THE ELECTROLYTES
      REM ***************************************************************
      REM *   SUBSCRIPT A REPRESENTS INGOING CATION                      *
      REM *   WHILE B IS OUTGOING CATION,                                *
      REM *   X IS DEFINED AS THE ANION ASOCCIATED                       *
      REM *   AND COMMON IN BOTH SALTS                                   *
      REM ***************************************************************
      OPEN "A:/ACTC.DAT" FOR OUTPUT AS #1
      INPUT " TOTAL NORMALITY="; TN
      PRINT " enter electrolyte parameters for activity coefficients"
      PRINT " ELECTROLYTE AX "
      INPUT " coefficient of the cation ="; NUA
      INPUT " coefficient of the anion="; NUXA
      INPUT " charge of the cation="; ZA
      INPUT " charge of the anion="; ZX
      INPUT " beta 0 ="; BT0AX
      INPUT " beta 1="; BT1AX
      PRINT " ELECTROLYTE BX "
      INPUT " coefficient of the cation ="; NUB
      INPUT " coefficient of the anion="; NUXB
      INPUT " charge of the cation="; ZB
      INPUT " beta 0 ="; BT0BX
      INPUT " beta 1="; BT1BX
      ATH = .3915
      SB = 1.2
      ALPHA = 2
      WRITE #1, " EAS   IOS   GAMA   GAMB   GAMAB   GAMBA   CGAM "
      REM ASSIGNMENT OF THE MOLARITY VALUES OF EACH ELECTROLYTE
      MAX = 0
      DELM = TN / 20
5     MBX = (TN - (MAX * ZA * NUA)) / (ZB * NUB)
      NUAX = NUA + NUXA
      NUBX = NUB + NUXB
      REM CALCULATION OF THE IONIC STRENGTH OF EACH ELECTROLYTE
      IOSAX = 0
      IOSBX = 0
      MA = MAX * NUA
      MB = MBX * NUB
      MXAX = MAX * NUXA
      MXBX = MBX * NUXB
      IOSAX = .5 * ((MA * ZA ^ 2) + (MXAX * ZX ^ 2))
      IOSBX = .5 * ((MB * ZB ^ 2) + (MXBX * ZX ^ 2))
      REM CALCULATION OF THE TOTAL IONIC STRENGTH OF THE SOLUTION
      IOS = IOSAX + IOSBX
      REM CALCULATIONS OF THE SOLUTION EQUIVALENT FRACTIONS
      EAS = ZA * MA / TN
      REM APPLICATION OF THE PURE ELECTRODE ACTIVITY COEFFICIENT MODEL
      DEF FNG (X) = 2 * (1 - ((1 + X) * EXP(-X))) / (X ^ 2)
```

```
        REM CALCULATIONS OF THE MOLALITIES FOR TOTAL IONIC STRENGTH
        MAX = (IOS * 2) / ((NUA * (ZA ^ 2)) + (NUXA * (ZX ^ 2)))
        MBX = (IOS * 2) / ((NUB * (ZB ^ 2)) + (NUXB * (ZX ^ 2)))
        BPHAX = BT0AX + (BT1AX * EXP(-ALPHA * (IOS ^ .5)))
        BPHBX = BT0BX + (BT1BX * EXP(-ALPHA * (IOS ^ .5)))
        BAX = BT0AX + (BT1AX * FNG(ALPHA * (IOS ^ .5)))
        BBX = BT0BX + (BT1BX * FNG(ALPHA * (IOS ^ .5)))
        FG = -ATH * (((IOS ^ .5) / (1 + (SB * (IOS ^ .5)))) +((2 / SB) * (LOG(1 + (SB * (IOS ^ .5))))))
        BGAX = BAX + BPHAX
        BGBX = BBX + BPHBX
        GAMA = EXP(ABS(ZA * ZX) * FG +(MAX * (2 * NUA * NUXA / NUAX * BGAX)))
        GAMB = EXP(ABS(ZB * ZX) * FG +(MBX * (2 * NUB * NUXB / NUBX * BGBX)))
        REM REASSIGNMENTS OF THE MOLARITY VALUES
        MAX = MA / NUA
        MBX = MB / NUB
        REM GLUECHKAUF METHOD FOR MIXTURE OF TWO ELECTROLYTES
        K1 = ZB * (2 * ZB - ZA + ABS(ZX))
        K2 = ZA * ((ZB + ABS(ZX)) ^ 2) * (1 / (ZA + ABS(ZX)))
        K3 = .5 * (ZA * ZB * ABS(ZX) * ((ZA - ZB) ^ 2) *(1 / (ZA + ABS(ZX))))
        K4 = ZA * (2 * ZA - ZB + ABS(ZX))
        K5 = ZB * ((ZA + ABS(ZX)) ^ 2) * ((1 / (ZB + ABS(ZX))))
        K6 = .5 * (ZA * ZB * ABS(ZX) * ((ZB - ZA) ^ 2) * (1 / (ZB + ABS(ZX))))
        GAMAB = 10 ^ ((LOG(GAMA) / 2.302585) - ((MB / (4 * IOS)) *      ((K1 * LOG(GAMA) /
        2.302585) - (K2 * LOG(GAMB) / 2.302585) - (K3 / (1 + (1 / SQR(IOS)))))))
        GAMBA = 10 ^ ((LOG(GAMB) / 2.302585) - ((MA / (4 * IOS)) *    ((K4 * LOG(GAMB) /
        2.302585) - (K5 * LOG(GAMA) / 2.302585) -  (K6 / (1 + (1 / SQR(IOS)))))))
        REM CALCULATIONS OF ACTIVITY RATIOS
        CGAM = (GAMBA ^ (ZA * (ZB + ABS(ZX)) / ABS(ZX))) *   (GAMAB ^ (-ZB * (ZA +
        ABS(ZX)) / ABS(ZX)))
        WRITE #1, EAS, IOS, GAMA, GAMB, GAMAB, GAMBA, CGAM
        MAX = MAX + DELM / ZA
        IF EAS > 1 THEN GOTO 10
        GOTO 5
10      END
```

A.1.4.1. List of Abbreviations Used in the Program

TN = Total normality of the solution

NUA = stoichiometric coefficient of cation A in salt AX

NUXA = stoichiometric coefficient of anion X in salt AX

ZA = charge of the cation A

ZX = charge of the anion X

BT0AX = $\beta_{AX}^{(0)}$ = constant specific to AX

BT1AX = $\beta_{AX}^{(1)}$ = constant specific to AX

NUB = stoichiometric coefficient of cation B in salt BX

NUXB = stoichiometric coefficient of anion X in salt BX

ZB = charge of the cation B

BT0BX = $\beta_{BX}^{(0)}$ = constant specific to BX

BT1BX = $\beta_{BX}^{(1)}$ = constant specific to BX

ATH = A_ϕ = Debye-Hückel parameter (0.3915 $(kg / mol)^{1/2}$ at 25 ^oC)

SB = b = universal parameter (1.2 $(kg / mol)^{1/2}$)

ALPHA = α = constant (2.0 $(kg / mol)^{1/2}$ for 1-1-, 1-2-, and 2-1- type salts at 25 ^oC)

MAX = molarity of salt AX

DELM = increment value of molarity of salt AX

MBX = molarity of salt BX

NUAX = summation of the stoichiometric coefficients of cation A and anion X in salt AX

NUBX = summation of the stoichiometric coefficients of cation B and anion X in salt BX

IOSAX = ionic strength of the electrolyte AX

IOSBX = ionic strength of the electrolyte BX

IOS = total ionic strength of the solution

EAS = equivalent fraction of cation A in solution phase

FNG (X) $= g(x) = 2\left[1-(1+x)\exp(-x)\right]/x^2$

BPHAX $= B_{AX}^{\varphi} = \beta_{AX}^{(0)} + \beta_{AX}^{(1)} \exp(-\alpha I^{1/2})$

BPHBX $= B_{BX}^{\varphi} = \beta_{BX}^{(0)} + \beta_{BX}^{(1)} \exp(-\alpha I^{1/2})$

BAX $= B_{AX} = \beta_{AX}^{(0)} + \beta_{AX}^{(1)}\, g(\alpha I^{1/2})$

BBX = $B_{BX} = \beta_{BX}^{(0)} + \beta_{BX}^{(1)}\, g\,(\alpha\, I^{1/2})$

FG = $f^{\gamma} = -A_{\varphi}\left[I^{1/2}/(1 + b\, I^{1/2}) + (2/b)\ln(1 + b\, I^{1/2})\right]$

BGAX = $B_{AX}^{\gamma} = B_{AX} + B_{AX}^{\varphi}$

BGBX = $B_{BX}^{\gamma} = B_{BX} + B_{BX}^{\varphi}$

GAMA = mean activity coefficient of the pure salt AX

GAMB = mean activity coefficient of the pure salt BX

K1 = $k_1 = z_B\,(2\,z_B - z_A + z_X)$

K2 = $k_2 = z_A\,(z_B + z_X)^2\,(z_A + z_X)^{-1}$

K3 = $k_3 = 0.5\left[z_A\, z_B\, z_X\,(z_A - z_B)^2\,(z_A + z_X)^{-1}\right]$

K4 = $k_4 = z_A\,(2\,z_A - z_B + z_X)$

K5 = $k_5 = z_B\,(z_A + z_X)^2\,(z_B + z_X)^{-1}$

K6 = $k_6 = 0.5\left[z_A\, z_B\, z_X\,(z_B - z_A)^2\,(z_B + z_X)^{-1}\right]$

GAMAB = mean activity coefficient of the electrolyte AX in the presence of BX

GAMBA = mean activity coefficient of the electrolyte BX in the presence of AX

CGAM = activity ratio

A.1.4.2. Outputs of the Program

Table A.2. Output of the Computer Program for Mixed $AgNO_3$ – $NaNO_3$ Solutions.

A_s	I	$\gamma_{\pm(AgNO_3)}$	$\gamma_{\pm(NaNO_3)}$	$\gamma_{\pm(AgNO_3)}^{(NaNO_3)}$	$\gamma_{\pm(NaNO_3)}^{(AgNO_3)}$	Γ
0	0.1	0.7287	0.7581	0.7432	0.7581	1.0403
0.05	0.1	0.7287	0.7581	0.7425	0.7573	1.0403
0.1	0.1	0.7287	0.7581	0.7418	0.7566	1.0403
0.15	0.1	0.7287	0.7581	0.7410	0.7558	1.0403
0.2	0.1	0.7287	0.7581	0.7403	0.7551	1.0403
0.25	0.1	0.7287	0.7581	0.7396	0.7543	1.0403
0.3	0.1	0.7287	0.7581	0.7389	0.7536	1.0403
0.35	0.1	0.7287	0.7581	0.7381	0.7528	1.0403
0.4	0.1	0.7287	0.7581	0.7374	0.7521	1.0403
0.45	0.1	0.7287	0.7581	0.7367	0.7514	1.0403
0.5	0.1	0.7287	0.7581	0.7359	0.7506	1.0403
0.55	0.1	0.7287	0.7581	0.7352	0.7499	1.0403
0.6	0.1	0.7287	0.7581	0.7345	0.7491	1.0403
0.65	0.1	0.7287	0.7581	0.7338	0.7484	1.0403
0.7	0.1	0.7287	0.7581	0.7330	0.7477	1.0403
0.75	0.1	0.7287	0.7581	0.7323	0.7469	1.0403
0.8	0.1	0.7287	0.7581	0.7316	0.7462	1.0403
0.85	0.1	0.7287	0.7581	0.7309	0.7454	1.0403
0.9	0.1	0.7287	0.7581	0.7302	0.7447	1.0403
0.95	0.1	0.7287	0.7581	0.7294	0.7440	1.0403
1	0.1	0.7287	0.7581	0.7287	0.7432	1.0403

Table A.3. Output of the Computer Program for Mixed $Zn(NO_3)_2$ – $NaNO_3$ Solutions.

A_s	I	$\gamma_{\pm(Zn(NO_3)_2)}$	$\gamma_{\pm(NaNO_3)}$	$\gamma^{(NaNO_3)}_{\pm(Zn(NO_3)_2)}$	$\gamma^{(Zn(NO_3)_2)}_{\pm(NaNO_3)}$	Γ
0	0.1	0.6197	0.7581	0.6081	0.7581	1.4688
0.05	0.1025	0.6174	0.7561	0.6065	0.7577	1.4774
0.10	0.105	0.6153	0.7542	0.6050	0.7573	1.4859
0.15	0.1075	0.6131	0.7523	0.6035	0.7570	1.4943
0.2	0.11	0.6111	0.7504	0.6020	0.7567	1.5026
0.25	0.1125	0.6090	0.7486	0.6006	0.7564	1.5109
0.3	0.115	0.6071	0.7468	0.5993	0.7561	1.5190
0.35	0.1175	0.6052	0.7451	0.5980	0.7559	1.5270
0.4	0.12	0.6033	0.7433	0.5967	0.7557	1.5350
0.45	0.1225	0.6015	0.7416	0.5954	0.7554	1.5429
0.5	0.125	0.5997	0.7400	0.5942	0.7552	1.5507
0.55	0.1275	0.5979	0.7383	0.5930	0.7551	1.5584
0.6	0.13	0.5962	0.7367	0.5919	0.7549	1.5660
0.65	0.1325	0.5945	0.7351	0.5908	0.7547	1.5736
0.7	0.135	0.5929	0.7336	0.5897	0.7546	1.5811
0.75	0.1375	0.5913	0.7320	0.5886	0.7545	1.5885
0.8	0.14	0.5897	0.7305	0.5876	0.7543	1.5959
0.85	0.1425	0.5882	0.7291	0.5866	0.7542	1.6032
0.9	0.145	0.5867	0.7276	0.5856	0.7541	1.6104
0.95	0.1475	0.5852	0.7261	0.5847	0.7540	1.6176
1	0.15	0.5837	0.7247	0.5837	0.7540	1.6247

Table A.4. Output of the Computer Program for Mixed $Cu(NO_3)_2$ – $NaNO_3$ Solutions.

A_s	I	$\gamma_{\pm(Cu(NO_3)_2)}$	$\gamma_{\pm(NaNO_3)}$	$\gamma_{\pm(Cu(NO_3)_2)}^{(NaNO_3)}$	$\gamma_{\pm(NaNO_3)}^{(Cu(NO_3)_2)}$	Γ
0.05	0.1025	0.6150	0.7561	0.6047	0.7576	1.4902
0.10	0.105	0.6128	0.7542	0.6030	0.7572	1.4988
0.15	0.1075	0.6106	0.7523	0.6015	0.7568	1.5073
0.2	0.11	0.6085	0.7504	0.5999	0.7564	1.5157
0.25	0.1125	0.6064	0.7486	0.5985	0.7560	1.5241
0.3	0.115	0.6044	0.7468	0.5970	0.7557	1.5323
0.35	0.1175	0.6024	0.7451	0.5956	0.7553	1.5405
0.4	0.12	0.6005	0.7433	0.5942	0.7550	1.5485
0.45	0.1225	0.5986	0.7416	0.5929	0.7547	1.5565
0.5	0.125	0.5967	0.7400	0.5916	0.7544	1.5644
0.55	0.1275	0.5949	0.7383	0.5903	0.7541	1.5723
0.6	0.13	0.5931	0.7367	0.5891	0.7539	1.5800
0.65	0.1325	0.5914	0.7351	0.5879	0.7536	1.5877
0.7	0.135	0.5897	0.7336	0.5867	0.7534	1.5953
0.75	0.1375	0.5880	0.7320	0.5856	0.7532	1.6028
0.8	0.14	0.5864	0.7305	0.5844	0.7530	1.6103
0.85	0.1425	0.5848	0.7291	0.5833	0.7528	1.6177
0.9	0.145	0.5833	0.7276	0.5823	0.7526	1.6250
0.95	0.1475	0.5817	0.7261	0.5812	0.7524	1.6323
1	0.15	0.5802	0.7247	0.5802	0.7523	1.6395

A.2. Calibration Data of Japanese Reference Rock Standards

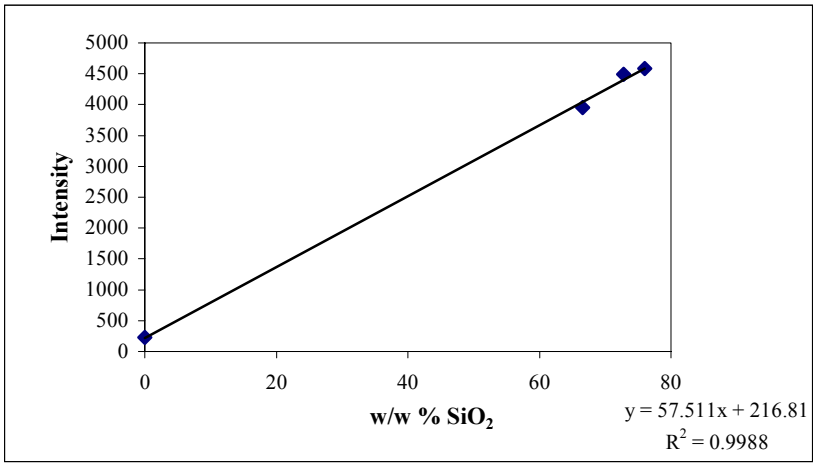

Figure A.6. Calibration Curve of SiO_2.

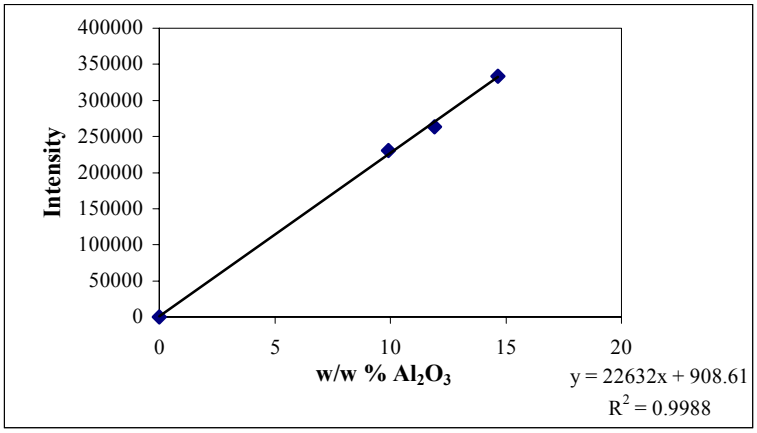

Figure A.7. Calibration Curve of Al_2O_3.

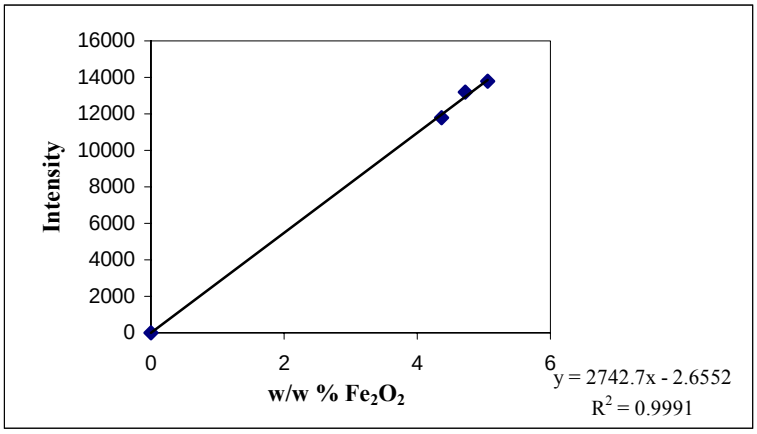

Figure A.8. Calibration Curve of Fe_2O_3.

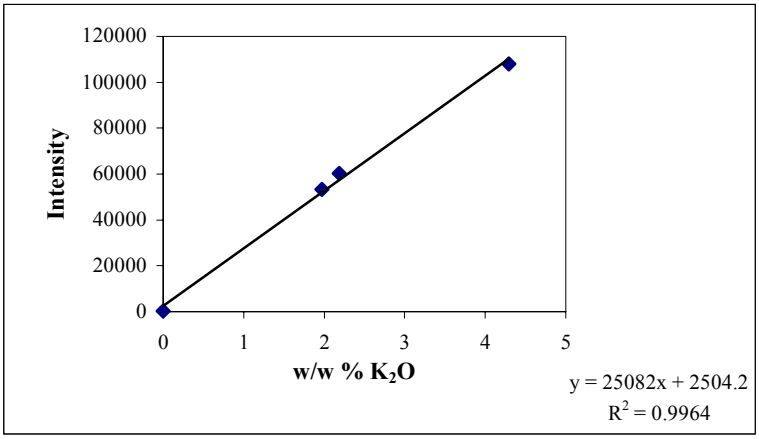

Figure A.9. Calibration Curve of K_2O.

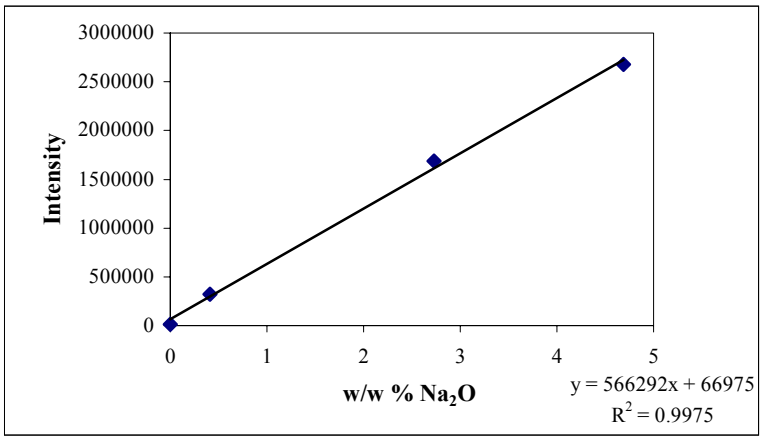

Figure A.10. Calibration Curve of Na_2O.

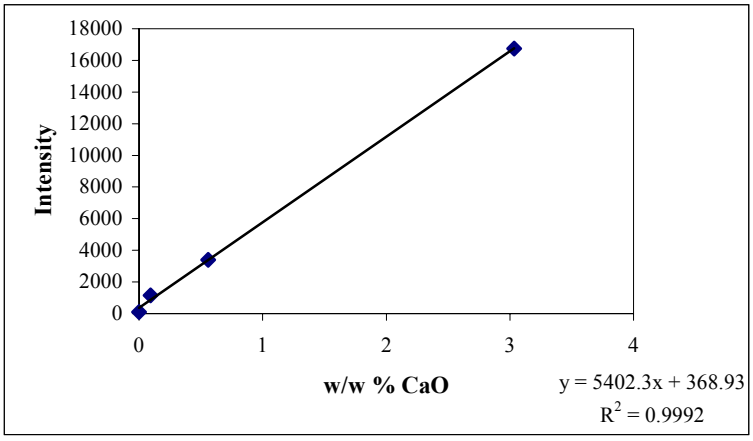

Figure A.11. Calibration Curve of CaO.

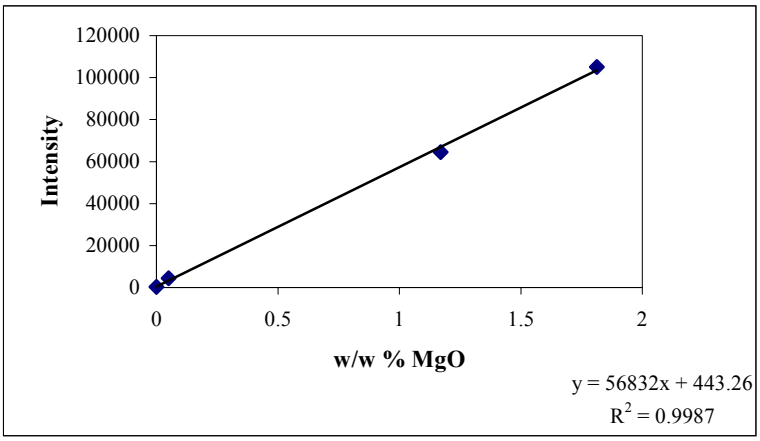

Figure A.12. Calibration Curve of MgO.

Table A.5. Calibration Curve Data for SiO_2.

certified w/w % SiO_2	Intensity	calculated w/w % SiO_2	% error
0	224		
66.55	3956	65.017	2.304
72.76	4490	74.302	2.119
76	4580	75.867	0.175

Table A.6. Calibration Curve Data for Al_2O_3.

certified w/w % Al_2O_3	Intensity	calculated w/w % Al_2O_3	% error
0	219		
9.908	230982.3	10.166	2.603
11.9	263843	11.618	2.371
14.65	333711.3	14.705	0.375

Table A.7. Calibration Curve Data for Fe_2O_3.

certified w/w % Fe_2O_3	Intensity	calculated w/w % Fe_2O_3	% error
0	5		
4.368	11792.33	4.299	1.590
4.72	13205.33	4.814	1.986
5.059	13787	5.026	0.656

Table A.8. Calibration Curve Data for K_2O.

certified w/w % K_2O	Intensity	calculated w/w % K_2O	% error
0	253		
1.971	53313	2.026	2.776
2.183	60330.33	2.305	5.611
4.29	107910.3	4.202	2.041

Table A.9. Calibration Curve Data for Na_2O.

certified w/w % Na_2O	Intensity	calculated w/w % Na_2O	% error
0	13771		
0.411	323196	0.452	10.086
2.727	1687199	2.861	4.918
4.69	2676669	4.608	1.740

Table A.10. Calibration Curve Data for CaO.

certified w/w % CaO	Intensity	calculated w/w % CaO	% error
0	96		
0.093	1149.267	0.144	55.32
0.56	3398.567	0.561	0.14
3.034	16750.33	3.032	0.06

Table A.11. Calibration Curve Data for MgO.

certified w/w % MgO	Intensity	calculated w/w % MgO	% error
0	234		
0.05	4388.67	0.069	38.85
1.17	64500	1.127	3.664
1.81	105022	1.840	1.497

A.3. Experimental Data of Binary Exchange Studies

Table A.12. Experimental Data for Ion Exchange between Ag^+ and Na^+.

Sample #	Zeolite Mass (g)	Solution Volume (ml)	M_i (ppm)	M_i (M)	M_f (ppm)	M_f (M)	A_s	A_z
1	0.5001	25	544.9	0.0051	155.1	0.0014	0.0144	0.0966
2	0.7	25	1103.1	0.0102	248.7	0.0023	0.0231	0.1513
3	0.4999	25	2143.1	0.0199	730.3	0.0068	0.0677	0.3503
4	0.4001	25	1975.3	0.0183	951.8	0.0088	0.0882	0.3170
5	0.6003	25	4130.19	0.0383	1636.5	0.0152	0.1517	0.5148
6	0.5001	25	4143.8	0.0384	1879.3	0.0174	0.1742	0.5612
7	0.6001	25	6710.1	0.0622	3258.5	0.0302	0.3021	0.7129
8	0.5	25	6735.8	0.0624	3718.7	0.0345	0.3447	0.7479
9	0.6	25	8625.2	0.0800	4569.8	0.0424	0.4236	0.8377
10	0.4999	25	8673.6	0.0804	5278.8	0.0489	0.4894	0.8416
11	0.6001	25	10737	0.0995	6362.8	0.0590	0.5899	0.9033
11*	0.6001	25	0	0	947.3	0.0412	0.5880	0.9178
12	0.2496	25	0	0	412	0.0179	0.8208	0.9596
13	0.3999	25	0	0	629.7	0.0274	0.7262	0.9155

* Up to (*) initial and final solution concentrations were measured in terms of silver. The remaining data were provided from sodium measurements.

Table A13. Experimental Data for Ion Exchange between Zn^{2+} and Na^{+}.

Sample #	Zeolite Mass (g)	Solution Volume (ml)	M_i (ppm)	M_i (M)	M_f (ppm)	M_f (M)	A_s	A_z
1	0.6000	10	378.5	0.0058	68.43295	0.0010	0.0209	0.0845
2	0.5002	10	368.6	0.0056	79.1472	0.0012	0.0242	0.0946
3	0.5996	10	691.8	0.0106	217.0192	0.0033	0.0664	0.1295
4	0.5000	10	724.9	0.0111	248.9371	0.0038	0.0761	0.1557
5	0.6001	10	1365.4	0.0209	628.6605	0.0096	0.1923	0.2008
6	0.4997	10	1309.3	0.0200	614.5973	0.0094	0.1880	0.2274
7	0.7500	10	1858.4	0.0284	869.191	0.0133	0.2658	0.2157
8	0.5000	10	1954.4	0.0299	1102.512	0.0169	0.3372	0.2787
9	0.7499	10	2768.6	0.0423	1363.378	0.0208	0.4170	0.3065
10	0.5001	10	2725.6	0.0417	1763.249	0.0270	0.5393	0.3147
11	0.7499	10	3236.8	0.0495	1843.572	0.0282	0.5639	0.3039
11*	0.7499	10	0	0	1020	0.0444	0.5564	0.3163
12	0.4999	10	0	0	709.31	0.0308	0.6915	0.3300
13	0.2499	10	0	0	406.37	0.0177	0.8233	0.3782
14	0.2500	25	0	0	191.95	0.0083	0.9165	0.4464

* Up to (*) initial and final solution concentrations were measured in terms of zinc. The remaining data were provided from sodium measurements.

Table A.14. Experimental Data for Ion Exchange between Cu^{2+} and Na^{+}.

Sample #	Zeolite Mass (g)	Solution Volume (ml)	M_i (ppm)	M_i (M)	M_f (ppm)	M_f (M)	A_s	A_z
1	0.6004	10	316.5	0.0050	82.4	0.0013	0.0259	0.0656
2	0.5005	10	310.8	0.0049	93.6	0.0014	0.0286	0.0739
3	0.6013	10	629.6	0.0099	210.9	0.0032	0.0645	0.1189
4	0.5003	10	620.2	0.0098	259.6	0.0040	0.0794	0.1237
5	0.6006	10	1220.8	0.0192	581.0	0.0089	0.1777	0.1839
6	0.4989	10	1263.5	0.0199	650.7	0.0100	0.1990	0.2129
7	0.7512	10	1900.6	0.0299	822.3	0.0126	0.2515	0.2468
8	0.4997	10	1720.6	0.0271	1068.9	0.0163	0.3269	0.2296
9	0.7504	10	2569.7	0.0404	1393.0	0.0213	0.4261	0.2727
10	0.7508	10	3199.6	0.0504	1647.1	0.0252	0.7481	0.3585
11*	0.5024	10	0	0	704.3	0.0306	0.6937	0.3260
12	0.2505	10	0	0	429.2	0.0187	0.8133	0.3985
13	0.2475	25	0	0	207.8	0.0090	0.9096	0.4881

* Up to (*) initial and final solution concentrations were measured in terms of copper. The remaining data were provided from sodium measurements.

A.4. Sample Calibration Curves for the Direct Calibration Method and the Standard Addition Method

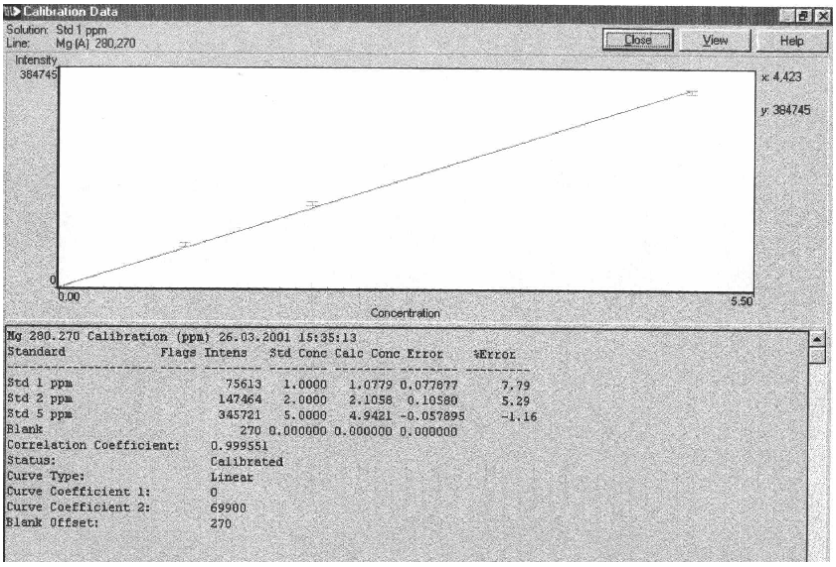

Figure A.13. Sample Calibration Curve for the Direct Calibration Method.

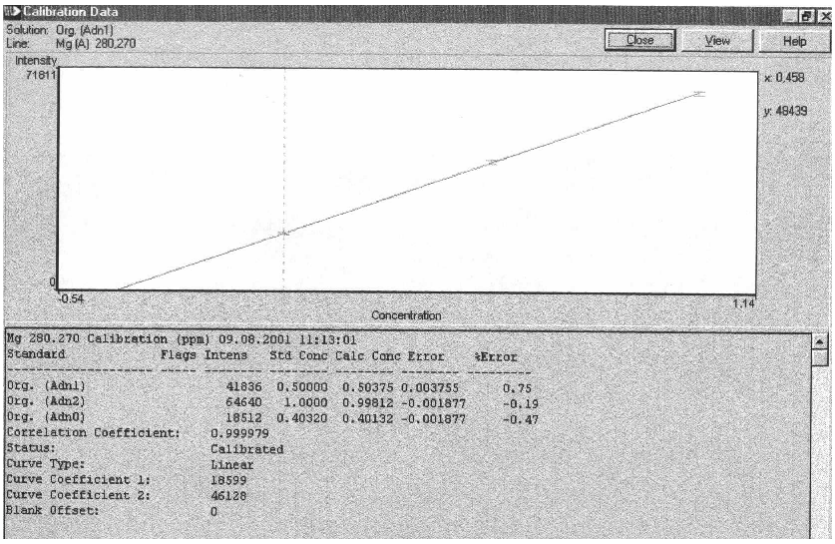

Figure A.14. Sample Calibration Curve for the Standard Addition Method.